Understanding and Targeting Fatty Acid-CoA Ligase ACSL4 in Advanced Human Prostate Cancer

by

Jinjin Wu

Department of Pathology
Duke University

Date: June 6, 2024

Approved:

Ming Chen, Supervisor

Jiaoti Huang

Yiping He

Jennifer Freedman

Soman N Abraham

Dissertation submitted in partial fulfillment of
the requirements for the degree of Doctor
of Philosophy in the Department of
Pathology in the Graduate School
of Duke University

2024

ABSTRACT

Understanding and Targeting Fatty Acid-CoA Ligase ACSL4 in Advanced Human Prostate Cancer

by

Jinjin Wu

Department of Pathology
Duke University

Date: June 6, 2024

Approved:

Ming Chen, Supervisor

Jiaoti Huang

Yiping He

Jennifer Freedman

Soman N Abraham

An abstract of a dissertation submitted in partial fulfillment of the requirements for the degree of Doctor of Philosophy in the Department of Pathology in the Graduate School of Duke University

2024

Abstract

Prostate cancer (PCa) ranks as the most prevalent non-cutaneous malignancy among men. While localized prostate cancer can often be cured, the recurrence of metastatic castration-resistant prostate cancer (mCRPC) remains a formidable challenge and is the leading cause of mortality in PCa patients. Recent findings from our lab and others highlights the pivotal role of RB1 loss in driving lineage plasticity, metastasis, and lethality of prostate tumors. One downstream target of RB1 loss/E2F activation is acyl-CoA synthetase long-chain family member 4 (ACSL4), a fatty acid ligase crucial for the utilization of long-chain fatty acids. Dysregulated fatty acid metabolism fuels oncogenic processes and tumor progression through excessive energy production and lipogenesis, and reprogramming fatty acid metabolism shows promise in advanced cancer therapy. ACSL4 has been reported to be upregulated in cancers of various histological origins, including prostate cancer, and its elevated expression is correlated with cancer aggressiveness. However, the metabolic regulation and clinical significance of ACSL4 in prostate tumorigenesis and progression remains elusive. Through both gain-of-function and loss-of-function approach aiming to examine the outcome of high ACSL4 level in PCa patients, we revealed ACSL4 as an oncogenic driver that promoted prostate cancer progression via enhanced cell proliferation and ATP production. Further characterization via untargeted lipidomic profiling and RNA sequencing has unveiled a distinct metabolic profile and transcriptomic landscape resulting from ACSL4 overexpression, characterized by altered organelle membrane composition, extracellular matrix component and increased neuroendocrine markers that support cancer progression.

These findings underscore the potential of ACSL4 as a novel target for advanced cancer therapy. By employing a structure-based virtual screening approach targeting ATP binding domains of ACSL4, followed by *in vitro* drug testing, we successfully identified four candidate ACSL4 inhibitors. These inhibitors demonstrated significant efficacy in suppressing prostate cancer (PCa) cell proliferation in a dose-response manner. Notably, we showed that these candidate inhibitors exhibit enhanced effectiveness in inhibiting cell proliferation in isogenic ACSL4-high PCa cells. Moreover, we assessed inhibition selectivity through an isotope-labeled ACSL4 activity assay for these inhibitors. Moving forward, our focus will shift towards analyzing pharmacodynamics/pharmacokinetics (PD/PK) for these inhibitors and modifying drug structures to facilitate in vivo application.

The first three chapters of this dissertation are introductory information that reviews the role of lipid metabolism in cancer progression and therapy resistance through the regulation of energy production, phospholipid composition and lipid storage, and the clinical significance of targeting lipid metabolism and fatty acid activation as a cancer therapy. Chapter 1 provides a comprehensive review of the current knowledge of how altered lipid metabolism contributes to aberrant cellular activities and oncogenic events in cancer cells, particularly in prostate cancer. Fatty acid activation is key to lipid utilization, and upregulation of multiple Acyl-CoA synthetase, including ACSL4, is frequently observed in cancer patients. The dissertation aims to bridge the existing gap in knowledge by unraveling the biological mechanisms underlying the positive correlation between prostate tumorigenesis and ACSL4 as a long-chain fatty acid activator.

Furthermore, it seeks to explore the therapeutic potential of targeting ACSL4 as a viable option for managing advanced prostate cancer.

Chapter 2 provided the background of lipid metabolism, and the impact of dysregulated lipid metabolism on cancer cell activities as a result of oncogenic signaling. In this chapter, we highlight the current understanding of the intricate interplay between cancer lipid metabolism and well-known oncogenic signaling. By elucidating these connections, we illuminate how altered lipid metabolic pathways contribute to the reshaping of cellular components, modulation of energy production levels, and perturbation of lipid storage mechanisms, all of which drive cancer progression.

Chapter 3 discusses the knowledge and considerations in the current field on the potential of targeting various pathways in lipid metabolism as effective cancer therapies. Given the pivotal role of dysregulated lipid metabolism during tumorigenesis, there has been significant clinical interest in developing pharmacological inhibitors to target altered lipid metabolic activities in cancer. Recent studies have discovered multiple targets as key fatty acid metabolic regulators during oncogenesis with several inhibitors demonstrating effectiveness in both preclinical studies and clinical trials. Most of these drugs exert their effects on tumorigenesis and tumor expansion by targeting enzymes in different lipid metabolic pathways, including *de novo* fatty acid synthesis, metabolic substrates, fatty acid degradation and lipid storage. The major obstacle in this field has been related to target specificity, as many enzymes within the same family share high structural similarities, leading to off-target issues for many lipogenesis inhibitors. In addition, inhibition of some crucial steps in fatty acid metabolism can cause severe side effects due to accumulation of unexpected side products and toxicity to normal tissues.

In many cases, single treatment with lipid synthesis inhibitors shows only moderate efficacy. Therefore, it is imperative for future studies to discover novel targets more specific to oncogenesis and explore the potential of combinatorial treatment with other therapeutic options such as chemotherapy and androgen deprivation therapy to achieve best efficacy with minimized toxicity.

Chapter 4 provides the basis for this thesis project based on our previous findings and preliminary data on the key modulators of advanced prostate cancer progression and metastasis. The Retinoblastoma Transcriptional Corepressor 1 (RB) is a key cell cycle regulator and tumor suppressor through regulating essential transcriptional activities via the RB1/E2F signaling axis. Loss of RB1 activity is known to drive cancer cell proliferation and correlates with cancer aggressiveness. Consistently, our preliminary data also showed that co-deletion of RB1 and PTEN in a mouse model led to a highly aggressive and lethal metastatic prostate cancer compared with PTEN deletion only. In addition to its well-established role in mitotic cell cycle regulation, RB1 has been reported to execute tumor-suppressing function through controlling important oncogenic transcriptional activities. Importantly, our previous study identified an RB1 downstream effector called ACSL4, also known as Acyl-CoA Synthetase Long Chain Family Member 4. We showed that RB1/E2F negatively regulates ACSL4 transcription through multiple binding sites on its promoter region, and ACSL4 levels are found to be significantly upregulated in RB-loss PCa cells and patient samples. ACSL4 catalyzes the activation and membrane incorporation of fatty acids by promoting fatty acid utilization and subsequently regulates cell lipid metabolism. Moreover, ACSL4 has been reported to be overexpressed in advanced cancers, including metastatic castration-resistant prostate cancer (mCRPC) and neuroendocrine prostate cancer (NEPC), and its upregulation is often associated with therapy resistance and poor prognosis. In addition to RB1, multiple genes have been reported to regulate ACSL4 level in cancer cells, including the well-known oncogenic signaling AR. However, the role of ACSL4 in reshaping cancer fatty acid metabolism thus promoting tumorigenesis remains elusive. Understanding the biological function of ACSL4 in the context of cancer metabolic landscape will provide great insight into novel targeted therapy by inhibiting ACSL4 activity.

Chapter 5 discusses the findings from the first part of this thesis project, which focuses on characterizing the impact of ACSL4 on prostate tumorigenesis through its regulation on cancer cell activities. To explore the role of ACSL4 in cancer cell proliferation and to understand the underlying mechanism, we examined ACSL4 levels in common human PCa cell lines, and generated ACSL4 overexpression cell lines to represent the clinical observation of ACSL4 upregulation. Examination of cell proliferation through crystal violet assay showed that ACSL4 overexpression led to significantly increased cell growth in human PCa cell lines. In addition, ACSL4-overexpressing xenograft tumors had increased growth rate *in vivo*. Further characterization through the seahorse assay revealed that these cells showed significantly higher oxygen consumption rate (OCR) and extracellular acidification rate (ECAR), indicating boosted ATP-dependent cell viability that accounts for the increased cell proliferation. ACSL4 activates intracellular fatty acids, preferably long-chain fatty acids by esterification of CoA to free fatty acids and generate Acyl-CoA. One metabolic fate of Acyl-CoA is to be diverted into mitochondria, where they are further catalyzed into

Acetyl-CoA and participate in tricarboxylic acid (TCA) cycle. Acceleration of TCA cycle due to increased Acetyl-CoA production can cause excessive ATP production supporting cancer cell growth. This result is also consistent with the previous finding that cancer cells tend to shift fatty acid utilization towards *de novo* synthesis. To confirm these results through loss-of-function studies, we sought to generate ACSL4 knockout and knockdown cell lines. Interestingly, shRNA knockdown of ACSL4 could not be stabilized due to impaired cell viability in parental DU145 and PC-3 cell lines. Alternatively, we found that cells with double knockdown of RB1 and ACSL4 can be stably passed with the knockdown effects well maintained. Our previous study found that RB1 loss granted PCa cells growth advantage and supported cancer progression, and that RB1 deficient PCa is highly lethal and lacks effective therapy options. Examination of the double knockdown PCa cells revealed that the proliferation of these cells was significantly impaired compared. Consistently, we found that ACSL4 knockout PCa cells had a significantly decreased cell proliferation rate and ATP production level. This result provides strong rationale for targeting ACSL4 activity as an efficient way to treat advanced prostate cancers with RB1 deficiency.

To further investigate the role of ACSL4 in reshaping cancer cell fatty acid metabolic landscape, in chapter 6 we aim to dissect the mechanism behind the effect of ACSL4 on PCa tumor growth. To this end, we performed untargeted lipidomic profiling analysis and RNA sequencing analysis on ACSL4 overexpression cells and control cells. Here we emphasize the role of ACSL4 in reshaping cancer cell lipid metabolic landscape to support cancer cell growth and drug resistance. Our lipidomic profiling analysis revealed upregulated lipid species in ACSL4 overexpressing PCa cells including triglyceride (TG), bismethyl phosphatidic acid (BisMePA), cholesteryl ester (ChE) and phosphatidylethanolamine (PE). Notably, upregulation of TG and PE has been associated with increased risk of tumor metastasis and progression. ACSL4 preferably consumes long-chain fatty acids including arachidonic acid (AA), eicosatetraenoic acid (EA), stearic acid (SA) and palmitic acid (PA) as substrates. Particularly, BisMePA and ChE with AA, EA and SA acyl tails are also enriched in ACSL4 overexpressing PCa cells. Interestingly, upregulation of BisMePA was observed for both ACSL4-specific acyl chains and in total amount. BisMePA is a major component of lysosomal and endosomal membranes, regulating endo-lysosomal capacity and cell response to stress, and elevated BisMePA could promote cancer cell survival and drug resistance. Interestingly, RNA-seq analysis on ACSL4-overexpressing cells revealed significant change of a set of genes that regulates lysosome stability and activity, consistent with our lipidomic data. Moreover, we found that ACSL4 OE may play a role in remodeling cancer cell extracellular matrix (ECM) to favor cancer cell migration and drug resistance as indicated by significant changes in the ADAMTS family and A2M. Intriguingly, we also noticed that ACSL4 OE cells had a distinct pattern of neuroendocrine prostate carcinomas (NEPC) signature genes expression independent of AR signaling compared with the wildtype cells, which warrants further study of how ACSL4 is involved in lineage plasticity during the progression of NEPC.

Given these results, it is imperative to explore the feasibility of pharmacological inhibition of ACSL4 for clinical application. Chapter 7 focuses on the discovery of novel ACSL4 inhibitors as potential treatment for advanced prostate cancer. Structure-based virtual screening (SBVS) utilizes computational docking approach based on the protein

3D structures, which has been widely applied in the discovery of novel small molecule ligands in early-stage drug discovery. To identify ACSL4 inhibitors, we performed SBVS by rendering and docking ACSL4 structure against 100,000 ligands obtained from three Maybridge compound libraries. These ligands were docked against ATP binding pocket and K572 acyl group accommodating channel on ACSL4 structure, respectively to optimize target selectivity. Standard docking followed by precision docking of the top hits generated each round was performed to maximize targeting accuracy. As a result, we identified 158 hits in total on ACSL4 structure, from which we selected top 15 hit compounds for subsequent *in vitro* screening. SBVS complements high-throughput screening (HTS) through computational approach and provides valuable insights into novel compound discovery, however, downstream *in vitro* validation is required to examine the pharmacological effects of these candidate molecules. Therefore, we established an *in vitro* drug testing system using human PCa cell lines to test the potency of the 15 top candidates. We found that 4 out of 15 compounds effectively inhibited PCa cell proliferation in a dose-response manner and their inhibitory effects positively correlated with cellular levels of ACSL4. Notably, we highlight the potency of our candidate inhibitors on suppressing PCa cell growth compared with the only previously reported ACSL4 inhibitor PRGL493, particularly in aggressive ACSL4-high PCa cells such as RB1-deficient PC-3 and neuroendocrine prostate cancer (NEPC) cell line H660. Achieving inhibitor selectivity for desired targets in the development of new drugs is often challenging and can lead to severe side effects due to off targeting. Here we performed an isotope-labeled enzyme activity assay to assess the inhibitor selectivity of our candidate inhibitors on ACSL4 activity. Through measuring the consumption and conversion of arachidonic acid (AA) to AA-CoA by ACSL4 activity, we confirmed that 2 of our candidate inhibitors showed high selectivity towards ACSL4 inhibition.

Chapter 8 highlights the potential of ACSL4 inhibitors in the context of clinical application. ACSL4 is known to regulate cancer cell sensitivity to ferroptosis through increased lipid peroxidation. Chemotherapeutic agents inducing cancer cell apoptosis such as docetaxel have been widely used to treat patients with metastatic prostate cancer. It has been debated that the effect of chemotherapy in certain contexts also involves other types of cell death including ferroptosis, arguing that ACSL4 inhibitor could weaken the potency of chemotherapy. Therefore, we investigated the mechanism of action of docetaxel and ACSL4 inhibitors in the context of prostate cancer. We showed that docetaxel treatment mainly induced apoptosis in PCa cell lines PC-3 and DU145, given that the inhibition of cell growth was only rescued by apoptosis inhibitors Z-VAD, not ferroptosis inhibitors ferrostatin and deferoxamine (DFO). This result indicates that inhibition of ACSL4 will not attenuate the effect of chemotherapy. Consistently, ACSL4 overexpressing PCa cells are more resistant to docetaxel treatment. Therefore, we further sought to maximize the therapeutic efficacy for ACSL4 inhibitors, and we found that combinational treatment of ACSL4 inhibitors and docetaxel displayed a synergistic effect on PCa cells, which was partially rescued by apoptosis inhibitor Z-VAD. Our data provides evidence for a novel precision therapeutic option for advanced PCa patients with high ACSL4 expression.

Chapter 9 concludes the findings of this study and offers directions for future research. It underscores the significance of targeting fatty acid metabolism and ACSL4 as a pivotal metabolic regulator and oncogenic driver in tumorigenesis and progression, providing valuable insights into treatment options for targeted therapy in advanced prostate cancer.

Dedication

I dedicate my dissertation work to my parents, Tao Jin and Weibing Wu, whose unconditional love, unwavering support, and boundless encouragement have been the guiding force behind every step of my life. To my husband, Bofeng Zhang, whose patience, understanding, and steadfast love have been my source of strength throughout this endeavor. To my friends, who always stand by me with endless encouragement through all the challenges.

Table of Contents

List of Tables

List of Figures

Acknowledgements

As I embark on the final stage of presenting my PhD thesis, I am filled with a profound sense of gratitude and humility. This work represents the culmination of years of dedication, perseverance, and collaboration, and I am deeply indebted to the many individuals who have supported and inspired me along the way.

First, I wish to extend my deepest gratitude to my mentor, Dr. Ming Chen, whose guidance and support have been invaluable throughout this journey. Your dedication to excellence and your unwavering belief in my abilities have been a constant source of inspiration.

I would like to express my heartfelt appreciation to the members of my lab, whose collaboration and support enriched every aspect of my research. Mu-En Wang, Alyssa Bawcom, Wei-Ling Tu, Yi Lu, Eden Jacobs, and Jaylen Kim, as well as previous lab members Jiaqi Chen, Meredith Davis, and Blake Zhang, your contributions have played a significant role in shaping the outcome of this thesis.

I would like to thank my committee members, Yiping He, Jiaoti Huang, Jennifer Freedman, and Soman Abraham for their insightful feedback and constructive advice, which have helped to refine this work and elevate its quality.

To my family, Tao Jin and Weibing Wu, whose unconditional love and support sustained me through the highs and lows of this academic journey, I owe an immense debt of gratitude. To my husband, Bofeng Zhang, your patience, understanding and unwavering love have been the bedrock of my success.

To my friends, Aijing Lin, Yi Li, Yi Fan, and Zoe Loh who provided much-needed joy and encouragement, support, and perspective along the way, I am deeply grateful. Your presence in my life has made this journey all the more meaningful.

Lastly, I would like to acknowledge the countless individuals whose names may not appear on these pages but whose contributions, in ways big and small, have left an indelible mark on this thesis. Your support has been invaluable and deeply appreciated. Thank you all for being a part of this incredible journey.

1. Introduction

Alteration of lipid metabolic landscape is a hallmark of cancer. Cancer cells have distinctive metabolic characteristics that allow rapid production of energy and macromolecules to support cancer cell replication, stress response, and activation of oncogenic signaling. [1-4] Cells can obtain fatty acids through either exogenous uptake or endogenous *de novo* synthesis, and cancer cells often shift their sources of fatty acid acquisition to maximize the lipid utilization efficiency and energy production. [5] Reprogramming of lipid synthesis in cancer cells also leads to a distinct group of phospholipids that further modulates cellular membrane composition and enhances cancer cell survival. [4-6] Moreover, recent studies have suggested that cancer cells can adapt themselves to maintain lipidomic homeostasis and avoid lipotoxicity or ferroptosis due to excessive lipid intake through an optimal ratio of fatty acyl chain species. [7, 8] It has been reported that tumor lipidome consists of a significantly increased proportion of saturated fatty acyl chains, particularly monounsaturated fatty acyl chains (MUFAs). [9, 10] This change of lipid species composition also implies response and resistance to anti-cancer therapies. [7, 11]

Cancer cells can reprogram fatty acid metabolism to support tumorigenesis and therapy resistance through various oncogenic signaling. Several key metabolic enzymes are directly regulated by oncogenes and/or tumor suppressors, such as the regulation of phosphoinositide 3-kinase and AKT (PI3K–AKT) pathway on CoA, and MYC oncogenic signaling on PGC1α and SREBP1. [12-14] On the other hand, dysregulated lipid metabolism is also noted to cause oncogenic signaling and genetic alterations, such as the crosstalk between FASN and estrogen signaling. [13] Moreover, products of lipid metabolism could also modulate cancer epigenome, thereby regulating gene expression and cellular stemness. [15]

Prostate cancer (PCa) is featured in a wide range of lipidomic remodeling, including alterations in fatty acid transport, *de novo* lipogenesis and ATP generation that is highly dependent on β-oxidation. [16-18] Particularly, dysregulated androgen receptor (AR) signaling contributes to the altered lipid metabolic activities such as steroidogenesis and β-oxidation that promote prostate cancer progression in a hormone-dependent manner. [19] In addition, enhanced uptake of extracellular lipids has been associated with castration-resistant prostate cancer (CRPC), with a distinct lipid content of increased glycerophospholipids being observed in patients developed with therapy resistance. [16, 20] Understanding the mechanistic basis of the dysregulated lipid metabolism in PCa will shed light on further clinical studies and development of novel targeted therapies.

Targeting altered lipid metabolism in cancer cells has been proven promising in the development of anticancer therapy through restricting fatty acid origins. Direct targeting FASN and several rate-limiting enzymes such as ACYL and SREBP interrupts *de novo* fatty acid synthesis and efficiently removes the fuel for cancer cell proliferation. For example, TVB-2640, an FASN inhibitor achieved success in pre-clinical and clinical studies, in spite of the fact that standalone treatment demonstrated only moderate efficacy from an early clinical trial. [21] On the other hand, exogenous fatty acid uptake via surface receptors like CD36 and FABPs is also a crucial step for cancer cells to obtain abundant lipid source to support their proliferation and invasion. To this end, dmrFABP5, an FABP5 inhibitor has shown potency in suppressing PCa cells proliferation and migration. [22] Currently challenges of clinical application of these inhibitors come from the toxicity arisen from accumulation of byproducts, and potential off-target effects. [23] Therefore, discovery of novel therapeutic targets is still a pressing need for anti-cancer therapies.

Fatty acid activation is the first and a crucial step in utilizing the free fatty acid molecules for β-oxidation, energy production and phospholipid synthesis. During fatty acid activation, free fatty acids are converted to an energy-rich derivative of coenzyme A (CoA) called fatty acyl-CoA in an ATP-dependent manner. The activated fatty acid is then transported to mitochondria undergoing fatty acid oxidation or participates in the production of membrane phospholipids. ACSL4 is a long-chain acyl-CoA synthetase that preferably catalyzes long-chain fatty acid activation. [24, 25] The role of ACSL4 in cancer has been implicated in recent studies where upregulation of ACSL4 is observed in many aggressive cancer types including triple-negative breast cancer, castration-resistant prostate cancer, and hepatocellular carcinoma. [26-28] Moreover, excessive fatty acid oxidation and aberrant phospholipid synthesis triggered by ACSL4 overexpression has been linked to increased tumor metastatic potential and drug resistance. [28-32] Intriguingly, our previous study revealed that ACSL4 transcription is regulated through RB1/E2F tumor suppressive signaling. [33] Therefore, understanding the biological function of ACSL4 as a lipid metabolic regulator during tumorigenesis is essential for exploring its potential as a therapeutic target in advance prostate cancer.

Our study aims to dissect the role of ACSL4 in regulating PCa development, and to explore the therapeutic opportunity by targeting ACSL4 activity. While many small molecule inhibitors targeting key enzymes for fatty acid synthesis have been proven efficient in pre-clinical studies, strategies targeting ACSL activity have largely failed due to off targets and unpredicted side effects. [34, 35] Structural-based virtual screening (SBVS) has been widely applied in early drug development and provides valuable information to accelerate the identification of novel small molecule inhibitors with high target selectivity. Through a drug screening strategy combining virtual screening with an *in vitro* drug testing system, we aim to develop novel inhibitors targeting ACSL4 activity with high potency and selectivity, thus provide insight into improving PCa treatment outcome through targeted therapies.

2. Lipid Metabolism Supports Cancer Progression and Therapy Resistance

It has been widely acknowledged that cancer cells reprogram their lipidome to meet the needs for abundant ATP and macromolecules production to support rapid growth. As a result, the lipid metabolic networks in cancer undergo drastic changes to acquire adaptability to multiple stresses during tumorigenesis. Fatty acids, through dietary uptake or *de novo* biosynthesis, serve as the fundamental building blocks that can be further utilized as substrates for ATP generation, as well as lipid sources to be incorporated into various membrane components. Recent findings have revealed that aberrant fatty acid metabolism is a hallmark in various cancer types. In this chapter, we will discuss the basic processes and biological functions of lipid metabolism pathways, and how these metabolic changes are regulated by oncogenic signaling and subsequently lead to oncogenic events.

2.1 Overview of Lipid Metabolism

2.1.1 Lipid Metabolism Pathways

In cells, functional lipids such as fatty acids, glycolipids, cholesterol, and phospholipids undergo the processes of being synthesized, and degraded to serve as sources of energy production, cellular membrane construction or lipid droplet storage. This complex metabolic network is called lipid metabolism. Lipid metabolism plays a fundamental role in the regulation of various cellular processes, including cell proliferation, response to stress, survival and apoptosis, inflammatory responses, and membrane homeostasis.

Cells can obtain free fatty acids (FAs) from exogenous uptake, as well as through *de novo* lipogenesis. The exogenous uptake from dietary FA sources is facilitated by several cell surface transporters, including CD36, FABPs and FATPs. [5, 36] When long chain fatty acids are activated and enter cytoplasm, they are shuttled into the mitochondria through carnitine shuttling system. [37] In the mitochondria, activated fatty acids (i.e. Acyl-CoAs) undergo oxidative reaction to form of acetyl-CoA. As the major source of ATP production, Acetyl-CoA undergo fatty acid oxidation (FAO) or tricarboxylic acid (TCA) cycle, converted into citrate, aconitase 2 (ACO2) and ultimately oxidized to CO2, through which procedure reduced electron carriers (NADH/FADH2) is produced and pass electrons to mitochondrial ETC to yield ATP. [5] In addition, the intermediate carbon and hydrogen sources generated during TCA cycle can be exported to the cytoplasm to participate in NADPH and dNTP production. [38] If not immediately used as substrates for downstream metabolic activities, free FAs and their synthetic derivatives will be redirected and stored as lipid droplets (LDs) and serve as backup sources for NADPH and acetyl-CoA production in the mitochondria. The major carbon sources of *de novo* lipogenesis are the citrates synthesized from glucose, glutamine, and acetate. Citrate undergoes a serial synthetic step through enzymes including ACLY, ACC and FASN, and are converted into acetyl-CoA, malonyl-CoA, and eventually palmitate. Palmitate is subsequently desaturated and elongated by stearoyl-CoA desaturase (SCD), fatty acid desaturase (FADS2), and FA elongases (ELOVLs) to form a different types of lipid species including monounsaturated fatty acids (MUFAs) and polyunsaturated fatty acids (PUFAs). [4, 39]

2.1.2 Impacts of Lipid Metabolism on Cellular Component and Activities

Alteration in fatty acid metabolic activities is implied in various downstream cellular activities in cancers. First, increased exogenous fatty acid uptake directly fuels cancer cells for all downstream cellular activities including ATP generation, de novo lipid synthesis, or lipid storage. Indeed, recent studies have revealed that several genes involved in the uptake of exogenous FAs are upregulated in cancer cells, such as CD36, FATPs and FABPs. [20, 40]. Particularly, high CD36 has been linked to poor prognosis in multiple cancer types, such as breast, ovarian, gastric and prostate. [11, 40, 41] In the aggressive Pten-deleted prostate cancer, it was reported that CD36 promoted increased FA uptake, which served as the major source of lipid biosynthesis and increased storage in LDs and altered lipid composition by increasing acyl-carnitines (ACs), monoacylglycerols (MAGs) and other lysophospholipids. [11] A major destiny of these elevated uptake of exogenous FAs is the storage in LDs synthesized as the form of triacylglycerols (TAGs) and sterol esters. [42] The excessive production of LDs in cancer cells not only maintains lipid homoeostasis by preventing lipotoxicity, but also provide a backup source of ATP and NADPH under metabolic stress and energy deprivation.

Interestingly, cancer lipid metabolism is also featured by the diversion of lipid source preference towards *de novo* synthesized lipids. [43] Such high level of lipid synthesis provides cells with FAs sources to maintain their high flexibility and adaptability to generate various lipid species with distinct functions. Intracellular biosynthesis of lipids is largely regulated through the sterol regulatory element-binding proteins (SREBPs) which transcriptionally regulate various genes involved during FA synthesis. [44] Particularly, palmitate is the most abundant lipid species generated through *de novo* lipogenesis, with high flexibility that can be desaturated and elongated to produce additional MUFAs and PUFAs. [45] Consequently, these FAs can be further used to synthesize of more complex lipids. For example, as a source FA of palmitate, oleate can not only feed into palmitate synthesis by GPAT1 and LPATs, but also can be incorporated into TAGs for storage. [46, 47] Such flexible roles in multiple lipid metabolic activities grants oleate important regulatory functions in structural and signaling controls and biosynthesis of complex glycerolipids. [48]

2.2 Oncogenic Reprogramming of Lipid Metabolism in Cancer

In cancer cells, reprogramming of tumor lipidome has been widely accepted as a consequence of oncogenic signaling due to genetic aberrations. On the other hand, as early oncogenic events, some aberrant lipid metabolism activities could also initiate oncogenic signaling to drive tumorigenesis. Moreover, there has been increasing evidence that regulation of fatty acid metabolism in cancer is closely associated with specific molecular and metabolic contexts. These complexities include exogenous (environmental) factors such as diets and endogenous regulatory networks which collectively shape the oncogenic lipidome to support cancer cell expansion.

2.2.1 Lipid Metabolism Alterations by Oncogenic Signaling

Many aberrant lipid metabolisms during tumorigenesis are directly regulated by oncogenic signaling through oncogenes and tumor suppressors. For example, the well-known oncogenic mutant KRAS signaling enhances glycolysis by upregulating hexokinase 1/2 (HK1 and HK2) in pancreatic cancer cells and redirecting glutamine flux to malate to promote pyruvate synthesis. [49] In addition, the MYC oncogene amplification has been reported to drive the upregulation of key enzymes in lipid biosynthesis and mitochondrial glutaminase (GLS1), leading to increased glutamine metabolism and energy production. [50, 51]

As one of the most oncogenic signaling pathways, the phosphoinositide 3-kinase and AKT (PI3K–AKT) pathway is frequently hyperactivated in various cancer and has also been reported to regulate metabolic processes through increasing glucose uptake, glutamine anaplerosis and remodeling cellular lipidome. [52, 53] However, how fatty acid metabolism plays a part in this complex metabolic network in the context of cancer is still understudied. With the activation of PI3K-AKT signaling, metabolic activities associated with biosynthesis of substrates required for lipogenesis and energy production in mitochondria are upregulated. Activated AKT contributes to *de novo* lipid synthesis by shuttling of required substrates as sources for anabolism, and producing NADPH to fuel lipogenesis. [54] It has been reported that AKT can phosphorylate ACLY and activate it to increase acetyl-CoA synthesis. [55] AKT signaling has also been found to promote the translocation of intracellular SREBP1c from ER membrane to Golgi apparatus where it is activated. [56] These findings collectively indicate that oncogenic signaling could significantly regulate lipid metabolic activities which eventually contributes to tumorigenic events.

2.2.2 Oncogenic Signaling Regulated by Aberrant Lipid Metabolism

On the other hand, hyperactivation of lipogenic activities could also occurs as early markers during tumorigenesis such as in hyperplastic and preinvasive lesions. [57]

Therefore, it is reasonably proposed that increased *de novo* lipogenesis and the metabolic activities may also reciprocally activate specific oncogenic signaling and promote the transformation into malignant phenotypes, instead of only representing a secondary phenomenon. One such example is the bi-directional crosstalk between fatty acid synthase (FASN) and estrogen receptor α (ERα) signaling in breast cancer. Inhibition of the FASN activity led to a sensitization of ERα to ER signaling activation and downstream upregulation of estrogen receptor element (ERE) and mitogen-activated protein kinase (MAPK)–ERK signaling to promote tumor development. [53] In addition, *de novo* lipid biosynthesis by FASN has also been linked to HER2 overexpression, as upregulation of the ets-DNA-binding protein PEA3, a suppressor of HER2 transcription was observed upon inhibition of FASN, leading to activated HER2 transcription in breast cancer. [58]

Dysregulated fatty acid metabolism can also contribute to oncogenic events through altered cellular components. Lipid homeostasis is maintained through a good ratio of saturated to unsaturated FAs and is crucial for preventing the cells from lipotoxicity-associated cell death. For example, it has been reported that the hyperactivation of Stearoyl-CoA desaturase (SCD), an ER membrane protein that catalyzes the formation of the monounsaturated FAs could significantly protect cancer cells from lipotoxicity and ER stress due to accumulation of saturated FAs, thus improving cancer cell survival. [59]

2.3 Lipid Metabolism and Therapy Resistance

Cancer cells reprogram their lipidome not only to fulfill their need for rapid expansion, but also to promote their survival against metabolic and environmental stress. As a result, cancer cells have developed dynamic metabolic adaptability to enhance stress response. Such adaptation to metabolic alterations requires flexibility and plasticity, where cancer cells adjust themselves to be able to utilize different metabolic substrates, and to process these substrates under different conditions.

In the context of cancer progression, the tumor microenvironment reshapes tumor cells and enables metabolic plasticity and flexibility to develop therapy resistance. As an example, autophagy and exosome secretion are found to be significantly upregulated in many types of cancer cell, which provide abundant metabolites such as amino acids and fatty acids to support the flexible adaptation and enhance cell survival under stressful conditions such as nutrient deprivation and chemotherapy. [60] As reported in a previous study, the angiogenesis inducer miR-126 was found to upregulate a set of genes involved in oxidative stress resolution and gluconeogenesis through blocking the transcription of insulin receptor substrate-1 (IRS-1) in malignant mesothelioma, leading to chemo-resistance. [61]

Tumor cells metabolic flexibility and plasticity increase their resistance in most anti-cancer therapies. One major contributor to the development of such resistance is the genetic heterogeneity nature of most tumor types. Clones with the ability to resist anti-cancer therapies undergo selection to enrich and expand the impact of a specific signaling pathway that supports the required metabolic adaptation and resolves stress imposed by the drug. As the counteraction against the anti-proliferation effects of therapeutic agents, cancer cells develop metabolic plasticity mainly to restore rapid growth rate. One most direct adaptation is through upregulated glucose metabolism following chemotherapy treatment. For example, patients receiving cisplatin chemotherapy for cervical cancer showed a significant upregulation in several key glycolytic regulators such as HK2, PFK, PKM2, and GLUT-1. [62, 63] As a result, the accumulation of intermediate product due to overactivated glycolysis leads to upregulated lactate production which creates a hypoxic environment and prevent the drug penetration into tumor cells. Meanwhile, accelerated glycolysis increases the basal energy consumption and could also activate stress response machinery like autophagy that help tumor cells to avoid apoptosis.

In conclusion, the evolution and progression of tumor is largely affected by the pressure to satisfy its metabolic needs under multiple stresses, including undergoing therapeutic treatment. Therefore, targeting such metabolic adaptation in cancer cells should be considered as a powerful treatment option in future pre-clinical research and clinical practice. Combinatorial treatment with current chemotherapeutic agents will abolish the drug resistance developed in cancer cells, meanwhile restricting tumor growth.

3. Reprogramming Lipid Metabolism as a Novel Target for Cancer Therapy

As one of the major contributors of cellular energization and synthetic lipid source that allow for well-maintained flexibility and adaptability in cancer cells, the altered lipid metabolic system has been widely acknowledged as an effective anti-cancer therapeutic target. While most well-known drugs proven effective in cancer therapies are small molecule pharmacological inhibitors targeting key enzymes involved during *de novo* fatty acid synthesis, recent studies have identified several novel therapeutic options that utilized the nature of hyperactivated lipid metabolic activities in cancer cells, such as ferroptosis induction. In addition, given the essential functions of cancer lipid metabolism in developing drug resistance, combinatorial treatment of lipid inhibitors and chemotherapy or radiotherapy has also shown promising efficacy in inhibiting tumor growth. In this chapter, we will discuss the current therapeutic agents that specifically target altered lipid metabolism in cancer treatment development.

3.1 Targeting De Novo Fatty Acid Synthesis

Since cancer cells shift their FA source towards biosynthetic FA, targeting FA *de novo* synthesis has become the most promising direction and several pharmacological inhibitors have been shown effective in various cancer types. First, given the fundamental role of FASN in controlling synthetic MUFAs and PUFAs, it has received most interest as a potential target. The first generation of FASN inhibitors such as C75 and cerulenin showed high efficacy in pre-clinical studies by inhibiting tumor growth, improving survival, and sensitizing several types of tumors to chemotherapy. [31, 64]

However, later studies have found that these FASN inhibitors demonstrated systemic adverse effects including weight loss and anorexia, which highlighted the major obstacle of FASN inhibitor where the viability of both malignant and normal tissues are significantly impaired without further specific targeting strategies. [65] This might be due to the universal expression of FASN in both healthy and tumor tissues, and the high FASN activity in those actively proliferating tissues. One such example is that the proliferative ovarian surface epithelial cells showed comparable FASN expression with ovarian cancer cells, and FASN inhibitors showed similar efficacies in inhibiting the growth of these two cell lines. [65]

To address this issue, recent studies have developed the next-generation FASN inhibitors such as TVB-3166 and TVB-2640, which have also shown great efficacies in the inhibitor of tumor growth in some preclinical studies for breast and colorectal cancer, with a much lower systemic toxicity during early-phase clinical trials. [66, 67] Compared with the first-generation inhibitors, TVB-3166 and TVB-2640 showed no effect in the activation of CPT1 in normal tissue, which was the major contributor of the adverse effects observed in the first generation FASN inhibitors. [66] Notably, there are currently two clinical trials going on evaluating the synergistic effects of TVB-2640 and chemotherapy in HER2+ breast cancer and astrocytoma (Clinical Trial ID: NCT03179904, NCT03179904). Therefore, clinical application of FASN inhibitors needs to be cautious in the determination of FASN as a tumor-specific biomarker instead of general upregulation.

3.2 Therapeutic Targeting of the Metabolic Substrates for Lipid Synthesis

Another strategy to target cancer *de novo* synthesis is through limiting the metabolic substrates supply to decelerate lipogenic reactions. Among all enzymes that regulate intermediate lipogenic reactions, the most promising target is ACYL. ACYL is found to be upregulated in multiple cancer types including breast, colorectal, and liver cancers. [68] ACLY catalyze the production of acetyl-CoA, which is the major substrate for the first step of *de novo* lipogenesis. ACLY inhibitors such as ETC-1002 and hydroxycitrate are clinically used as treatment for cardiovascular disease and type II diabetes by decreasing LDL in patients with low toxicity. [69, 70] In addition, there is pre-clinical evidence that supports the favorable outcome of ACLY inhibitors as anti-tumor treatments. First, inhibition of ACYL through both genetic and pharmacological strategies significantly reduced tumor growth in prostate and lung xenograft models. [68] Such high efficacy may from the dual role of acetyl-CoA generated by ACLY in both ATP generation as they are transported to mitochondria, as well as serve as the building blocks for FA synthesis. The current limitation for ACLY clinical application in cancer treatment comes from the relatively high dose required in order to effectively inhibit ACLY activity. Therefore, current therapeutic options suggest ACLY inhibitors to be used particularly for patients with high glucose consumption rate. In addition, ACLY is also found to regulate oncogenic signaling such as AMPK pathway. In CRPC patients, ACLY inhibition led to increased ER stress and re-sensitized CPRC cells to AR inhibitors. [71] While most ACLY inhibitors are currently used for treatment of diabetes and hypercholesterolaemia, it would be worthwhile to investigate the feasibility of repurposing these drugs for anti-cancer therapies.

3.3 Decrease Fatty Acid Desaturation

As the rate-limiting step for MUFA and subsequent PUFA synthesis, fatty acid desaturation can also be exploited therapeutically to reduce cancer cell lipid source thus preventing tumor growth. FA desaturation is executed through SCDs to synthesize MUFA, which can be further used to synthesize other lipid species including glycerophospholipids. [72] Overexpression of SCDs is frequently observed in breast and colorectal cancer patients and is associated with poor prognosis through increased EMT. [72] Several SCD inhibitors, such as SSI-4, BetA and MF-438, have been proven effective to reduce tumor size in pre-clinical and clinical studies, particularly in combination with dietary lipid restriction. [73, 74] Reduced SCD activity significantly limits the MUFA and PUFA source through biosynthesis, leading to increased ER and mitochondrial stress, thus leading to tumor cell growth inhibition and apoptosis.

Given the presence of the compensatory FA desaturation mechanism through FADSs that generate sapienate directly from palmitate and incorporated into cell membranes, SCD inhibitors only showed therapeutic benefits to specific patient population. [75] This outcome was significantly improved by combinatorial treatment of SCD and FADS2 inhibitors in a pre-clinical model. [75] Therefore, when deciding therapeutic strategy regarding targets in FA synthesis pathways, it is important to take into consideration of a more comprehensive stratification criteria with patient genomic background to better predict the clinical outcomes.

3.4 Ferroptosis in PUFAs-Enriched Cancers

Recently studies also shed light on targeting cancer cell vulnerability based on their lipidome profile including ferroptosis. Fatty acid, especially PUFAs pool largely affects the ferroptosis sensitivity. [76] Long-chain PUFAs such as arachidonic acid (AA) and docosahexaenoic acid (DHA) synthesized and elongated by FADSs and ELOVL have been shown to drastically increase ferroptosis sensitivity through contributing to the total lipid peroxidation pool. [77, 78] Given the upregulation of PUFA synthesis and metabolism in cancer, targeting ferroptosis may create a therapeutic window through utilizing the high lipid level in cancer cell. Indeed, several cancers with low expression of ELOVLs and FADSs and low basal synthetic rate of AA and DHA are shown to be resistant to ferroptosis inducer treatment, which could be reversed by supplying cancer cells with dietary long-chain PUFAs. [79] Functionally, knock down of FADS2 and ELOVL5 decreased cancer cell to RSL3-induced ferroptosis. [79] On the other hand, MUFAs such as oleic acid (OA) are known to protect cells from ferroptosis. [80] Although the mechanism underlying the protective function of MUFAs to ferroptosis is still elusive, it has been shown that uptake of OA reduced the intracellular level of ferroptosis-related phospholipids, such as PC-PUFAs or PE-PUFAs without affecting free PUFAs levels, suggesting that MUFAs may play a competitive role with PUFAs for incorporation into phospholipids thus protecting cells against ferroptosis. [80]

As we discussed, there is an increase of FA uptake through CD36 in malignant tumors, which is preferentially incorporated into phospholipids, DAG, and TAG rather than β-oxidation. [81] Tumors overexpressing CD36 and cPLA2 could promote the release of PUFAs from phospholipids, while CD36 overexpression can also be implied in increased lipid storage and thus protective against ferroptosis. [82] On the other hand, The ACSLs family members have been reported to be closely linked to ferroptosis, while they have distinct roles to affect ferroptosis sensitivity in cancers. ACSL3 mediates MUFA phospholipid incorporation and is needed for MUFA-mediated ferroptosis inhibition, while ACSL4 is one major contributor to lipid peroxidation pool and thus increasing cancer cell sensitivity to ferroptosis. [83] Notable, several studies including us have shown that tumor cells with high ACSL4 levels have a significantly lower IC50 to the treatment with ferroptosis inducers such as RSL3 and IKE. [33, 84]

The major obstacle to the clinical application of ferroptosis inducers, as well as other inhibitors targeting lipid metabolism for anti-cancer treatment is to ensure low toxicity to normal tissues like heart, liver, and kidney, which are also susceptible to ferroptosis and may lead to severe side effects. In conclusion, given the complexity of the fatty acid metabolic networks and feedback regulations, inhibiting single enzyme or pathway may not be sufficient to achieve the maximal therapeutic effects. Targeting cancer lipid metabolism holds great promise not only for novel and low-toxicity therapeutic options through dietary intake, but also for the exploration of the combinatorial strategies that improve the potential of current therapies.

4. ACSL4 as a Critical Effector of RB1 Loss-Driven Cancer Progression

In many cancers, over-activation of oncogenic signaling and inactivation of tumor suppressors promote cancer initiation and development through various mechanisms. One such important mechanism is through altered transcriptional regulation on key factors involved in tumorigenic activities. In hormone-dependent cancers like prostate cancer and breast cancer, dysregulated transcriptional activities such as the well-established AR, RB1, and ERG signaling, are a major driver mechanism. [85] Identification of downstream targets of these altered transcriptional factors (TFs) is crucial while challenging to define the biological processes that directly drive tumorigenesis and progression, as well as discovery of novel therapeutic targets for anti-cancer treatment. Recent studies have discovered many fatty acid metabolism regulators as key downstream target of oncogenic transcriptional regulations that further affecting not only the energy production level but also the remodeling the tissue microenvironment that favors cancer cell proliferation, migration, and invasion.

4.1 RB1 and Cancer Aggressiveness, Metastasis and Lethality

The retinoblastoma transcriptional corepressor 1 (RB1) is one of the most well-known tumor suppressor genes with profound effects on tumor development and progression. RB1 inactivation is frequently observed in a wide range of cancers, including retinoblastoma, sarcoma, and carcinomas of the breast, lung, and prostate. [86, 87] The classical pathway of RB1 activation serves as a key cell cycle regulator in response to anti-proliferation signals such as antimitogens. When dephosphorylated, RB1 can bind E2F family of transcriptional factors (i.e. E2F1, E2F2, E2F3) and prevents their binding to the genome, thus stopping unscheduled entry into mitotic cell cycle. [86] E2Fs regulate the expression of a group of genes that are important in cell proliferation, particularly those driving the progression of G1 phase and into the S-phase during mitotic cell cycle [86]. RB1 inactivation is thus associated with cancer initiation and progression. To drive proliferation, cancer cells counteracts the effects of RB1, through bypassing the phosphorylation of RB and activation of CDK-cyclin complexes by growth factors or hormones, or silencing RB1 expression through genetic alterations like mutations or deletions. [86] As a result of RB1 deactivation, cancer cells are granted dysregulated growth rate without inhibitory signals, and refractory to therapeutic agents against upstream mitogenic and hormonal pathways.

Moreover, RB/E2F has recently been recognized to play broader roles beyond its classical function in regulating cell cycle progression specifically through S-phase entry. There has been increasing evidence suggesting that RB inactivation is associated with lineage plasticity, tumor metastasis and therapy resistance that further drives cancer aggressiveness and lethality. [88, 89] Consistent findings are observed in clinical investigation of genetic status of RB1 and validated by the results obtained in genetically engineered mouse models. RB1 loss was identified as the single contributor to the progression of many advanced cancer types following tumorigenesis initiated by other genetic events such TP53 inactivation or PTEN loss, dictating poor survival of cancer patients. [88-90]

Consistently, observation from our genetically engineered mouse models to study the function of different tumor suppressor genes confirmed the indispensable role of RB1 in the advancement of the aggressiveness in prostate cancer development. Mice with PTEN deletion, a tumor suppressor with a well-established function in prostate tumorigenesis, developed spontaneous and indolent primary prostate tumors without distal metastasis (Figure 1A, B). However, prostate-specific double knockout of PTEN and RB1 led to a severe phenotype of prostate cancer, as indicated by a shortened tumor onset time, high frequency of multiple organ metastasis and a drastically reduced overall survival (Figure 1A, B). Collectively, these findings from our preliminary data and previous studies highlight the need for the identification of downstream effectors of RB1, not only to dissect the specific function of RB1 loss during cancer progression, but also to tailor novel therapeutic strategies targeting RB1 deficiency-driven mechanisms to reduce prostate cancer mortality.

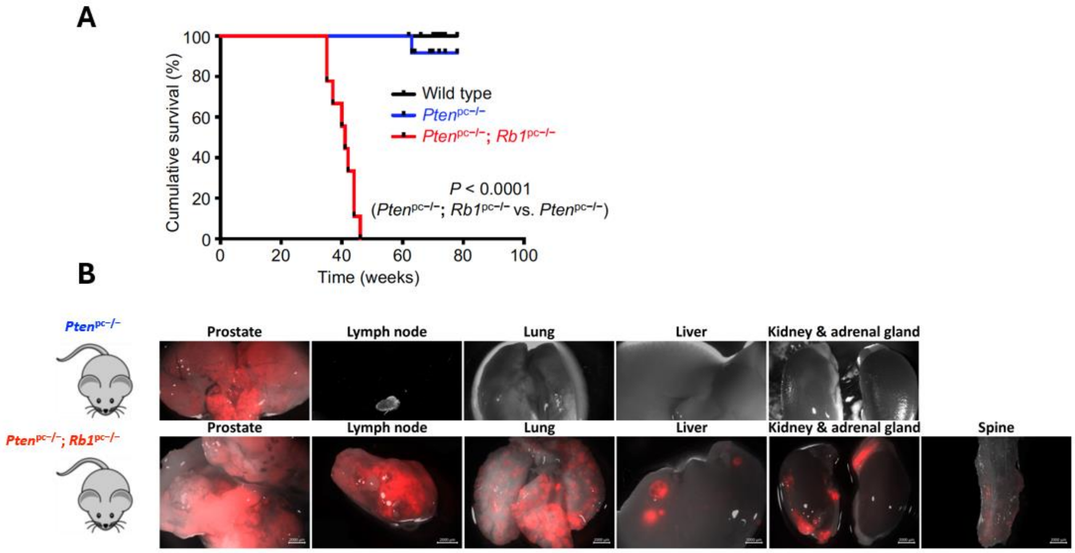

Figure 1. Rb1 loss drives lineage plasticity, metastasis, and lethality of PCa. 1A. Cumulative survival of wild type, prostate-specific PTEN deletion and prostate-specific PTEN and RB1 double deletion. 1B. Fluorescent imaging showing the spontaneous primary tumor and metastasis into distal organs in PTEN KO and PTEN/RB1 double KO mice. Tumor cells with PTEN or PTEN/RB1 deletion showed fluorescence from RFP expression driven by Probasin-Cre. P-value indicated in figure.

4.2 Identification of ACSL4 as a Downstream Target of RB1/E2F Signaling

In a previous study, we explored the RB1/E2F regulation on transcriptional activities throughout the genome to fully elucidate the role of RB1 in cancer development and discover novel therapeutic target downstream RB1 inactivation. We examined E2F1 ChIP-Seq databases generated from prostate cancer cell lines associated with ferroptosis sensitivity. Interestingly, we identified a pro-ferroptotic gene, ACSL4, with 3 distinct E2F1-binding regions on its promoter in all the ChIP-Seq data sets, which expression is thereby regulated. [33] Consistently, we showed that PC3 cells with RB shRNA knockdown had a significantly increased E2F1 binding to the ACSL4 promoter, with an upregulation of ACSL4 and E2F-targed mRNA expression, whereas RB1 overexpression resulted in downregulated levels of ACSL4 and E2F-target genes. [33] Clinically, we found that patients with RB inactivation and deletion express a significantly higher ACSL4 level. [33] These findings collectively support the hypothesis that ACSL4 is a downstream target of the RB/E2F pathway.

Notably, ACSL4 is a key enzyme promoting ferroptosis through facilitating lipid peroxidation of polyunsaturated fatty acids. [91] Ferroptotic cell death is a promising target in cancer treatment proven by previous studies done by us and other groups. [92] However, the role of ACSL4 during cancer initiation and development has been underestimated, particularly given the fact that ACSL4 is upregulated upon RB1 loss and associated with advanced status of multiple cancer types. Therefore, investigating the oncogenic role of ACSL4 and underlying mechanism is key to the understanding of biological processes due to the upregulation of ACSL4, as well as the discovery of novel therapeutic target for anti-cancer treatment.

4.3 Overview of ACSL4

The first step of fatty acids utilization by cells is the activation by acyl-CoA synthases (ACS) that catalyzes the conversion of free fatty acids (FAs) to FA-CoAs. Based on the length of the carbon chain of the substrates, the ACS family members are classified into very long-chain acyl-CoA synthase, long-chain acyl-CoA synthase (ACSL), medium-chain acyl-CoA synthase (ACSM), and short-chain acyl-CoA synthase. Long-chain acyl-coenzyme A (CoA) synthase 4 (ACSL4) is an enzyme that functions to incorporate Coenzyme A (CoA) into specific long-chain fatty acid substrates, such as arachidonic acid and palmitic acid. Such acylation reactions provide a substrate for the β-oxidation and phospholipid synthesis. Intracellularly, ACSL4 protein is mainly found in the inside of the plasma membrane, with sporadic expression in the endoplasmic reticulum (ER) and lipid droplets. [93] ACSL4 is broadly expressed in multiple organs such as adrenal gland, epididymis, brain, lung, ovary, placenta, liver, and testis and its expression is found to be specifically high in steroidogenic cells. ACSL4 plays a key role in modulating fatty acid metabolism landscape by providing an active form of substrate for reactions and deciding phospholipids composition to regulate cellular activities.

4.3.1 Structure of ACSL4

The ACSL4 gene is located on the X chromosome, specifically Xq22. 3-q23. The ACSL4 gene contains 17 exons, and it encodes a 74.4 kDa protein, named after FACL4, composed of 670 amino acids assembling 17 peptides. The structure of ACSL4 has been identified through crystallographic techniques, which can be generally divided into four subunits based on their geographical location and distinct function: the N-terminal membrane-bound domain, the transmembrane structural domain, the adenylate-bound domain, and the C-terminal catalytic domain. [94] The N-terminal region located at the anterior side of ACSL4 contains two unstable subregions (N1 and N2) segmented by several leucine amino acids. While the function of this subunit is not completely understood, it has been proposed that the N-terminal region facilitates the acylation reaction of substrate, including recognition and binding of fatty acids to CoA. In addition, the N-terminal region could also anchor protein localization since it contains a fatty-acid-binding pocket for long-chain fatty acids. [95] The adenylate-bound domain has two subunits that recognize adenosine triphosphate (ATP) and CoA molecules, respectively, and links them together for acylation reaction. Importantly, the C-terminal structural domain catalyzes the acylation reaction and forms the ACSL4 catalytic active center consisted of an acylase kinetic triad (Lysine (Lys)-Aspartate (Asp)-Cysteine (Cys)), where Lys and Asp drive protonation and deprotonation to catalyze the acylation reaction after fatty-acid binding to CoA. [95] In addition to the major domains, the ACSL4 protein structure also contains post-translational modification sites, such as for phosphorylation, glycosylation, and ubiquitination etc.. [96]

There are five sub-families of ACS that have been characterized, ACSL1, ACSL3, ACSL4, ACSL5 and ACSL6. The structure of ACSL4 protein shares high similarity to other ACSLs, making it difficult to specifically target ACSL4 for the development of pharmacological inhibitors. The catalytic active center of all ACSLs contains a conserved acylase kinetic triad, and ACSLs members shares highly conserved amino acid sequences except for the N-terminal regions, allowing for different substrate fatty acids binding specificity. [93]

4.3.2 ACSL4 and Long-Chain Fatty Acid Activation

ACSL4 plays an important role by producing a source of energy and building blocks for intracellular fatty-acid metabolism through catalyzing fatty acid activation. Fatty acids need to be activated before they can be further utilized for β-oxidation. Fatty acid activation occurs when free fatty acids enter the cytosol or are synthesized, where they react with coenzyme A (CoA) and are transformed into fatty acyl-CoA molecules in an ATP dependent manner. Briefly, long-chain fatty acids like arachidonic acid (AA) and eicosapentaenoic acid (EPA) undergo a two-step process of being activated by ACSLs. First, adenine monophosphate from ATP is transferred onto the fatty acid, releasing pyrophosphate and forming acyl-AMP. The pyrophosphate then gets hydrolyzed by pyrophosphatase into two orthophosphates. Next, the acyl-AMP reacts with CoA molecule to form acyl-CoA and AMP is released. After the fatty acid is activated, it will be transported into the matrix of the mitochondria by reacting with carnitine to form acyl carnitine that moves across the inner mitochondrial membrane through translocase. Once inside the mitochondrial matrix, the acyl-carnitine can be transformed back into acyl-CoA and the carnitine will be shuttled back into the cytoplasm by the translocase transporter.

Given the distinct structure of N-terminal domain for substrate binding between ACSLs family members, it is important to compare the specificity of ACSL4 activity to consume and activate different fatty acids to explore the unique role of ACSL4 in physiological and pathological contexts. Through isotopic and spectrophotometric measurement of recombinant ACSL4 consumption on various substrates of long-chain fatty acids, a previous study has identified the group of long-chain fatty acids preferentially targeted by ACSL4 as substrates. It was reported that ACSL4 preferentially utilizes arachidonate and eicosapentaenoate, with a higher affinity with most C8–C22 saturated fatty acids and C14–C22 unsaturated fatty acids. [24] Compared with other ACSLs family members, ACSL4 preferentially selects arachidonic acid (AA) as substrate. Other polyunsaturated fatty acids (PUFAs), such as adrenic acid (AdA), eicosapentaenoic acid (EPA), epoxyeicosatrienoic acids (EETs), and hydroxyeicosatetraenoic acids (HETEs), docosahexaenoic acid (DHA), are also substrates of ACSL4. Saturated fatty acids (SAs) such as palmitic acid can also be catalyzed by ACSL4, while the affinity is relatively lower compared to other ACSLs. [25]

4.4 ACSL4 as a Regulator of Fatty Acid Metabolism

With the classical role as an ACSL family member that esterifies long-chain FAs to fatty acyl-CoA, and a particular selectivity for PUFAs such as arachidonic acid (AA), ACSL4 not only serves as a major regulator of *de novo* lipogenesis and energy production through fatty acid β-oxidation, but also plays a significant role in modulating lipid peroxidation and phospholipid component.

Upon activation, FA-CoA is transported to mitochondria by CPT1, where they undergo β-oxidation and are transformed into Acetyl-CoA. On one hand, Acetyl-CoA participates in the tricarboxylic acid (TCA) cycle which generates ATP and provides energy source for cellular activities. On the other hand, citrate produced through TCA cycle can be used to synthesize acetyl-CoA, which will be further used for *de novo* FA synthesis through FASN and SCD. [97] To this end, ACSL4 plays an important role for this process by providing the building blocks, FA-CoA, to accelerate energy production and recycling through *de novo* lipogenesis.

ACSL4 is also largely involved in PUFAs incorporation into phospholipids (PLs). PLs are major components of intracellular and cell membranes and are important for maintaining normal cell activity. Phosphatidylcholine (PC), Phosphatidylethanolamine (PE), phosphatidylinositol (PI), and phosphatidylserines (PS) are major classes of PLs categorized from the structure of their head groups. A classical PL structure consists of a glycerol/sphingosine backbone, two fatty acyl tails, and a phosphate group. The activation of FAs and conversion to FA-CoA by ACSL4 is the first step of the incorporation of FAs into PLs, and perturbation of ACSL4 level significantly modulates the component of PLs by altering the proportion of PLs containing FAs catalyzed by ACSL4 such as AA-PLs, which are further incorporated into cellular membranes, or undergo lipid metabolism leading to dysregulated cell functions. [98] For example, adipocyte-specific ACSL4 knockout mice showed reduced incorporation of AA into all PLs species, but not other lipid species when fed with high-fat diet. AA-PLs were shown to increase cell sensitivity to apoptosis, and such modulation of PLs species could potentially contribute to dysregulated cell death and tumorigenesis. [99]

In addition, ACSL4 plays a role in regulation of eicosanoid biosynthesis and steroidogenesis. Intracellular AAs are a source of prostaglandins such as PGE2 and thromboxanes oxidized by cyclooxygenases (COXs), and ACSL4 contributes to this production of eicosanoids. [100] Moreover, ACSL4 could also regulate steroidogenesis through steroidogenic acute regulatory protein (StAR). During steroidogenesis, cholesterol is converted into various steroid hormones, which is a key biological process involved in many hormonal-dependent tumorigenesis such as breast cancer and prostate cancer. StAR plays an important role by transferring cholesterol to the inner mitochondrial membrane, which is then converted into pregnenolone, and the transcriptional activity of StAR was shown to be upregulated by cAMP-dependent addition of AA to multiple eicosanoid species such as EET, 5-HETE, and 5-hydroperoxyeicosatetraenoic acid. [101]

4.5 ACSL4 and Fatty Acid Metabolism in Cancer

4.5.1 ACSL4 Pan Cancer

In previous chapters, we discussed that altered cancer cell lipid metabolic network is a hallmark of cancer, as aberrant lipid level supports the energy needs to drive uncontrolled cancer cell proliferation. Given the role of ACSL4 in fatty acid activation as the first step of all downstream lipid utilization processes, it is not surprising that ACSL4 may be a key regulator during cancer development. Interestingly, according to previous epidemiological data, ACSL4 showed distinct regulations among different cancer types. For example, ACSL4 level is found to be high in colon and liver tumor specimens compared to normal tissue. [102] On the other hand, ACSL4 is downregulated in ovarian cancer and lung cancer. [103, 104] This might be due to the bidirectional effect of ACSL4 in promoting cell proliferation, while sensitizing cells to ferroptosis through accumulation of lipid peroxides, which will be further discussed in this chapter. Notably, the suppression impact of high ACSL4 on tumor growth in certain cancer types was only induced with the presence of other ferroptosis inducers such as high fat diet. [104] Moreover, one recent study revealed that ACSL4 may play different roles during cancer progression, as ACSL4 level was found to be upregulated in late stages of breast cancer and prostate cancer, with an aggressive phenotype resistant to hormonal therapies. [27, 28] However, the mechanism of action underlying the complex regulation of ACSL4 on multiple cellular activities remains inconclusive.

Among ACSL family members, ACSL3 and ACSL4 share the highest structural and functional similarities, with consensus regulation on lipid synthesis and ferroptosis sensitivity. It has been reported that the expression of ACSL3 and ACSL4 was both increased in liver cancer, while their expression patterns were distinct in different subtypes. [105] Therefore, to study the functions of ACSL4 in cancer, it would be valuable to elucidate the role of ACSL3 as they may have complementary effects in regulating cellular activities.

4.5.2 ACSL4 and Prostate Cancer Aggressiveness

In prostate cancer, the expression of ACSL4 is particularly found to be upregulated in advanced stages of PCa which seems to increase over the progression of prostate cancer. Prostate cancer is the most prevalent cancer in men and has the second leading cause of cancer-related deaths in the US. [106] As the standard of care, the majority of patients diagnosed with prostate cancer undergo androgen deprivation therapy (ADT) to diminish androgen receptor (AR) signaling through either surgical removal of prostate gland or pharmacologically administration of AR inhibitors [107]. However, over the course of disease recurrence, many patients will develop resistance to ADT and are diagnosed with castration-resistant prostate cancer (CRPC). It was reported that more than 30 percent of the patients undergoing ADT would eventually develop AR-independent CRPC tumors. According to the recent statistics, the number of patients developed with AR-independent prostate tumor has increased by three time since the wide application of the second generation of anti-androgen treatments such as enzalutamide and abiraterone. [108] On top of that, there is an increasing number of patients develop that a subtype of aggressive prostate cancer feature by small neuroendocrine features, neuroendocrine prostate cancer (NEPC). CRPC and NEPC are characterized by resistance to anti-androgen therapies and poor prognosis.

PCa progression is often accompanied by increased fatty acid biosynthesis and lipid metabolism, suggesting the critical role of altered ACSL4 activity in the promotion of a malignant phenotype. [109] Interestingly, a previous study revealed the co-expression of ACSL4 and hormone-independent markers in breast cancer and prostate cancer, indicating hormonal therapy resistance in ACSL4-high tumors. [110] Consistently, ACSL4 expression was found to increase in CRPC patients compared to early-stage hormone-sensitive PCa patients. [28] There is also evidence showing that ACSL4 is involved in the advancement of tumor aggressiveness in PCa through increasing steroidogenesis that supports hormonal-dependent tumor growth. [111] However, the comprehensive understanding of the participation of ACSL4 in PCa and during aggressive PCa development remains largely unsolved, taking into consideration its regulation on cell proliferation and drug resistance through altered energy production, lipid profiles and impacts on transcriptional landscape in cancer cells, which hinders the emphasis of direct targeting ACSL4 as an effective therapeutic option in advanced PCa.

4.5.3 Transcriptional Regulation of ACSL4 in Cancer

Multiple regulatory mechanisms have been reported to regulate expression of ACSL4. First, the expression of ACSL4 can be transcriptionally regulated by several transcription factors (TFs). Meta-analysis of ChIP-seq databases and predicted binding sequences revealed multiple binding sites for some TFs at the promoter region of ACSL4. For example, specificity protein 1 (Sp1) and cyclic adenosine monophosphate (cAMP) response element-binding (CREB) are both found to be able to bind to ACSL4 promoter and induce its transcription according to their predicted binding sequence. [112] In addition, it has been reported that the transcriptional enhanced associate domain 4 (TEAD4) also binds to ACSL4 promoter and upregulate its expression moderated by its coactivator Yes-associated protein (YAP). [113] Similar to what we found, another study identified a 43-base pair-sequence on ACSL4 promoter region that functional drives upregulation, and retinoid-related orphan receptor alpha (RORα), Sp1 and E2F elements are found to participate in the regulation of promoter activity. [114]

In addition to the TFs, several enzymes and molecules involved in fatty acid metabolism have also been shown to regulate ACSL4 level. For instance, peroxisome proliferator-activated receptor delta (PPARδ), while activated by its specific ligands, could induce the transcriptional and protein levels of ACSL4. [115] In addition, ACSL4 expression was found to be downregulated following the activation of Src and integrin α6β4, which increase the resistance of ferroptosis triggered by intrinsic signals. [116] Interestingly, the ACSL4 specific substrate arachidonic acid (AA) was shown to downregulate ACSL4 through uptake by promoting the protein ubiquitination and degradation, suggesting and reciprocal feedback regulation between ACSL4 and its target long-chain fatty acids. [117] Collectively, the regulation of ACSL4, particularly in the context of cancer, is driven by the comprehensive effects combining genetic and microenvironment factors.

5. ACSL4 Promotes Prostate Tumorigenesis through Enhanced Fatty Acid Oxidation

In this chapter, we highlight our functional studies to explore the role of ACSL4 during tumorigenesis, particularly in prostate cancer. Given the function of ACSL4 in fatty acid activation and ATP production which implies its oncogenic role, we aim to perform our investigation through gain-of-function and loss-of-function studies followed by characterization of tumor proliferation and apoptosis phenotypes. Such studies will not only establish biological foundation for the previous findings on the upregulation of ACSL4 in some cancer patients in populational studies, but also provide proof-of-concept evidence for the feasibility to target ACSL4 as a potent anti-cancer treatment option. For this part, we will further discuss the therapeutic strategies in chapter 7. In addition, in vivo tumorigenesis may show a more complex response to ACSL4 level provided with the impact from dietary uptake of fatty acids. Therefore, we sought to validate our data from *in vitro* assays through an *in vivo* xenograft model.

5.1 Introduction and Rationale

In the previous chapter, we discussed that ACSL4 is a key downstream effector of RB1/E2F signaling, and the expression was upregulated when RB1 is inactivated in prostate cancer (PCa) cells. As a result, the fatty acid (FA) activation efficiency is largely increased, indicating a higher conversion rate from free long-chain FAs into fatty acyl-CoAs. This upregulation of cell FA-CoA level may grant PCa cells growth advantages *in vitro* and *in vivo* through multiple potential mechanisms. First of all, fatty acyl-CoAs can be transferred into mitochondrial matrix through a carnitine-dependent translocase activity and further converted into acetyl-CoA, which subsequently serves as a fundamental fuel ATP production by undergoing β-oxidation and tricarboxylic acid (TCA) cycle. Therefore, one main downstream effect upon altered ACSL4 level will be the change of the cancer cell ATP generation rate. This change in intracellular ATP production is directly reflected in PCa cell growth by providing abundant energy resource for division, as well as the PCa cell ability to resist apoptosis due to nutrient deprivation. In addition, increased acyl-CoAs generated through ACSL4 could reshape PCa cell lipidomic landscape modulated by incorporation of preferentially selected lipid species by ACSL4. On one hand, phospholipids serve as the building blocks for cellular membranes that could potentially affect various cell activities and stress response. [118] On the other hand, several lipid species such as eicosanoids and sphingolipids also have essential functions as signaling molecules to modulate cell transcriptome and epigenome. [119] A comprehensive effect of ACSL4 in cancer cells is summarized in Figure 2. Indeed, ectopic ACSL4 level is observed in multiple cancer types. [102] In prostate cancer, ACSL4 is particularly overexpressed in advanced PCa including CRPC and NEPC. [28] However, the biological consequence caused by such ACSL4 overexpression and the underlying mechanism still remain elusive.

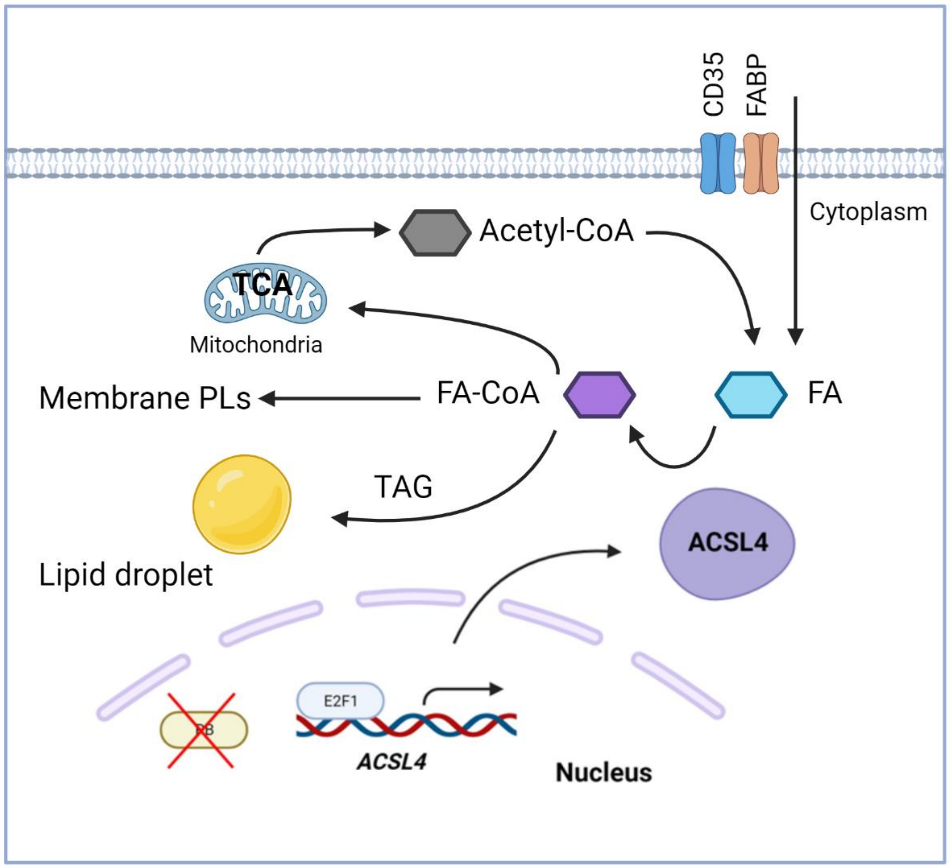

Figure 2. ACSL4 is a downstream target of RB1/E2F signaling with an essential role fatty acid metabolism. E2F1 directly binds to the promoter region of ACSL4 and activates ACSL4 transcription. ACSL4 is mainly located in ER and Golgi apparatus and functions by activating specific free long-chain fatty acids and converting them into Acyl-CoA. The major metabolic destinies of Acyl-CoA include contribution to ATP generation through β-oxidation in mitochondria, incorporation into phospholipids, and formation of lipid droplet for lipid storage.

To determine the role of ACSL4 as a lipid metabolic regulator in PCa, we sought to perform gain-of-function studies in ACSL4-low PCa cells and loss-of-function studies in ACSL4-high PCa cells. These functional analyses will be valuable to fully elucidate the biological function and to determine the regulatory effect of ACSL4 in PCa. We expect that ACSL4 overexpression will lead to upregulated ATP generation by PCa cells, and subsequently promote PCa cell growth. Given the complexity of in vivo conditions such as dietary FA uptake and energy deprivation in tumor microenvironment, particularly in the context of cancer FA metabolism, an *in vivo* xenograft model will be valuable to validate our findings from *in vitro* observations. Upon establishment of the *in vitro* models, overexpression and knockout/knockdown of ACSL4 were validated through western blot. In this chapter, we will describe our investigation to study the effects of ACSL4 in PCa through functional analyses of cell growth by crystal violet assay, ATP generation assay and xenograft mouse model analyses.

5.2 Materials and Methods

5.2.1 Cell Lines and Cell Culture, Transfection, Lentiviral Transduction, and Stable Cell Line Establishment

PC-3, C4-2, 22Rv1, DU145 and HEK293T were purchased from ATCC. All cell lines were checked for mycoplasma infection using the MycoAlert Mycoplasma Detection Kit (Lonza). Human prostate cancer cells PC3, C4-2, 22Rv1, and DU145 were cultured in RPMI medium. HEK293T cells were cultured in DMEM medium. Complete growth media were supplied with 10% fetal bovine serum, 2 mM glutamine and 100 U/mL of penicillin-streptomycin (Thermo Fisher). All cells were maintained at 37°C with

5% CO_2. To establish ACSL4 overexpressed LNCaP and 22Rv1, and ACSL4 knockout PC3 and DU145 cell lines, HEK293T cells were used for virus packing. Briefly, pLenti-PCMV6 empty vector or pLenti-PCMV6-ACSL4 constructs for overexpression, pLentiCRSPR v2-sgCtrl and pLentiCRSPR v2-sgACSL4 for knockout, psPAX2, pMD2.G plasmids, and PEI (DNA:PEI = 1:4) were mixed in Opti-MEM (Thermo Fisher) for 15 min and transfected into HEK293T cells. At 48 and 72 hours after transfection, the virus-containing medium was collected and filtered with a 0.45 μm filter. The virus-containing suspension was mixed with fresh culture medium at 1:1 ratio and supplemented with 4 μg/ml of polybrene (Santa Cruz), and then applied to the cells. 48 hours after virus infection, cells were selected using puromycin for 48 hours. For CRISPR knockout cell lines, single-cell clones were isolated and validated using Western blotting.

5.2.2 Plasmids, SgRNA Design and Construction

pLenti-PCMV6 and LentiCRISPR v2 were purchased from Addgene. The sgRNAs targeting ACSL4 were designed using Broad Institute GPP sgRNA Designer (https://portals.broadinstitute.org/gpp/public/). The sgRNA oligo pairs containing BsmBI compatible ends (Supplemental Table 1) were synthesized from IDT and annealed. Golden gate assembly with the BsmBI enzyme was used to clone the annealed oligos into LentiCRISPR v2 vectors. Human ACSL4 full-length cDNA was cloned into pLenti-PCMV6 vector to generate its overexpression plasmid. Ampicillin and puromycin were purchased from Sigma-Aldrich. Crystal violet was purchased from Sigma-Aldrich. Polyethylenimine (PEI) was purchased from Polysciences. RPMI, DMEM, Opti-MEM–reduced serum media, and FBS were from Thermo Fisher Scientific. The antibodies for

Western blotting are listed below: anti-GAPDH (D16H11) was purchased from Cell Signaling Technology; anti-ACSL4 (A305-358A) was purchased from Bethyl Laboratories. Anti-AR (N-20) antibody was purchased from Santa Cruz Biotechnology. Anti-PSA (K92110R) antibody was purchased from Meridian Bioscience.

5.2.3 Western Blotting, Cell Proliferation Assay, and ATP Generation Assay

Western blotting was performed to validate the successful overexpression and knockout of ACSL4 in desired cell lines. Briefly, cells were lysed in RIPA buffer (Boston BioProducts) supplemented with Complete Protease Inhibitor Cocktail and Phosphatase Inhibitor Cocktail 2 (Sigma-Aldrich). The protein content of each sample was quantified using the BCA protein assay kit (Thermo Fisher Scientific). Cell lysates were diluted, mixed with 6× Laemmli buffer (Boston BioProducts), and boiled at 95°C for 5 minutes. Denatured proteins were separated on NuPAGE 4%–12% Bis-Tris gels with MOPS buffer SDS running buffer (Thermo Fisher Scientific) and then transferred onto nitrocellulose membranes (GE Healthcare) using the standard wet transfer method. Membranes were blocked with 5% milk at room temperature for 1 hour and then incubated with specific antibodies at 4°C overnight. The HRP-conjugated secondary antibodies and ECL substrate (GE Healthcare) were applied to visualize the bands of specific proteins.

Crystal violet assay was performed to analyze cell proliferation rate. Briefly, 1.0×10^4 cells/well for 22Rv1 and LNCaP, 8×10^3 cells/well for PC3 and 6×10^3 cells/well for DU145 were plated in 12-well plates (Falcon). Cells were harvested on day 0, 2, 4, 6. At each time point, culture medium was removed, and 10% Formalin was added directly to the cells for fixation at room temperature for 30 minutes. The cells were then stained with 0.1% crystal violet solution (Sigma-Aldrich) at room temperature. 1ml 10% acetic acid was used to solubilize the dye. The luminance signal was measured using Spectral 100ul of solution was used to detect O.D. at 595nm wavelength.

For ATP generation assay, ENLITEN® ATP Assay System Bioluminescence Detection Kit (Promega) was used according to the manufacturer's guide. For normalization, total cell protein was measured by Bicinchoninic acid (BCA) Protein Assay Kit (ThermoFisher Scientific) according to the manufacturer's guide, and ATP levels detected were normalized accordingly.

5.2.4 Animal Studies and Immunohistochemistry (IHC)

1×10^6 Ctrl or ACSL4 OE 22Rv1 cells were mixed with 100 μL Matrigel (Corning) and implanted subcutaneously into the right flanks of 6- to 8-week-old male nude mice (Foxn1nu, The Jackson Laboratory). The tumor volume was measured every other day using calipers and calculated as $L\times W^2\times0.52$, where L (length) stands for the largest tumor diameter and W (width) stands for the diameter perpendicular to the length.

Mouse tissues were dissected and fixed in 4% paraformaldehyde for histology and IHC analysis. For staining, the tissues were embedded in paraffin according to standard procedures. 5 μm sections were cut and processed for histology or immunostaining. The following primary antibodies were used: Ki67 (Thermo Fisher Scientific, SP6, 1:100), Cleaved Caspase 3 (Cell Signaling Technology, 9661, 1:100). The stained slides were visualized by a bright-field microscope.

5.2.5 Statistical Analysis

No statistical analysis was applied to determine sample size. The studies involving mice were randomized. The investigators were not blinded to allocation during experiments and outcome assessment. Statistical analyses were performed using GraphPad Prism software. For comparison of two experimental groups, an unpaired 2-tailed Student's *t* test was used. For comparison of more than two groups, 1-way or 2-way ANOVA with Tukey's multiple-comparison test was used. When data from multiple groups were not normally distributed, a Kruskal-Wallis test followed by Dunn's multiple-comparison test was used. For analysis of categorical data, 2×2 contingency tables were constructed, and data sets were compared using Fisher's exact test. Image J IHC Toolbox was used to quantify the percentage of positive stained cells for IHC. P-values of less than 0.05 were considered to be statistically significant.

5.3 Results

5.3.1 Generation of ACSL4 Overexpression and Knockout Cell Lines

To assess the effect of ACSL4 overexpression (OE) and knockout (KO) on prostate cancer cell proliferation, we evaluated cell growth through gain-of-function and loss-of-function experiments. ACSL4 expression was first determined in parental human prostate cell lines, which was found to be high in PC3 and DU145, intermediate in 22Rv1 and low in C4-2 and LNCaP (Figure 3A). We selected ACSL4-high expression cell lines PC3 and DU145 for loss-of-function studies, and ACSL4-low expression cell lines 22Rv1 and LNCaP for gain-of-function studies. ACSL4 overexpression in LNCaP and 22Rv1, and knockout in PC3 and DU145 were validated through western blotting (Figure 3B, C).

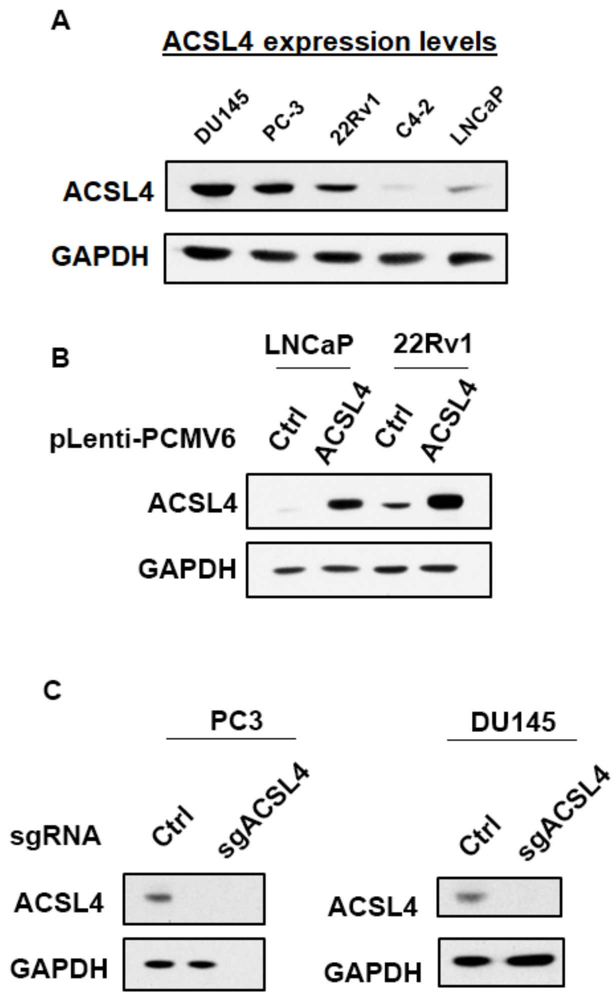

Figure 3. Western blotting shows the ACSL4 protein levels in parental human prostate cell lines and ACSL4 OE and KO cell lines. 1A. ACSL4 levels in parental PCa cell lines. 1B. Confirmation of ACSL4 OE in LNCaP and 22Rv1 cells. 1C. Confirmation of ACSL4 KO in PC3 and DU145 cells.

5.3.2 Effects of ACSL4 Overexpression and Knockout on Prostatβe Cancer Cell Proliferation and ATP Generation

We first sought to examine the cell proliferation rate upon ACSL4 overexpression (OE) and knockout (KO). We expect that ACSL4 overexpression will provide prostate cancer cells with more metabolic active Acyl-CoA, thus accelerating the generation of mitochondrial Acetyl-CoA through β-oxidation, leading to higher ATP production level that meets the needs for a more rapid proliferation rate in cancer cells. Indeed, we found that the proliferation rate of both LNCaP and 22Rv1 was significantly increased upon ACSL4 OE, with a more drastic change in LNCaP-ACSL4 (Figure 4A). This could be explained by the different dependency levels of LNCaP and 22Rv1, as representatives for early-stage and advanced-stage PCa, respectively, on additional energy source to act against tumor energy deprivation environment. [120, 121] Moreover, 22Rv1 has a moderate basal level of ACSL4 (Figure 3A), so there could also be less additional ATP generation from excessive ACSL4 level given limited intracellular free FAs. Consistent with this finding, ACSL4 KO led to a significant growth suppression in PC3 and DU145, with the proliferation of PC3-ACSL4 KO being almost completely inhibited (Figure 4B). This result suggested that ACSL4 is dispensable for maintaining the rapid proliferation of prostate cancer cells.

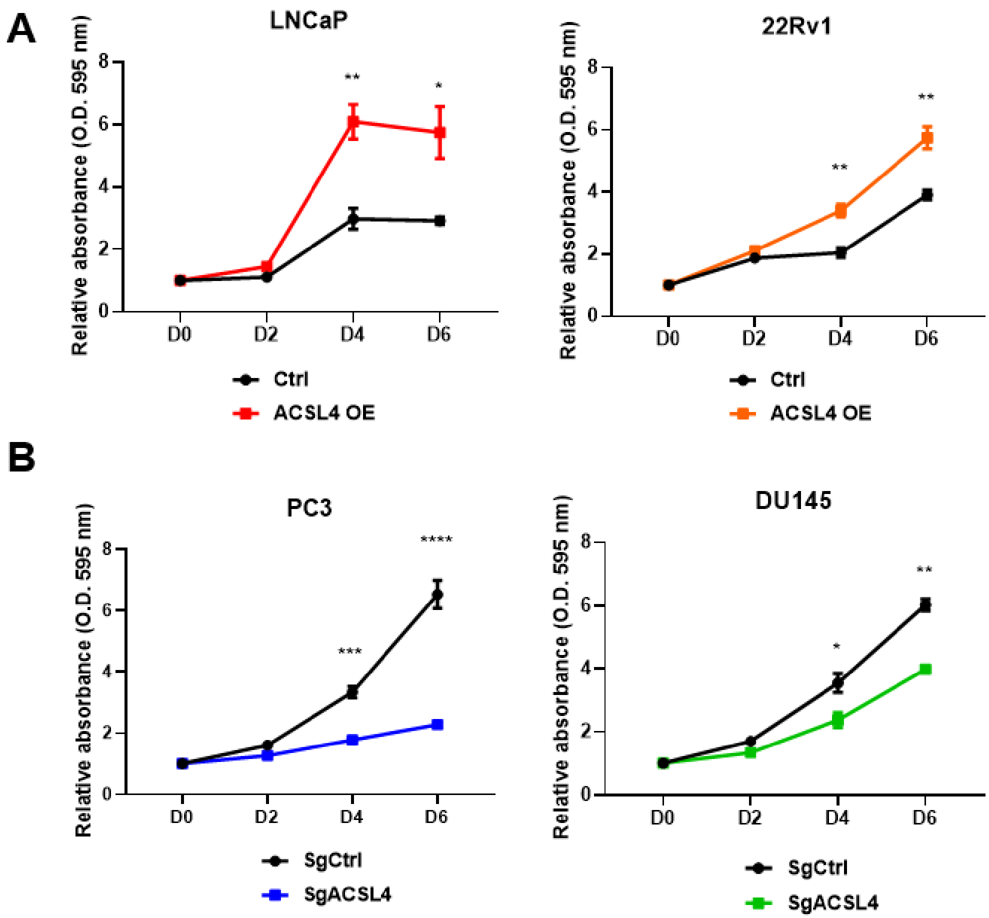

Figure 4. ACSL4 promotes the proliferation of prostate cancer cells. 4A. 6-day proliferation of control and ACSL4 OE LNCaP and 22Rv1 cells detected by crystal violet assay. 4B. 6-day proliferation of control and ACSL4 KO DU145 and PC3 cells detected by crystal violet assay. One-way ANOVA followed by unpaired t-test was used to determine statistical significance. *P < 0.05, **P < 0.01, ***P < 0.001, ****P < 0.0001. All data are shown as the mean ± SD from n = 3 biological replicates.

To further establish the association between the proliferation rate with ATP level upon ACSL4 OE and KO, we measured the total cellular ATP level in these cells. Despite the observation that cancer cells tend to obtain energy through anaerobic glycolysis rather than oxidative phosphorylation (the Warburg effect), high level of mitochondrial ATP synthesis is linked to increased tumor growth, metastasis, and poor prognosis. [122, 123] Consistent with these findings, we found that the total ATP level was significantly higher in ACSL4 OE cells compared to the control cells, which is more evident in LNCaP, and ACSL4 KO cells had significantly lower ATP level (Figure 5). These results suggested that ACSL4 promotes cancer cell proliferation through increased ATP generation, and that inhibition of ACSL4 activity may serve as a novel target for cancer therapy.

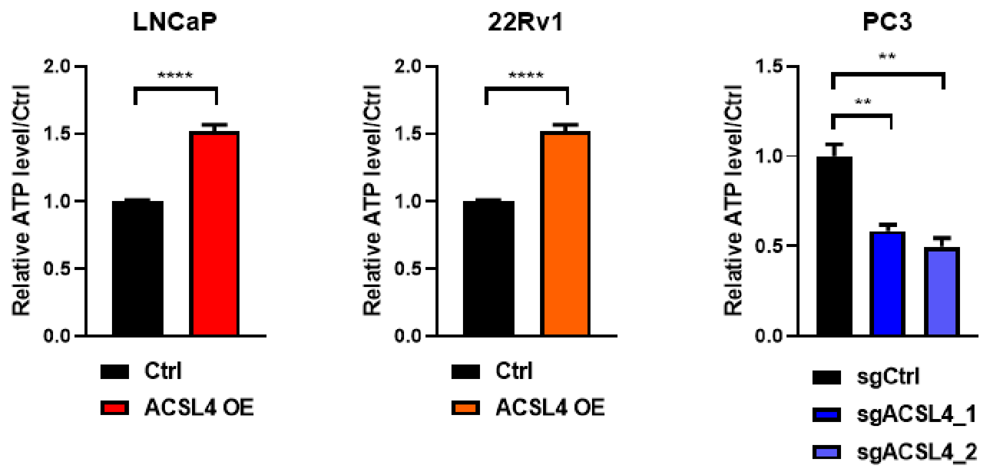

Figure 5. ACSL4 regulates energy production in prostate cancer cells. Total cellular ATP level in ACSL4 OE (LNCaP and 22Rv1) and ACSL4 KO (PC3) cells was measured by ENLIGHTEN ATP Assay Kit. Unpaired t-test was used to determine statistical significance. $*P < 0.05$, $**P < 0.01$, $****P < 0.0001$. All data are shown as the mean ± SD from n = 3 biological replicates.

5.3.3 ACSL4 Overexpression Promoted Tumor Growth *In Vivo*

To test if ACSL4 also drives tumor growth *in vivo*, we implanted 22Rv1-ACSL4 OE together with the control cells subcutaneously and examined the xenograft tumor growth. Notably, 22Rv1 cells developed xenograft tumors that grew rapidly within 30 days post-implantation, and ACSL4-overexpressing 22Rv1 cells demonstrated a significantly higher growth rate *in vivo*, as indicated by both tumor volume and tumor weight (Figure 6A, B, C). Mice body weight was not significantly impaired, and no metastasis was observed during the course of the study (Figure 6D). Histopathological analyses of the end-stage xenografts found that both 22Rv1-Ctrl and 22Rv1-ACSL4 OE primary prostate tumors demonstrated a typical adenocarcinoma morphology, with well-differentiated glandular structure (Figure 7A). Immunohistochemical staining showed that 22Rv1-ACSL4 OE tumors had a significantly higher expression of the proliferation marker of mitotic cells, Ki67 (Figure 7A, B). In addition, sporadic expression of cleaved Caspase 3 was found in 22Rv1-Ctrl tumors, indicating ongoing apoptosis inside the tumor, while we found no cleaved Caspase 3-positive cells in 22Rv1-ACSL4 OE tumors (Figure 7A, C). Collectively, these results confirm our findings *in vitro* and suggest that ACSL4 drives a highly proliferative phenotype of prostate tumor growth *in vivo*.

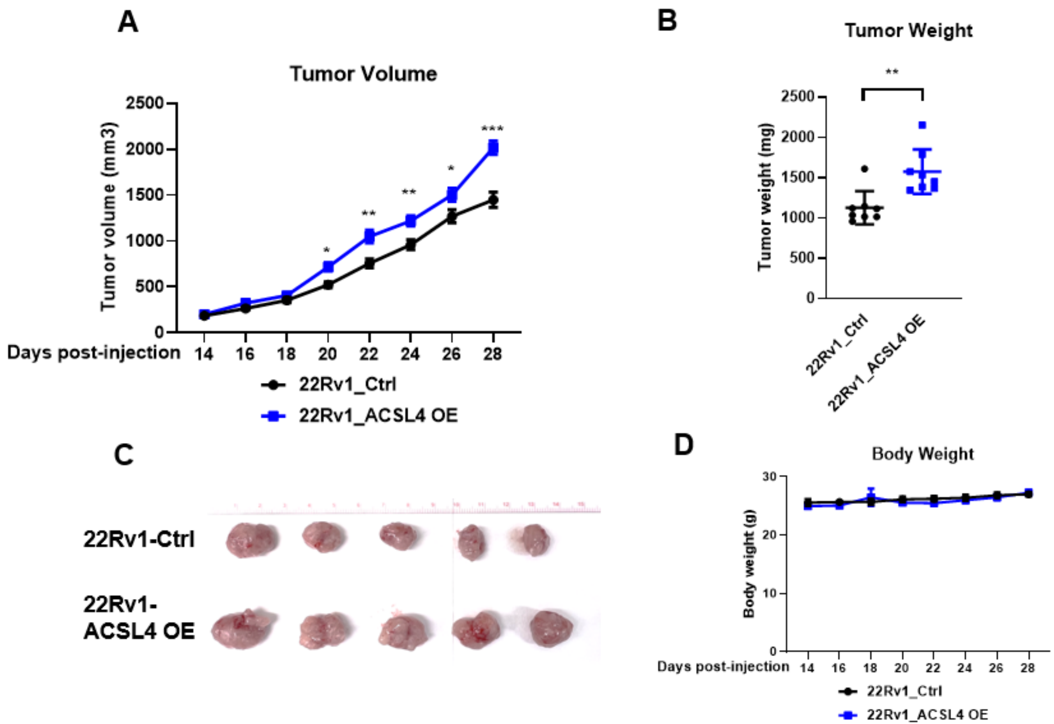

Figure 6. ACSL4 promoted xenograft tumor growth *in vivo*. 6A. Tumor volume over the course for 22Rv1-Ctrl and 22Rv1-ACSL4 OE xenografts. 6B. Final tumor weight measured after 28 days post-injection. 6C. Representative picture of the gross tumor isolated from 22Rv1-Ctrl and 22Rv1-ACSL4 OE xenografts. 6D. Body weight over the course of the study. In 6A and 6D, one-way ANOVA followed by unpaired t-test was used to determine statistical significance. In 6B, unpaired In t-test was used to determine statistical significance. **P* < 0.05, ***P* < 0.01, ****P* < 0.001. *****P* < 0.0001. Data are shown as the mean ± SD from n=8 mice per group.

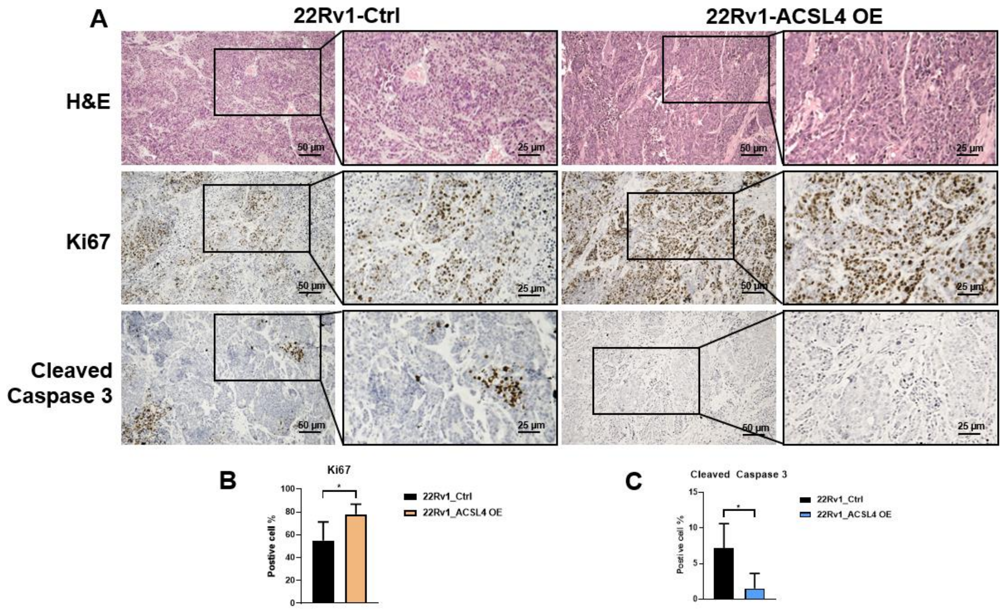

Figure 7. Histopathological analyses of 22Rv1-Ctrl and 22Rv1-ACSL4 OE xenograft tumors. 7A. H&E and IHC staining of control or ACSL4 overexpression 22Rv1 xenografts harvested 28 days post-implantation. 7B. Quantification of positive cell percentage of Ki67, and 7C. Cleaved Caspase 3 as shown in 7A. Unpaired t-test was used to determine statistical significance. **P* < 0.05. Data are shown as the mean ± SD from n=8 mice per group.

5.4 Discussion

Prostate cancer is featured by highly dysregulated lipid metabolism. This dysregulation is largely reflected in β-oxidation of fatty acids in mitochondria, and modulation on lipogenesis. [124] It has been suggested that increased lipids intake such as obesity and high fat diet is risk factors of prostate cancer, and supplementary FAs in diet was shown to promote prostate tumor growth in pre-clinical models. [125] In addition, pharmacological inhibition of fatty acid synthesis and metabolism have been reported to effectively restrict prostate cancer growth in preclinical cancer models, while clinical application of these drugs are often challenging due to low selectivity and toxicity. However, the molecular and biological consequences of altered lipogenesis pathways remain largely understudied, and there is an urgent need to elucidate how reprogramming cancer lipidome can regulate tumor progression and drug resistance.

In this chapter, we reported the oncogenic function of ACSL4, a long-chain fatty acid ligase as a driver of prostate tumor growth. ACSL4 expression is regulated by RB1/E2F signaling and contributes to the acceleration of cell cycle and proliferation downstream of RB1 inactivation. This was possibly achieved through boosting total cellular ATP level to support proliferation. While ATP generated through anaerobic glycolysis is mainly from utilization of glucose uptake, the observed total cellular ATP increase is likely from mitochondrial ATP synthesis by utilization of Acetyl-CoA produced through FA breakdown. As a result, ACSL4 overexpression provided abundant energy source needed for rapid tumor growth and promoted prostate cancer cell proliferation. *In vivo* tumor microenvironment is often challenged by energy and nutrient deprivation, therefore, ACSL4 overexpression may not be evident due to limited source. For future *in vivo* studies, it might be interesting to also compare how dietary FAs level may affect the effect of ACSL4 on tumor growth.

6. ACSL4 Reshapes Lipidomic and Transcriptomic Landscapes Leading to Prostate Cancer Progression

6.1 Introduction and Rationale

Current knowledge about the function of ACSL4 in promoting tumor progression through altering cancer cell lipidome and transcriptome remains largely elusive. One major outcome of dysregulated ACSL4 activity is reflected in the level of lipid utilization for downstream cellular activities, as well as shifted incorporation of certain lipid species into the cell lipidome. By selectively activating certain lipid species, ACSL4 overexpression may substantially alter the level of lipid utilization for energy production and storage, as well as shift cellular membrane composition. Elucidating such changes in lipid species following ACSL4 overexpression will be valuable for understanding the biological function of ACSL4 in the context of tumorigenesis.

In addition, certain products of lipid metabolism such as eicosanoids serve as important signaling molecules and regulate transcription and epigenetic modifications. ACSL4-targeting FAs such as arachidonate are known as major source compounds to synthesize eicosanoids like prostaglandins and leukotrienes which can regulate gene expression through direct interaction with TFs and transcriptional coactivators. [126, 127] As discussed in Chapter 4, ACSL4 has been shown to regulate oncogenic signaling such as ER and AKT. These changes, together with those regulated by lipid-based signaling molecules in cancer cells further lead to malignant transformation into advanced disease stages. The extracellular matrix (ECM) in cancer cells plays an essential role in the modulation of tumor microenvironment, tissue stiffness and intercellular signaling communication. These changes are reflected in the motility and mechanotransduction of cancer cells, thus enhancing their ability to migrate and metastasize. [128] In addition, cancer cell ECM is also one of the major contributors to therapy resistance as the matrix niche can serve as a physical barrier to drug delivery. [129] Understanding the regulatory role of ACSL4 on downstream lipidomic and transcriptional activities is essential for the development of novel target in prostate cancer through reprogramming lipid metabolic landscape.

6.2 Materials and Methods

6.2.1 Cell Lines and Cell Culture, Total RNA Extraction

Ctrl and ACSL4 OE LNCaP and 22Rv1 stable cell lines generated from Chapter 5 were cultured in complete RPMI medium. The total RNA from cells was extracted using TRIzol and the PureLink RNA mini kit (Thermo Fisher Scientific) following the manufacturer's instructions. To eliminate genomic DNA contamination, the PureLink DNase on-column digest kit (Thermo Fisher Scientific) was applied.

6.2.2 Untargeted Lipidomic Profiling

The lipidomic analysis was performed as we previously described. [130] Briefly, Ctrl and ACSL4 OE LNCaP and 22Rv1 cells in 10 cm dishes were at 80%–90% confluency in PBS, and protein content was measured using the BCA protein assay kit (Thermo Fisher Scientific) for sample normalization. Nonpolar lipids were extracted with MTBE and dried using a SpeedVac Vacuum Concentrator (Thermo Fisher Scientific) with no heat. Lipid samples were resuspended in 35 μL of 50% isopropanol/50% MeOH. 10 μL of samples were injected for reversed-phase (C_{14}) LC-MS/MS using a hybrid QExactive Plus Orbitrap mass spectrometer (Thermo Fisher Scientific) coupled to an

Agilent 1100 HPLC in DDA mode using positive/negative ion polarity switching (top 8 in both modes). The lipidomics data were analyzed using LipidSearch 4.1.9 software. The software identifies intact lipid molecules based on their molecular weight and fragmentation pattern using an internal library of predicted fragment ions per lipid class, and the spectra were then aligned based on retention time and MS1 peak areas are quantified across sample conditions.

6.2.3 Transcriptome Profiling (RNA-sequencing)

Total RNA isolated from Ctrl and ACSL4 OE LNCaP and 22Rv1 cells was submitted to for RNA-seq analysis service. Sequence reads were aligned to GRCh38 reference genome and visualized using Integrative genomics viewer. Read counts were subjected to paired differential expression analysis using the R package DESeq2. Top GO categories were selected according to the adjusted p-values and enrichment score and illustrated as number of genes downregulated in respective category. Heatmap was generated by Morpheus (Broad Institute).

6.2.4 Statistical Analysis

No statistical methods were applied to determine sample size. The investigators were not blinded during experiments and outcome assessment. Statistical analyses were performed using GraphPad Prism software. For comparison of two experimental groups, an unpaired 2-tailed Student's *t* test was used. Image J Wound Healing Toolbox was used to quantify the wound closure percentage for the migration assay. P-values of less than 0.05 were considered to be statistically significant.

6.3 Results

6.3.1 ACSL4 Overexpression Modulates Lipid Metabolite Composition in Prostate Cancer Cells

To investigate the effects of ACSL4 overexpression on modulating PCa cell lipidome, we performed a global lipidomic analysis in control and ACSL4 OE LNCaP and 22Rv1 cells by untargeted high-resolution liquid chromatography–tandem mass spectrometry (LC-MS/MS). The lipidomic profiling analysis identified a total number of 1984 lipid ions in both cell lines (Figure 8B), which belonged to 45 classes of lipids (Supplemental Table 3), resulting in a distinct group of lipid species detected in the ACSL4 OE groups for both LNCaP and 22Rv1 cell lines (Figure 8A). We found a total number of 207 lipid species that were significantly changed in LNCaP-ACSL4 OE, with 167 upregulated lipids and 40 downregulated lipids (Figure 8B). There were fewer altered lipid species detected in 22Rv1-ACSL4 OE, with a total number of 60 lipid species changed, 36 of which were upregulated and 24 were downregulated. (Figure 8B). The full list of significantly altered lipid species can be found in Supplemental Table 3.

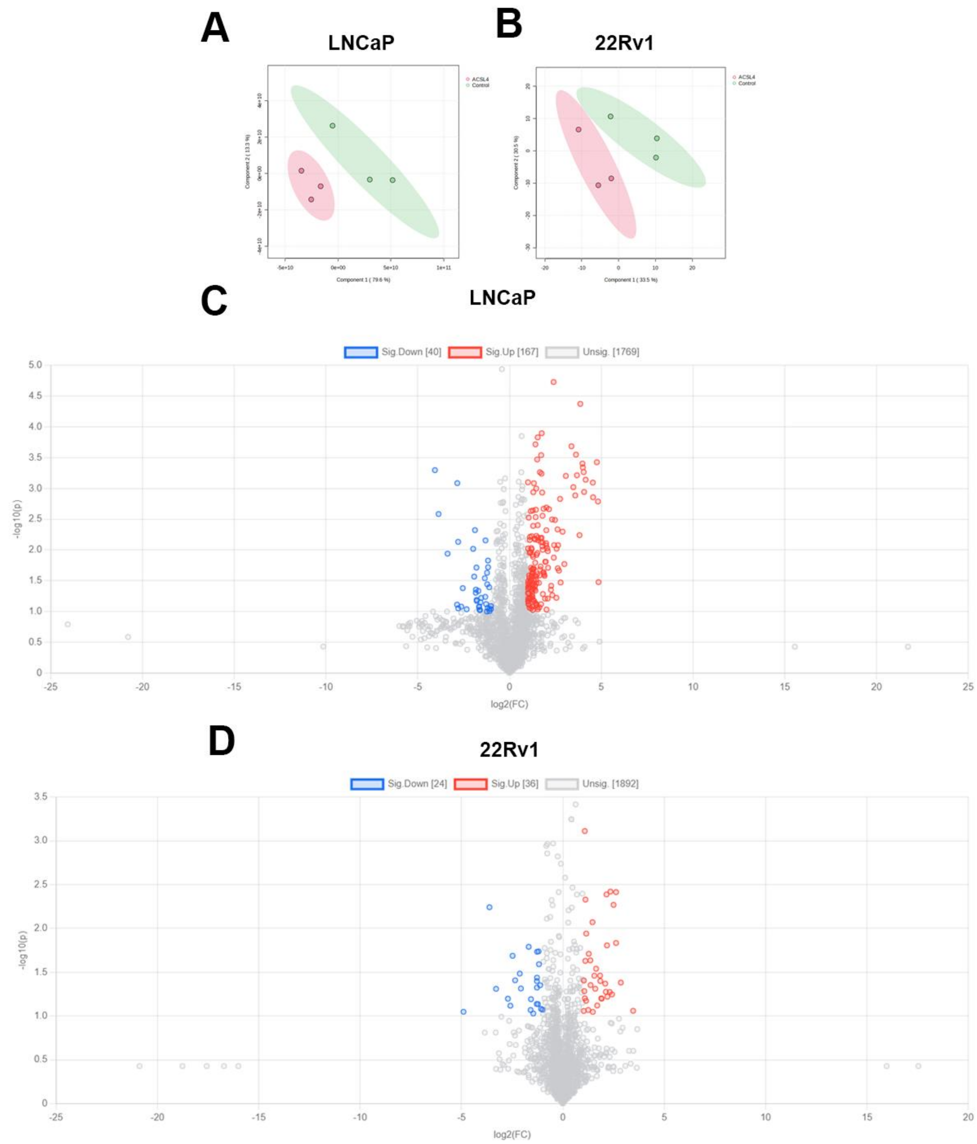

Figure 8. ACSL4 OE resulted in a distinct group of lipid species detected in LNCaP and 22Rv1 cells. 8A. PLS-DA analysis for separation of lipid species detected in control and ACSL4 OE cells. 8B. Volcano plot showing the significantly changed lipid species in control and ACSL4 OE cells.

Further analysis on significantly changed lipid species revealed that in LNCaP, there was a significantly increase in the total abundancy of multiple lipid species in ACSL4 OE cells, including triglyceride (TG), bismethyl phosphatidic acid (BisMePA), cholesterol ester (ChE), Phosphatidylethanolamine (PE), and stigmasteryl ester (StE) (Figure 9A). In addition, phospholipids with ACSL4-modified FA tails such as arachidonic acid (AA), eicosapentaenoic acid (EA), stearic acid (SA), and palmitic acid (PA) were also upregulated in ACSL4 OE cells (Figure 9B). Among all lipid species, bismethyl phosphatidic acid (BisMePA) and cholesterol ester (ChE) with ACSL4-modified acyl chains were found to be commonly enriched in ACSL4 OE cells, indicating a higher affinity of ACSL4-modified FA-CoAs to be incorporated into these two lipid species. In addition, the increase in the total abundancy of some lipid species suggests that there might exist a fast secondary step of incorporation of the ACSL4-modified lipids into the whole lipidome, which further contributes to various cellular activities. Interestingly, such increase in the lipid abundance of ACSL4 OE cells was only observed in LNCaP, as we found that there was no significant change in the majority of phospholipids with ACSL4-targeted FA chains except for phosphatidylserine (PS-EA), or in the total abundancy of lipid species in 22Rv1-ACSL4 OE cells (Figure 9, Figure 10).

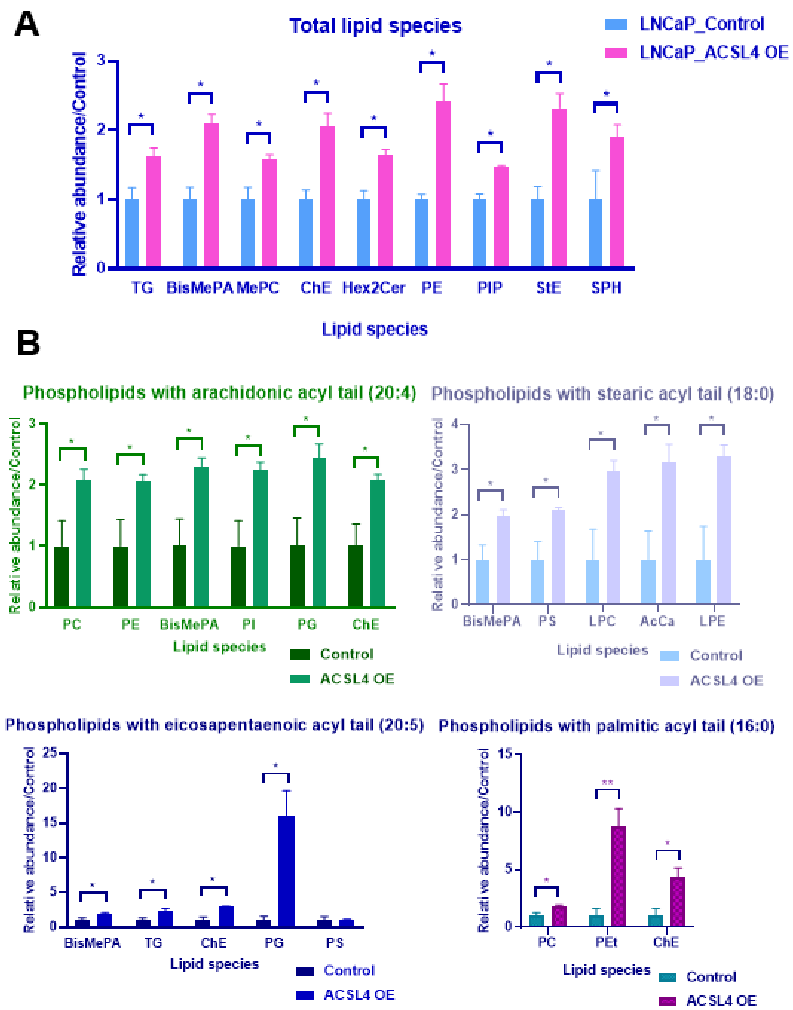

Figure 9. Total lipid species and phospholipids with ACSL4-targeted FA tails in LNCaP-ACSL4 OE cells. 9A. Changes in the total abundancy of lipid species in comparing control and ACSL4 OE cells. 9B. Changes in the phospholipids with ACSL4-targeted FA tails comparing control and ACSL4 OE cells. Unpaired t-test was used to determine statistical significance. **P* < 0.05. Data are shown as the mean ± SD from n=3 biological replicates.

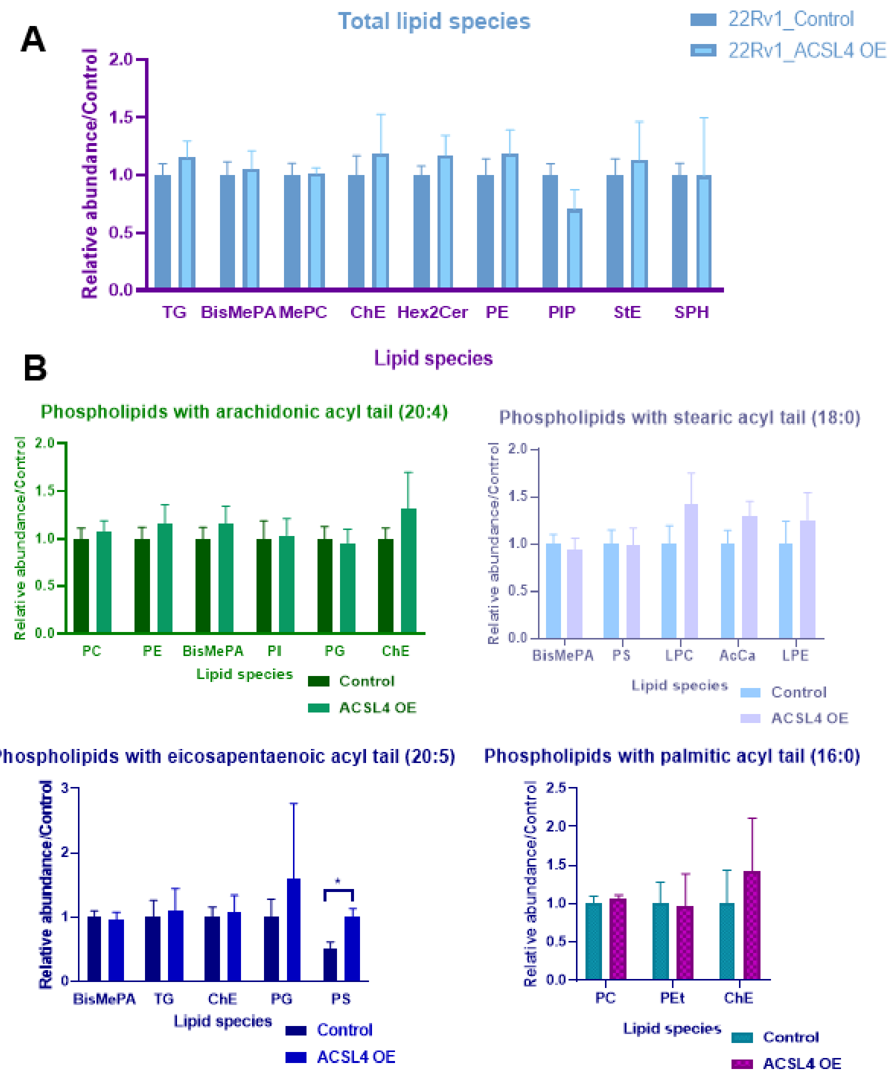

Figure 10. Total lipid species and phospholipids with ACSL4-targeted FA tails in 22Rv1-ACSL4 OE cells. 10A. Changes in the total abundancy of lipid species in comparing control and ACSL4 OE cells. 10B. Changes in the phospholipids with ACSL4-targeted FA tails comparing control and ACSL4 OE cells. Unpaired t-test was used to determine statistical significance. *P < 0.05. Data are shown as the mean ± SD from n=3 biological replicates.

6.3.2 RNA Sequencing Analysis Reveals a Distinct Transcriptomic Landscape Regulated by ACSL4

Next, we sought to investigate the changes in the transcriptomic prolife of ACSL4 OE cells through RNA-seq analysis. Overall, ACSL4 OE did not lead to drastic change in the gene expression, although principal component analysis revealed a distinct transcriptomic landscape in both LNCaP- and 22Rv1-ACSL4 OE cell lines (Supplemental Figure S1). Interestingly, we found that the expression of a set of genes involved in cancer cell extracellular matrix (ECM) were significantly altered, including the downregulation of A2M and ADAMTS3, and the upregulation of LAMC1 and ADAMTS1 (Figure 11C). Cancer cell ECM is often implied in intercellular communication through signaling molecules and cell motility, as well as tumor microenvironment stiffness that may affect extracellular permeability. [128] In addition, gene ontology analysis revealed that the differentially expressed genes are enriched in participating in ECM and extracellular structure organization, regulation of apoptosis and cell cycle (Figure 11A, B). Notably, we found that ACSL4 OE led to a distinct expression pattern of NEPC signature genes as reported by Beltran et al. [131] (Figure 12A, B). Multiple genes that were reported to be differentially expressed in NEPC patient samples compared with AdPC were consistently observed in both LNCaP- and 22Rv1-ACSL4 OE cells. Particularly, a NEPC marker, BRINP1, was found as one of the top changed genes in both cell lines. Mechanisms of the transformation of AdPC to NEPC have not been fully understood. It is widely acknowledged that the transition is characterized by the acquisition of neuroendocrine (NE) features and the loss of the adenocarcinoma epithelial (Ad) phenotype. [132] During this process, AdPC cells undergo lineage switching to NE cells and develop therapy resistance featured by loss of AR signaling. Our RNA-seq data revealed that the top changed NEPC genes upon ACSL4 OE were largely involved in the development of neuroendocrine features, as indicated by gene ontology analysis where genes with biological process of neuron development and synapse organization is highly enriched (Figure 11A). However, these changes seemed to be independent of AR signaling, as we found that while AR signaling was slightly upregulated in LNCaP-ACSL4 OE cells, 22Rv1, which expresses mutant AR-v7, did not show any significant change in AR genes upon ACSL4 OE (Figure 12A, B). In addition, consistent with our lipidomic profiling results, we also observed changes in the expression of several genes involved in the lysosome, endosome and endocytic vesicles in ACSL4 OE cells, such as EPHA3, CLU, GNAI1 and DPP4 (Supplemental Figure S2).

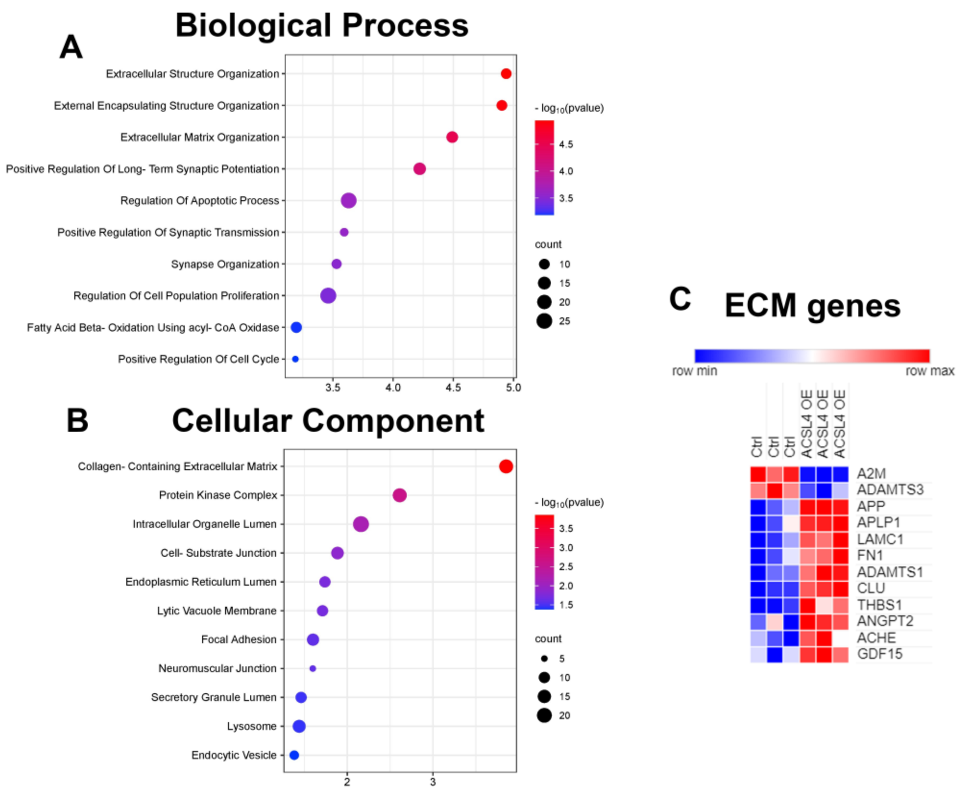

Figure 11. RNA-seq analysis revealed differentially expressed genes involved in cancer cell ECM. 11A. Enrichment analysis showing the top biological processes that are changed in ACSL-OE LNCaP cells. 11B. Enrichment analysis showing the top cellular components changed in ACSL-OE LNCaP cells. 11C. Heatmap showing the differentially expressed genes involved in regulation of ECM.

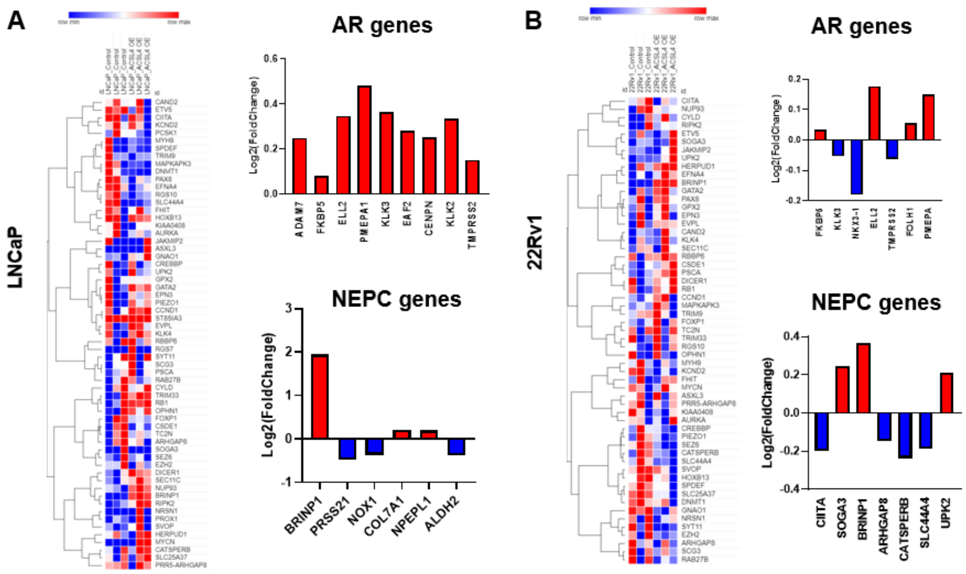

Figure 12. RNA-seq analysis revealed differentially expressed genes involved in NEPC development. 12A. Heatmap and bar graph showing the differentially expressed genes in NEPC signature and AR signaling in LNCaP ACSL4 OE cells. 12A. Heatmap and bar graph showing the differentially expressed genes in NEPC signature and AR signaling in 22Rv1 ACSL4 OE cells.

6.3.3 ACSL4 Overexpression Leads to Enhanced Migration and Chemotherapy Resistance in Prostate Cancer Cells

To validate the biological effects of ACSL4 overexpression on downstream expression of genes associated with cancer cell ECM, we sought to test the PCa cell ability of migration and response to chemotherapeutic agent treatment upon ACSL4 OE and KO. Consistent with our findings from RNA-seq, we found that both LNCaP- and 22Rv1-ACSL4 OE cells are more resistant to the treatment of docetaxel (Figure 13A, B). Resistance to docetaxel treatment was more evident in LNCaP cells, and discrepancies between 22Rv1 control and ACSL4 OE in docetaxel sensitivity was only observed under a high dose treatment (Figure 13A, B). In addition, the wound-healing assay also revealed a significant increase in the migration ability in 22Rv1-ACSL4 OE and a significant decrease in PC3-ACSL4 KO cells compared to the control cells (Figure 13C, D). Collectively, these results suggested that ACSL4 promotes prostate cancer malignancy through increased total lipid abundancy that supports downstream energy production and various cellular activities, as well as modulating cancer cell transcriptome to enhance their progression and therapy resistance.

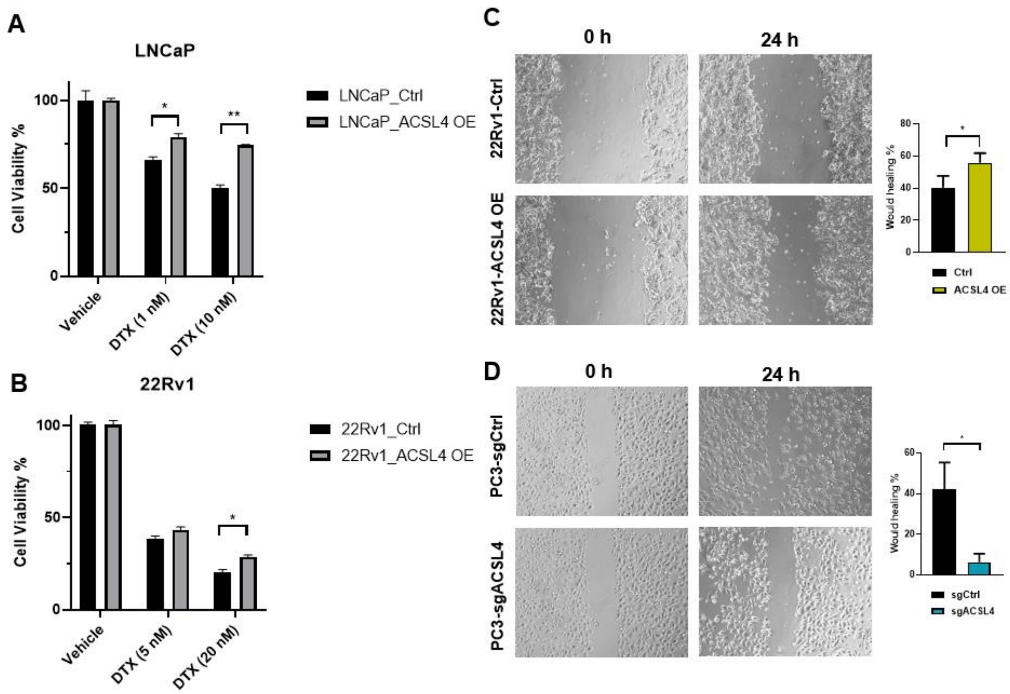

Figure 13. ACSL4 enhanced PCa cell resistance to docetaxel treatment and cancer cell migration. 13A. Treatment of LNCaP-Ctrl and LNCaP-ACSL4 OE cells with docetaxel for 24 h. 13B. Treatment of 22Rv1-Ctrl and 22Rv1-ACSL4 OE cells with docetaxel for 24 h. 13C. Wound-healing assay showing the migration of 22Rv1-ACSL4 OE compared to the control. 13D. Wound-healing assay showing the migration of PC3-sgACSL4 compared to the control. $^*P < 0.05$. $^{**}P < 0.01$. Data are shown as the mean ± SD from n=3 biological replicates.

6.4 Discussion

In this chapter, we identified a significant upregulation of total lipid species, as well as ACSL4-targeted lipid species after ACSL4 overexpression. ACSL4 overexpression led to a higher rate of incorporation of its targeted FA-CoAs into the lipidome, which subsequently underwent secondary incorporation into the lipidome through a dynamic process. As a result, this global increase of total lipids served as the fundamental source of energy production as shown in Chapter 5. Interestingly, this change was only observed in LNCaP-ACSL4 OE, but not in 22Rv1-ACSL4 OE. This was consistent with the observation that the ACSL4 OE effects on cell growth and ATP generation were more evident in LNCaP than 22Rv1, which might be due to the low efficiency of FAs uptake or limited FA synthesis rate in 22Rv1. BisMePA is mainly found in the lysosomal compartment of cells and in exosomes and is considered as a marker of lysosome. [133] Although the function of BisMePA in cancer is largely unknown, its function is implied in providing structural support for the development the complex intraluminal membrane system of lysosomes, thus enhancing resistance to phospholipases and prevent self-digestion of the lysosomal membranes. [134] BisMePA level is found to be elevated in some cancer types and it has been reported that breast cancer cells can divert PUFAs into BisMePA to develop adaptability and protect the lysosomes from increased reactive oxygen species (ROS) levels. [135] In line with these results, our data showed a common upregulation of BisMePA following ACSL4 upregulation across different FA chains, particularly with PUFA chains (BisMePA-AA and BisMePA-EA), suggesting its role in developing stress resistance in these cells.

It has been suggested that lipid metabolite can activate oncogenic signaling pathways. [10, 32] A previous study revealed upregulation in the ER and MTOR pathways in ACSL4-overexpressed colon and breast cancer cells. [136] However, the interaction between ACSL4 and its modulated lipid metabolic network with the regulation on cancer cell transcriptomic profile, particularly in the context of prostate cancer progression is poorly understood. Through RNA-seq analysis, we identified a distinct transcriptome upon ACSL4 overexpression in LNCaP and 22Rv1 cells. Interestingly, enrichment analysis revealed that there was a significant change in a set of genes associated with cancer cell ECM components such as ADAMTS1/3. Cancer cell ECM is largely implicated in modulating motility thus migration ability, as well as drug resistance. [128] [129] Consistently, we found that ACSL4 OE cells are more resistance to docetaxel treatment, and that ACSL4 KO cells demonstrated significantly impaired migration ability compared to the control cells. Interestingly, our data also revealed that ACSL4 overexpression led to a distinct expression of a set of genes that resembled NEPC signature. Notably, this change seemed to be independent of AR signaling, as we found that AR genes are only slightly upregulated in ACSL4 OE LNCaP cells, and no significant change in 22Rv1 cells. Among top changed genes, we found that BMP/Retinoic Acid Inducible Neural Specific 1 (BRINP1), an NEPC signature genes is significantly upregulated in both LNCaP- and 22Rv1-ACSL4 OE cells. In 22Rv1, although the change of BRINP1 was not as drastic, the expression of BRINP2, a BRINP family gene with similar function was significantly upregulated. Both BRINP1 and BRINP2 play an important role in controlling neurogenesis and neuron differentiation during development, and their expression was shown to be highly activity-dependent and could be induced by glutamate-induced signaling molecules such as BMP2 and kainic acid. [137, 138] Therefore, there might exist a potential interaction between ACSL4-mediated metabolites and BRINP family gene expression that accounts for its upregulation upon ACSL4 expression. BRINP1 was identified as a NEPC signature gene which is upregulated in NEPC samples compared to AdPC samples. [131] However, the function of BRINP1 during NEPC progression is unknown. Despite its reported negative regulation on cell cycle and mitosis, BRINPs may contribute to the PCa lineage plasticity and drive the transition of adenocarcinoma to an NEPC phenotype. [138] Further studies on how BRINPs play a role in NEPC cells will deepen the understanding of NEPC evolution and create new therapeutic opportunities for advanced prostate cancers.

7. Discovery of Novel ACSL4 Inhibitors that Effectively Targeted Prostate Tumor

7.1 Introduction and Rationale

Given the previous results that the proliferation rate, and the migration ability of PCa cells with ACSL4 KO were significantly suppressed, we hypothesized that inhibiting ACSL4 activity is a promising therapeutic strategy in advanced PCa. Currently, there are several small molecules that have been reported to pharmacologically inhibit ACSL4 activity. For example, triacsin C is a general inhibitor of long-chain fatty acyl CoA synthetase that blocks β-cell apoptosis induced ACSL family. [34] Despite promising data in several pre-clinical models, the clinical application of triacsin C in cancer therapy did not achieve success due to its non-specificity that caused toxicity to normal tissues. [35] Thus far, the only specific inhibitor that has been proven selective to inhibit ACSL4 activity is the recently published PRGL493, which demonstrated efficient suppressive effects on cell growth when treating several breast cancer and prostate cancer cell lines. [111] However, from both previous studies and our preliminary data, the *in vitro* IC50 of PRGL493 is higher than 20 μM in PCa cells, indicating insufficient potency. [111] Moreover, it is not known whether there is any off-target effect of PRGL493 that could result in severe side effects. Therefore, there is an urgent need to develop an ACSL4 inhibitor that suppresses prostate tumor growth more efficiently without severe adverse effects. In this chapter, we aim to develop novel ACSL4 inhibitors with a higher potency and better target selectivity for prostate cancer treatment.

The structure-based virtual screening (SBVS) utilizes the predicted structure of the targeted proteins and the well-established compound libraries that allows for a rapid screening for potential small molecules with high binding affinities with the target proteins through molecular docking. SBVS has been widely used as an effective tool for early-stage drug development. [139] Compared with traditional drug panel screening, SBVS offers an efficient platform to identify new compounds which accelerates the discovery of new uses of existing compounds in a much more cost-and time-effective manner. Through a virtual screening strategy to discovery new compounds that specifically target ACSL4 structure, followed by testing the pharmacological effects through our in vitro system, our study will provide great insight to the development of ACSL4 inhibitors with high potency and selectivity for advanced prostate cancer treatment.

7.2 Materials and Methods

7.2.1 Structure-Based Virtual Screening (SBVS)

Virtual screening workflow library selection and preparation

Compounds libraries were selected in this study and categorized in 2 groups. (a) Thermofischer's HitDiscover: A ready-to-screen collection of 52,000 Maybridge screening compounds (b) Maybridge library of high-throughput screening collections. These compounds were subjected into ligand preparation by Ligprep wizard application of Maestro (Schrodinger Release 2021.1: Maestro, LigPrep, Schrodinger, LLC, New York, NY, 2021). The Ligprep protocol performed processes on the ligand including 2D to 3D conversion, the addition of hydrogens, correction of bond length and angle, low energy structure, stereochemistries followed by minimization and optimization potential for liquid simulations (OPLS4) force field. Possible tautomers of the compounds were generated using Epik at the target pH of 7.4±1.0. At most 5 stereoisomers were generated for each chiral molecule.

Preparation of proteins

The human long-chain-fatty-acid-CoA ligase 4(ACSL4) AlphaFold structure prediction was loaded via Maestro (Schrodinger Release 2021.1). Each structure was prepared using Protein Preparation wizard application; water molecules were removed, all hydrogens were added and protonation states of His, Asn and Gln side chains were adjusted with default protocol. A restrained minimization was performed using OPLS4 force field. The resulting complex structures were used to generate Glide grids for docking by the Receptor Grid Generation module of Maestro. The scaling factor and partial charge cutoff of van der Waals radius scaling was set to 1.0 and 0.25, respectively. The size of grid box around the a) ATP binding site or b) around the K572 residue was adjusted less than 24 Å. Other parameters such as constraints, rotatable groups, and excluded volume, which are the default setting of the Maestro are used unless otherwise specified.

Glide molecular docking

Glide module (Grid-based ligand docking with energetics) of Maestro with default parameter was carried out to calculate the ligand-receptor interaction. The prepared ligands were docked into the binding site of the target protein using the extra precision algorithm (XP) with the ligand sampling treated as flexible. The ligand interaction tool was used to view the interaction diagram of the ligands with the residues at the active site of the target protein. The GScore, the output score of docking study, is calculated in kcal/mol and it includes ligand–protein interaction energies, hydrophobic interactions, hydrogen bonds, internal energy, p–p stacking interactions, and root mean square deviation (RMSD) and desolvation. The best fit compounds were chosen for each target by GScore, types of interactions, potential of bonding, steric clash and conformations.

Virtual screening workflow

Virtual screening was carried out with virtual screening work flow wizard application. Initially, ligand properties were calculated using Qikprop. Next, every ligand was filtered by Lipinski's rule of 5, followed by the removal of ligands with reactive functional groups. The ligand library was subjected to Glide module (Grid-based ligand docking with energetics) of Maestro. The glide virtual screening workflow (VSW) is a 3-level docking protocol involving high-throughput virtual screening (HTVS), standard precision (SP) and extra precision (XP) to calculate ligand-protein interaction. From the results of HTVS docking, 10% of the top-ranked compounds were further docked using the SP mode, and of these results, the top 10% were docked using the XP mode.

7.2.2 Cell Lines and *In Vitro* Drug Test

Human prostate cancer cell lines PC3, DU145, 22Rv1, C4-2 and LNCaP were cultured in complete RPMI medium. LNCaP-Ctrl, LNCaP-ACSL4 OE, 22Rv1-Ctrl, 22Rv1 ACSL4 OE, PC3-sgCtrl, and PC3-sgACSL4 stable cell lines generated from Chapter 5 were cultured in complete RPMI medium. Top hit small molecules generated by virtual screening were purchased from Maybridge (Supplemental Table 5). PRGL493 was purchased from Cayman Chemical (32748) To determine the inhibitory efficiencies of ACSL4 inhibitors and their IC50 doses, cell viability was measured using the CellTiter-Glo 3D Cell Viability Assay kit (Promega). Briefly, we plated the cells in white-walled 96-

well plates (Falcon) at the density of 1.0×10^3 cells/well and treated the cells with candidate inhibitors and PRGL493 as positive control for 6 days. Three doses (1 μM, 5 μM and 10 μM) for *in vivo* drug screening, and 5 doses selected based on screening results for IC50 determination were tested in cells. On day 6, one volume of the CellTiter-Glo 3D reagent was added into each well, mixed on a thermomixer at 750 rpm for 5 minutes, and then incubated at room temperature for another 20 minutes. The luminance signal for a 250-millisecond integration time was measured using a SpectraMax M3 Multi-Mode Microplate Reader (Molecular Devices).

7.2.3 Isotope-Labeled ACSL4 Enzyme Activity Assay

The ACSL4 enzyme activity assay was performed as previously described by measuring the formation of arachidonic acid (AA)-CoA from AA. [140] Briefly, recombinant ACSL4 protein (Abnova, H00002182-P01) was incubated in the presence or absence of ACSL4 inhibitors (PRGL493 and candidate inhibitors) for 10 min at 37 °C in a reaction mixture of 175 mM Tris (pH 7.4), 8 mM $MgCl_2$, 5 mM DTT, 10 mM ATP, 250 μM CoA with 50 μM AA trace-labeled with [14C]-AA (American Labeled Chemicals, ARC 0290-10 µCi), and 4 mg membrane fractions. in a final volume of 100 µl. Recombinant ACSL4 was first added to the mixture to initiate the reaction, and 1ml of ethyl acetate was added to terminate it. Then a phase extraction was performed, and the upper phase was removed, followed by the second extraction of the lower aqueous phase. The radioactivity of the final aqueous phase was determined by a liquid scintillation counter. A blank control was included for correction of the background.

7.2.4 Statistical Analysis

No statistical methods were applied to determine sample size. The investigators were not blinded during experiments and outcome assessment. Statistical analyses were performed using GraphPad Prism software. For comparison of two experimental groups, an unpaired 2-tailed Student's *t* test was used. For comparison of more than two groups, 1-way or 2-way ANOVA with Tukey's multiple-comparison test was used. When data from multiple groups were not normally distributed, a Kruskal-Wallis test followed by Dunn's multiple-comparison test was used. For determination of dose response and IC50, a non-linear regression with three parameters were used. P-values of less than 0.05 were considered to be statistically significant.

7.3 Results

7.3.1 Identification of Top Hit Molecules Targeting ACSL4 Structure

To identify novel inhibitors or lead compounds that selectively target ACSL4 by utilizing currently available drugs and chemical compounds, we performed a Structure-Based Virtual Screening (SBVS) on 2 published compound libraries. Virtual docking of compound structures from 2 previously established compound libraries (i.e. Thermofischer's HitDiscover HD and Maybridge library MSC) against the human long-chain-fatty-acid-CoA ligase 4(ACSL4) AlphaFold structure on 2 binding pockets were carried out as described in (Figure 14A). Upon removal of duplicated compounds with multiple hits on the ACSL4 structure, the screening result revealed 60 compounds from HD library and 53 compounds from MSC library predicted to bind the ACSL4 ATP pocket, as well as 87 compounds from the HD library predicted to bind the K572 pocket, the FA substrate entrance site with high binding affinity. Then we selected the top 10 hits from each output list with the highest docking scores, and we identified and removed 15 duplicated compounds. The finalized candidate list contains 15 compounds with predicted highest binding affinity with ACSL4 based on their chemical structures which were subsequently submitted for *in vivo* drug testing, namely ACSL4i #1 to #15 (Figure 14B). A full list of the 15 candidates with their detailed structural information is available in the supplemental materials (Supplemental Table 5).

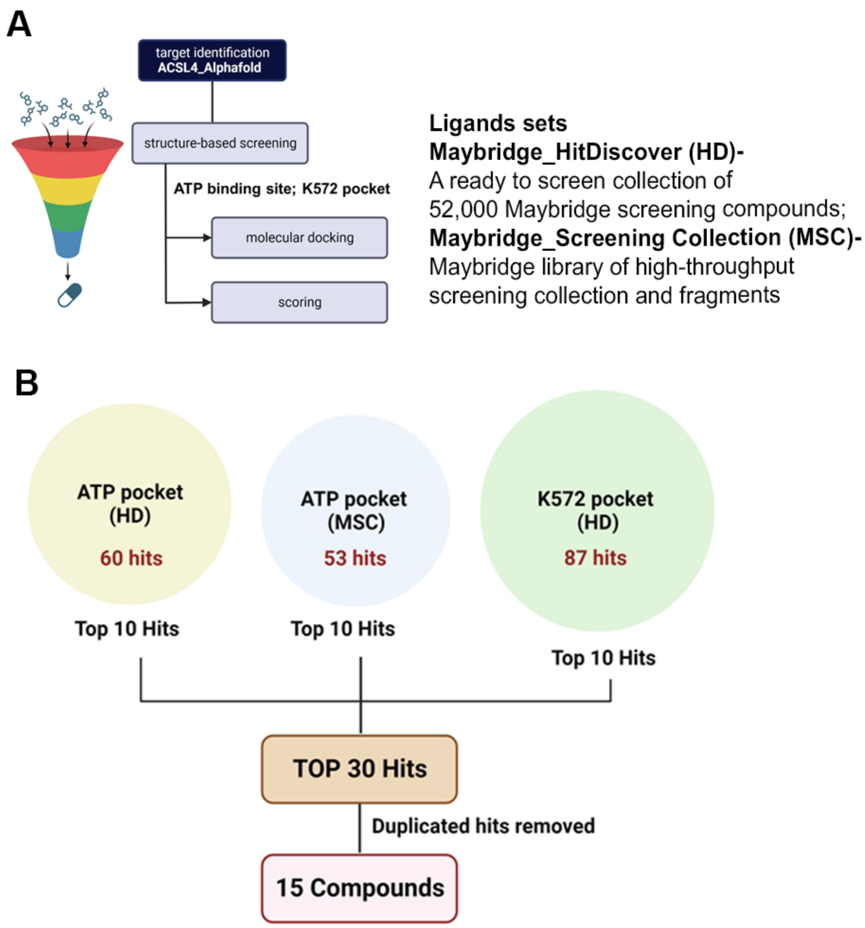

Figure 14. Workflow of the structure-based virtual screening to identify ACSL4 candidate inhibitors. 14A. Scheme showing the design and workflow of the structure-based virtual screening. 14B. Scheme showing the strategy for the identification of top hits from SBVS for following *in vitro* screening.

7.3.2 Identification and Characterization of Lead Candidate ACSL4 Inhibitors that Effectively Restricts Prostate Cancer Cell Growth

Virtual screening provided valuable information of the chance of binding of library compounds to the targeted protein (i.e. ACSL4) based on predicted affinity scores, while it does not predict the pharmacological efficacy or the actual effect on ACSL4 activity. Therefore, an in vitro drug system was established to evaluate the inhibitory effects of the 15 candidates on PCa cell proliferation. We first tested the inhibitory effects of the 15 candidates on cell viability of DU145 and PC3, 2 ACSL4-high cell lines under the same treatment dose. We compared the inhibitory effects of the 15 candidate compounds relative to PRGL493, the previously discovered ACSL4 inhibitor as a positive control. We found that 4 of the 15 candidate molecules, ACSL4i #6, #7, #10 and #13 significantly inhibited DU145 and PC3 cell viability. In PC3, treatment of the positive control PRGL493 for 6 days achieved 20% inhibition rate with a dose of 10 μM, while in PC3, treatment of ACSL4i #7 inhibited 80% of cell viability with the same dose, while #10 had a similar inhibitory efficiency with PRGL493, and #6 and #13 inhibited 10% of cell growth (Figure 15A). We next expanded the screening pool to 4 PCa cell lines, DU145, PC3, C42, and 22Rv1, and we also tested IC50 doses of these 4 candidate inhibitors in each individual cell line (Figure 15B, C). Consistently, we found that ACSL4i #6, #7, #10 and #13 demonstrated dose-dependent inhibitory effects on PCa cell viability, where ACSL4i #7 and #13 demonstrated higher efficacy in the inhibition of PCa cell proliferation than PRGL493 (Figure 15B, C). Despite variation of sensitivities across different cell lines, IC50 doses of ACSL4i #7 were significantly lower compared to PRGL493 (Figure 16). #13 had slightly lower IC50 doses in most cell lines tested, while #6 and #10 were comparative to PRGL493 in the inhibitory effects on cell growth (Figure 16). Notably, we found that the ACSL4 level among the cell lines that we tested did not fully correlate with the sensitivity of these cells to ACSL4 inhibitors treatment, including the positive control PRGL493. This might be due to the distinct basal level of fatty acid utilization for energy production and lipid incorporation rate in different PCa cell lines, and the resulting discrepancy in the dependency on ACSL4 activity to support cell proliferation. To this end, further tests using isogenic ACSL OE or ACSL4 KO cell lines are needed to fully elucidate the association between ACSL4 level and sensitivity to the treatment.

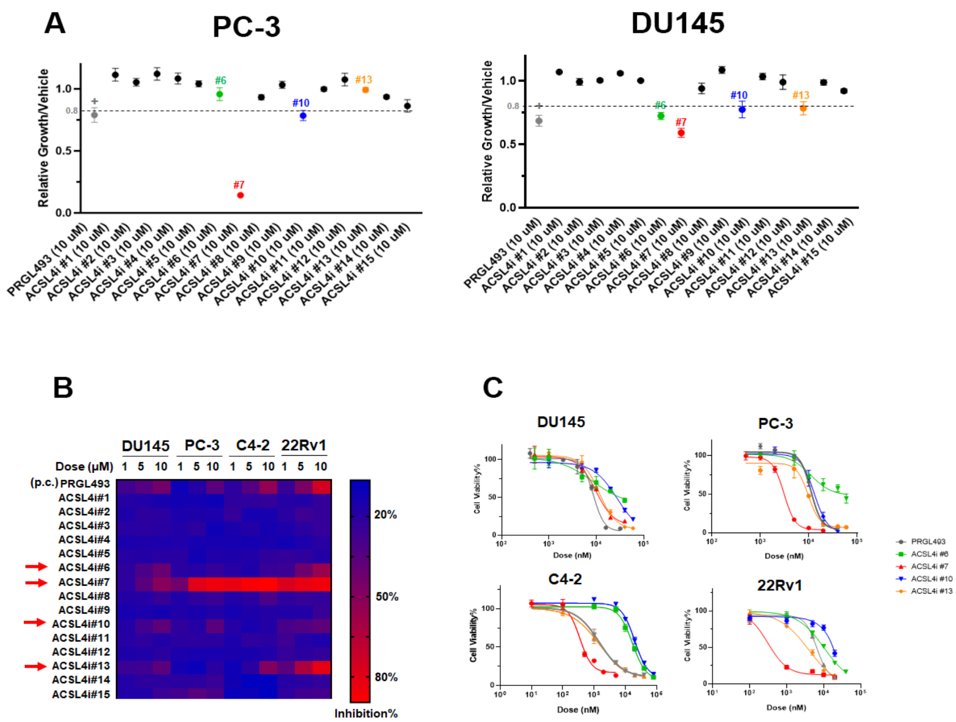

Figure 15. *In vitro* drug testing of the pharmacological effects of the 15 candidate ACSL4 inhibitors on PCa cell proliferation. 15A. Growth Inhibition of PRGL493 and the 15 candidate ACSL4 inhibitors in PC3 and DU145. 15B Heatmap showing the inhibition efficiencies of PRGL493 and the 15 candidate ACSL4 inhibited tested in different doses and cell lines. 15C. Dose-response of PRGL493 and ACSL4i #6, #7, #10, #13 in 4 PCa cell lines. Data are shown as the mean ± SD from n=3 biological replicates.

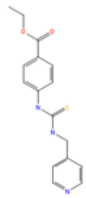

Cell line	IC 50 (μM)
PC-3	10.98
DU145	8.51
22Rv1	10.32
C4-2	16.94
LNCaP	>50

#6, ethyl 4-({[(4-pyridylmethyl)amino]carbothioyl}amino)benzoate

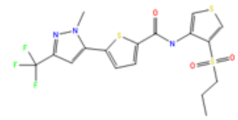

Cell line	IC 50 (μM)
PC-3	2.99
DU145	9.84
22Rv1	0.31
C4-2	0.35
LNCaP	2.5

#7, N2-[4-(propylsulfonyl)-3-thienyl]-5-[1-methyl-3-(trifluoromethyl)-1H-pyrazol-5-yl]thiophene-2-carboxamide

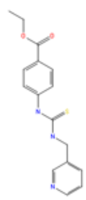

Cell line	IC 50 (μM)
PC-3	11.28
DU145	17.84
22Rv1	13.94
C4-2	19.88
LNCaP	9.54

#10, ethyl 4-({[(3-pyridylmethyl)amino]carbothioyl}amino)benzoate

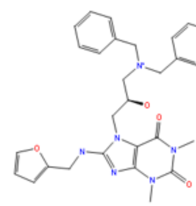

Cell line	IC 50 (μM)
PC-3	9.8
DU145	11.47
22Rv1	3.99
C4-2	1.43
LNCaP	4.06

#13, 7-[3-(dibenzylamino)-2-hydroxypropyl]-8-[(2-furylmethyl)amino]-1,3-dimethyl-2,3,6,7-tetrahydro-1H-purine-2,6-dione

Figure 16. Chemical structures and IC50 doses tested in PCa cell lines of 4 candidate ACSL4 inhibitors #6, #7, #10 and #13.

7.3.3 Pharmacological Inhibition of ACSL4 Activity Reduces Prostate Tumor Burden in Advanced RB1-Loss and Neuroendocrine Prostate Cancer Cells

Next, we sought to investigate whether ACSL4 inhibitors were also effective in inhibiting advanced prostate cancer growth. The RB1-deficient PCa cells PC3-shRB1 that we generated previously displays an aggressive phenotype with a significantly higher proliferation rate *in vivo* and *in vitro*. [33] In addition, several NEPC cell lines also have high level of ACSL4 expression. We first examined the effect of ACSL4 inhibition by comparing the growth inhibition of genetically double knockdown PC3-shRB1-shACSL4 cells and ACSL4 inhibitors-treated cells. We found that compared with RB1 single KD control, double KD of RB1 and ACSL4 led to a 40% reduction of cell growth. In addition, treatment with PRGL493 and the 4 ACSL4 candidate inhibitors resulted in a more drastic growth suppression, possibly due to the higher efficiency of inhibiting ACSL4 activity (Figure 17A). Notably, treatment of PC3-shRB1 cells with 5 μM ACSL4i #7 led to an 80% inhibition on cell proliferation (Supplemental Figure S4, Figure 17A). We also tested the efficacy of the ACSL4 inhibitors in an NEPC cell line, H660, and we found that PRGL493, ACSL4i #7 and #13 significantly suppressed the proliferation of H660 (Supplemental Figure S4, Figure 17B). These results served as a proof-of-concept study indicating that targeting ACSL4 is an effective therapeutic option for advanced prostate cancers.

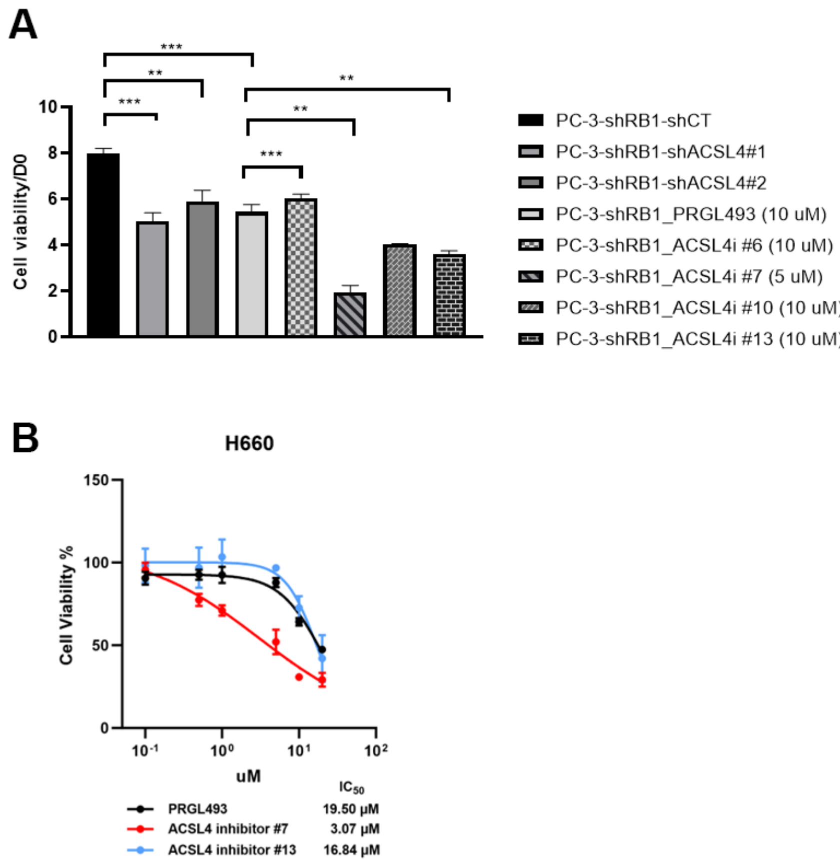

Figure 17. Inhibition of ACSL4 suppressed aggressive PC3-shRB1 and H660 cell proliferation. 17A. Relative cell growth rate comparing PC3-shRB1, PC3-shRB1-shACSL4 and treatment with PRGL493 and 4 ACSL4 inhibitors. 17B. Dose-response of H660 treated with PRGL493 and ACSL4i #7 and #13. ***P* < 0.01. ***P<0.001. Data are shown as the mean ± SD from n=3 biological replicates.

7.3.4 Evaluation of Inhibitor Selectivity and Identification of Potential Off-Target Effects

Target selectivity is the key to prevent off-target activities toward other proteins which may cause unwanted side effects. [141] There are several approaches to determine the drug selectivity to target proteins (i.e. ACSL4), one of which is to directly measure the consumption rate of an ACSL4 substrate co-treated with the inhibitors. In addition, determination of the dose-response shift in ACSL4 OE or KO cells also provides solid evidence for target specificity. To this end, we first tested the change in the IC50 doses of the ACSL4 inhibitors by comparing ACSL4 OE and ACSL4 KO cell lines. Determination of the IC50 doses in such isogenic cell lines also provides valuable information on treatment sensitivity to serve as a biomarker for patient stratification. We expect that ACSL4 OE cells will be more sensitive to ACSL4 inhibitors treatment with lower IC50 doses compared to the parental cell lines, and that ACSL4 KO will significantly increase the resistance to the inhibitor treatment. Indeed, we found that the IC50 doses were significantly lower for LNCaP-ACSL4 OE cells, and significantly increased in PC3-ACSL4 KO cells compared to the control (Figure 18A, B). Similar trends in the alteration of IC50 dose were observed in 22Rv1-ACSL4 OE cells, while the shift of the dose-response curve was not as evident as in LNCaP cells (Supplemental Figure S3). In addition, we also generated an ACSL4 KO mouse fibroblast cell line (MEF) to investigate the potential effect of ACSL4 inhibitor on normal cell lines. Notably, we found that compared to prostate cancer cell line, this mouse fibroblast cell line was more resistant to ACSL4 inhibitor treatment, and ACSL4 KO MEFs were even more resistant to inhibitor treatment (Supplementary Figure S3). These results suggest that our candidate inhibitors showed good specificity in targeting ACSL4 activity, and that ACSL4-high PCa cells are more sensitive to the inhibitor treatment.

Next, we sought to determine the drug selectivity by direct measurement of substrate consumption. Through the isotope-labeled ACSL4 activity assay, we found that our candidate inhibitor ACSL4i #7 and #10 demonstrated direct inhibition of the consumption and conversion of arachidonic acid (AA) to AA-CoA in a dose-dependent manner, indicating their specificity in targeting ACSL4 activity (Figure 19). Collectively, our data suggest that our candidates #7 and #10 are promising candidates for suppressing PCa cell proliferation through targeting ACSL4 activity, which could also serve as lead compound for the improvement and development of future ACSL4 inhibitors with better efficacy and selectivity.

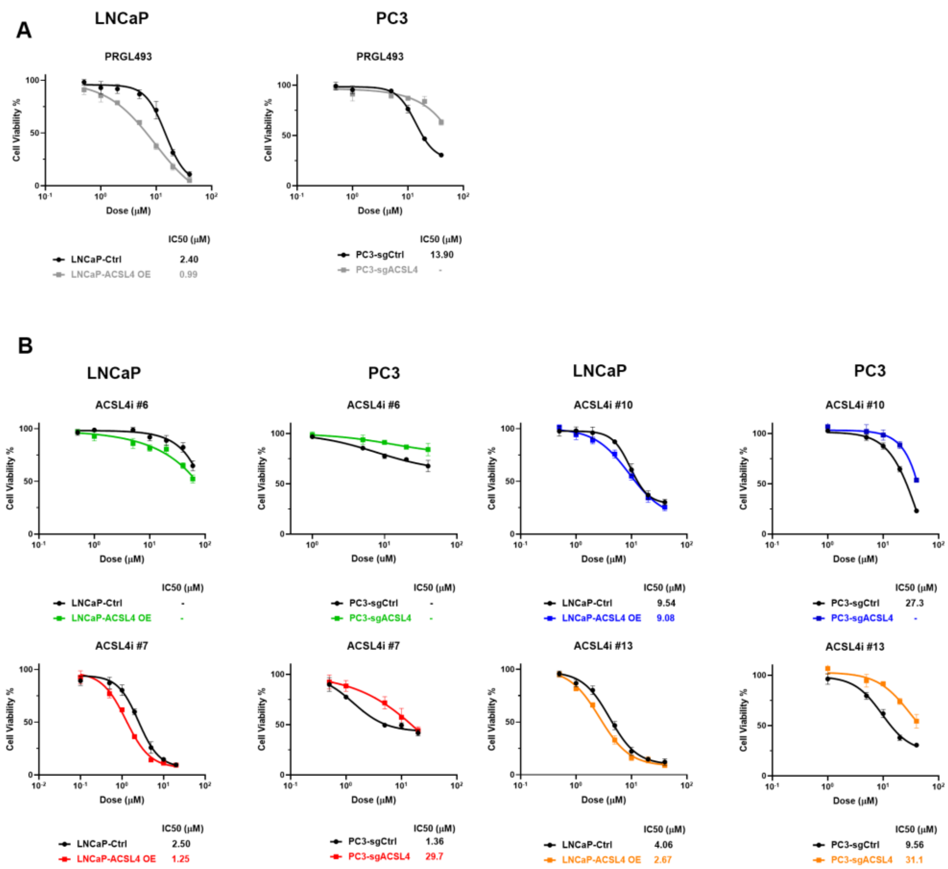

Figure 18. ACSL4 OE sensitized and ACSL4 KO de-sensitized PCa cells to ACSL4 inhibitor treatment. 18A. Dose-response of LNCaP-ACSL4 OE and PC3-ACSL4 KO treated with PRGL493 compared to the control cells. 18B. Dose-response of LNCaP-ACSL4 OE and PC3-ACSL4 KO treated with the candidate ACSL4 inhibitors compared to the control cells. Data are shown as the mean ± SD from n=3 biological replicates.

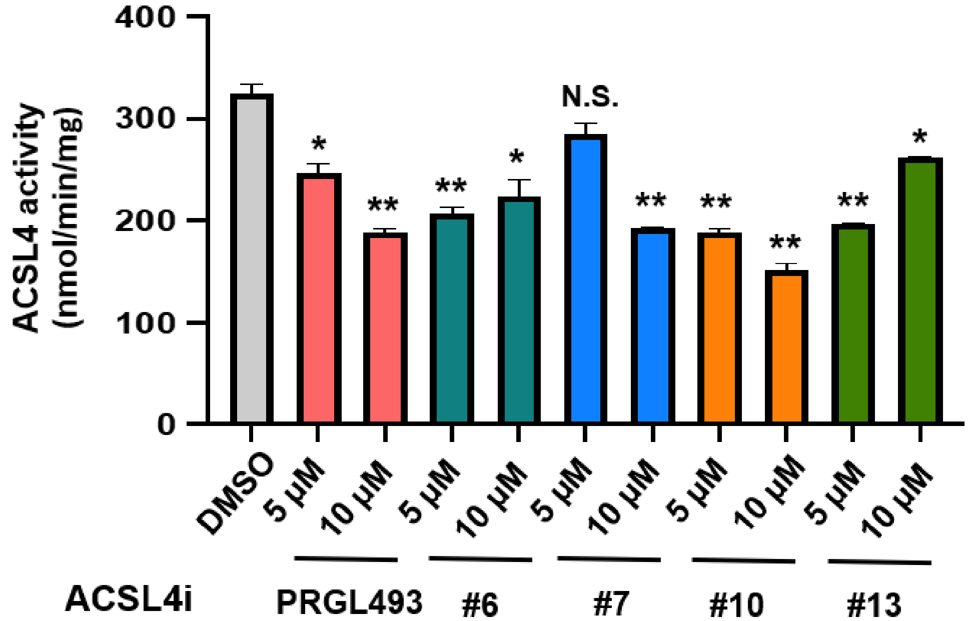

Figure 19. ***In vitro*** **ACSL4 activity assay showing the conversion rate of AA to AA-CoA treated with PRGL493 and the candidate ACSL4 inhibitors.** *P<0.5, **P < 0.01. Data are shown as the mean ± SD from n=3 biological replicates.

7.4 Discussion

In this chapter, we discovered several candidate ACSL4 inhibitors that effectively suppressed PCa cell proliferation through a combined virtual screening and *in vitro* testing. Virtual screening dictates the possibility of existed drugs to be repurposed and used to bind target proteins based on their 3D structures, while it does not indicate the inhibition of target protein activity or cancer cell proliferation. Thus, an *in vitro* drug system is usually required to validate the pharmacological effects during drug development. Through virtual screening we identified candidate compounds with high predicted binding affinity of library compounds to ACSL4, specifically to the ATP pocket and K572 pocket (substrate entrance tunnel). These 2 domains are the major enzymatically active sites that drive ACSL4 activity, and such screening strategy maximized the predicted efficacy for potential pharmacological inhibition of ACSL4 activity. The sequences of the ATP-binding domain share high similarities among all ACSL family members, while the substrate-binding domain are highly variable between different ACSL members. These structural variances determine the different preferentially selected FA substrates of different ACSLs. Therefore, identification of candidate compounds that target both domains allowed for the improvement of inhibition selectivity to ACSL4 without off-target effects on other ACSL family members. Among our top 15 candidate inhibitors, #1 to #10 are predicted to bind the ATP pocket, #11 to #15 are predicted to bind the K572 pocket, and #6, #10, and #12 are predicted to hit both sites on ACSL4 chemical structure. This information serves as an important reference for the determination of selectivity and the direction for possible structural modification.

The *in vitro* drug testing validated the inhibitory effects of 4 out of 15 candidate drugs on PCa cell proliferation. Following measurement of IC50 doses found that the dose-response did not fully correlate the basal level of ACSL4 among different PCa cell lines. This was possibly due to the different lipid metabolic profiles in different cell lines that decide the dependency on ACSL4 activity for oncogenic events. As an FA-CoA ligase, ACSL4 regulates cancer cell activities through activating FA for downstream energy production, which could be influenced by other pathways such as FA uptake or synthesis rate, and the proportion of ATP generation through lipid β-oxidation vs. glycolysis. In addition, ACSL4 activity could be compensated by its family members such as ACSL3, which could be activated upon ACSL4 inhibition through feedback regulation. Therefore, future studies may also include the investigation of other ACSL family members to fully elucidate the underlying regulatory mechanism in PCa.

The ACSL4 enzyme activity assay showed that ACSL4i #7 and #10 inhibited ACSL4 activity in a dose-dependent manner. However, the inhibition efficiency did not directly reflect the efficacy of PCa cell proliferation suppression. This might be due to the limited bioavailability and the efficiency of drug uptake *in vitro* thereby affecting the effective dose. Further experiments such as a PD/PK analysis will facilitate the understanding of *in vivo* mechanism of action and optimization of administration approaches. In addition, future work will focus on structural modification of #7 and #10 to improve bioavailability thus increasing the drug efficacy. Overall, ACSL4i #7 and #10 serve as promising lead compounds for the development of pharmacological ACSL4 inhibitors to treat advanced prostate cancers.

8. Inhibition of ACSL4 Activity Modulates Prostate Cancer Cell Sensitivity to Chemotherapy and Hormonal Therapy

8.1 Introduction and Rationale

Docetaxel is one of the most commonly used chemotherapeutic agents which is often given together with hormonal therapy for patients with advanced prostate cancer such as CRPC. [142] However, as the disease progresses, a significant proportion of CRPC patients will not respond to these docetaxel-based therapies and all patients will ultimately develop resistance. [143] Several mechanisms such as AKT signaling and AR signaling have been identified to play a role during the development of docetaxel resistance. [144] Since overall docetaxel treatment still confers significant survival benefit, it is important to overcome the issue of resistance in CRPC patients. In Chapter 5 we found that ACSL4 OE enhanced PCa cells resistance to docetaxel treatment. Therefore, we hypothesize that there exists a combinatorial benefit by treatment of ACSL4 inhibitors and docetaxel in ACSL4-high PCa. ACSL4 is known to induce ferroptosis sensitivity through increasing lipid peroxidation pool, meanwhile treatment of chemotherapeutic agents such as docetaxel causes generation of mitochondrial reactive oxygen species (ROS) which facilitates the lipid peroxidation reactions. [145] Therefore, it was proposed that chemotherapy could also induce ferroptotic cell death in addition to apoptosis, and it is controversial whether ablating ACSL4 activity will impair the efficacy of docetaxel treatment. Indeed, a previous clinical study reported that higher ACSL4 expression is related to better overall survival in breast cancer patients receiving neoadjuvant chemotherapy. [146] Therefore, examination of the combinatorial effects and potential interactions of ACSL4 inhibition and chemotherapy will provide valuable information for the clinical application of ACSL4 inhibitors in the context of advanced PCa. Another important clinical feature of advanced PCa that needs to be taken into consideration is the development of hormonal resistance. The initiation and progression of early-stage AdPC is often highly dependent on AR signaling and respond well to hormonal therapy, while patients will develop resistance to androgen deprivation, both through AR-dependent and AR-independent pathways and will eventually stop responding to castration even after the treatment of the second generation of anti-androgen therapies such as enzalutamide and abiraterone. [147] As we showed from RNA-seq analysis that ACSL4 OE slightly activated AR-regulated genes in LNCaP and that ACSL4 is particularly found to be upregulated in advanced PCa such as CRPC, it is important to investigate the effect of anti-androgen treatment to PCa cells with differential ACSL4 expression. In this chapter, we will explore the therapeutic potential of targeting ACSL4, especially considering the standard-of-care therapies that patients undergo and potential synergistic benefits through combinatorial treatment.

8.2 Materials and Methods

8.2.1 Cell Lines and Cell Culture, Docetaxel and Enzalutamide Treatment

LNCaP-Ctrl, LNCaP-ACSL4 OE, 22Rv1-Ctrl, 22Rv1-ACSL4 OE, PC3-sgCtrl, and PC3-sgACSL4 stable cell lines generated from Chapter 5 were cultured in complete RPMI medium. To analyze the effects of ACSL4 inhibitors, docetaxel and enzalutamide, cell viability was measured using the CellTiter-Glo 3D Cell Viability Assay kit (Promega). Briefly, we plated the cells in white-walled 96-well plates (Falcon) at the density of 1.0 ×

10^4 cells/well and treated the cells with ACSL4 inhibitors, docetaxel, or enzalutamide and rescued with Z-VAD, ferrostatin, or deferoxamine (DFO) for 48 hours. After the treatment, one volume of the CellTiter-Glo 3D reagent was added into each well, mixed on a thermomixer at 750 rpm for 5 minutes, and then incubated at room temperature for another 20 minutes. The luminance signal for a 250-millisecond integration time was measured using a SpectraMax M3 Multi-Mode Microplate Reader (Molecular Devices).

8.2.2 Statistical Analysis

No statistical methods were applied to determine sample size. The investigators were not blinded during experiments and outcome assessment. Statistical analyses were performed using GraphPad Prism software. For comparison of two experimental groups, an unpaired 2-tailed Student’s *t* test was used. For comparison of more than two groups, 1-way or 2-way ANOVA with Tukey’s multiple-comparison test was used. When data from multiple groups were not normally distributed, a Kruskal-Wallis test followed by Dunn’s multiple-comparison test was used. P-values of less than 0.05 were considered to be statistically significant.

8.3 Results

8.3.1 Combinatorial Treatment of ACSL4 Inhibitors with Docetaxel Demonstrated Synergistic Effects on Suppression of PCa Cell Growth

Given the previous result that ACSL4 OE LNCaP and 22Rv1 cells are more resistant to docetaxel treatment (Figure 13), we sought to investigate whether combinatorial treatment with ACSL4 inhibitors would re-sensitize ACSL4-high PCa cells and improve the effects of docetaxel treatment. ACSL4 OE will significantly increase cellular lipid peroxidation, which will be further upregulated by chemotherapy treatment through the generation of mitochondrial ROS, suggesting enhanced cell death through sensitization to ferroptosis (Figure 20A). [145] Therefore, we first sought to explore whether docetaxel treatment will also lead to ferroptosis in addition to apoptosis, which might be suppressed by ACSL4 inhibition. Notably, we found that in two ACSL4-high human prostate cancer cell lines PC3 and DU145, docetaxel treatment led to significantly reduced cell viability, which was almost completely rescued by co-treatment of the apoptosis inhibitor Z-VAD (Figure 20B). Inhibition of ferroptosis by ferrostatin or deferoxamine (DFO) did not rescue the cell death caused by docetaxel treatment (Figure 20B). This result indicated that in prostate cancer cell, docetaxel treatment only leads to cell death caused by apoptosis, not ferroptosis, and it is likely that ACSL4 inhibitor does not impair the efficacy of docetaxel treatment.

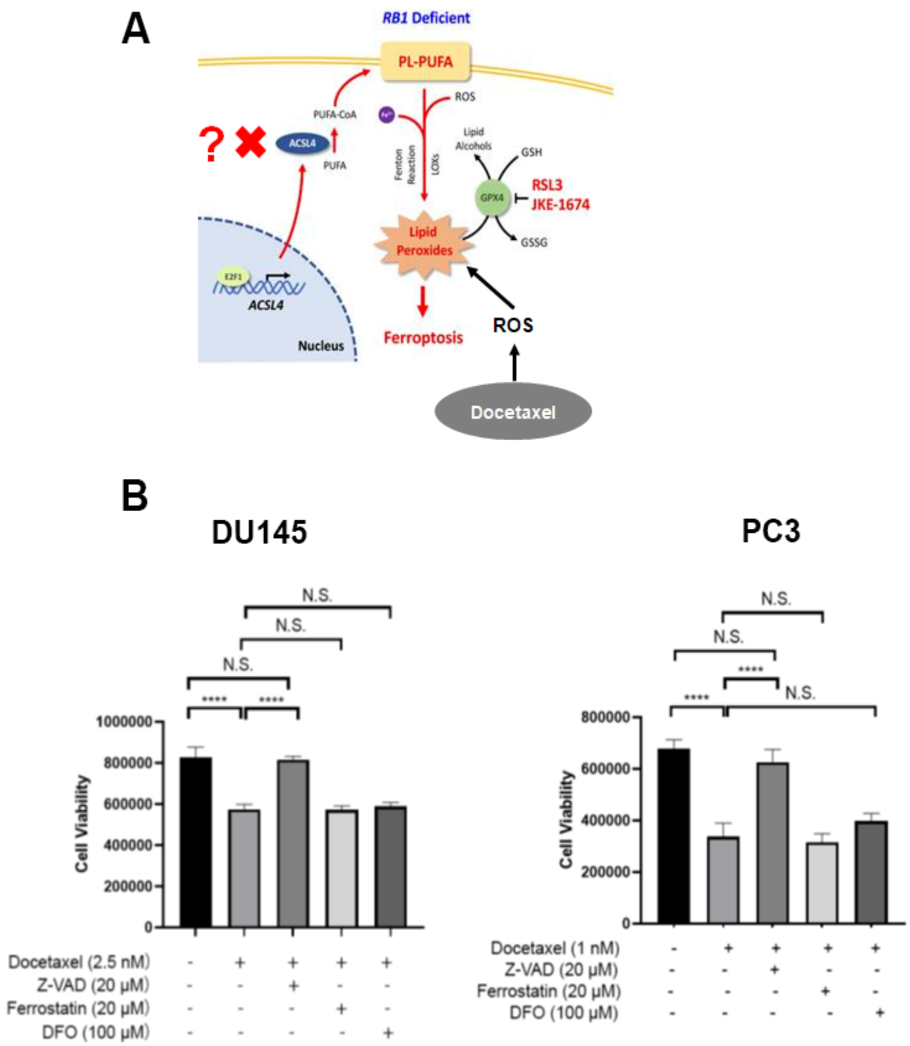

Figure 20. Docetaxel treatment induced prostate cancer cell death through inducing apoptosis not ferroptosis. 19A. Schematic demonstration of the potential role of mitochondrial ROS generated from chemotherapy treatment in the induction of ferroptosis. 19B. Treatment of DU145 and PC3 with docetaxel and rescue by apoptosis inhibitor Z-VAD, and ferroptosis inhibitors ferrostatin and DFO. ****$P < 0.0001$. Data are shown as the mean ± SD from n=3 biological replicates.

We next sought to investigate whether combinatorial treatment of ACSL4 inhibitors with docetaxel will demonstrate a synergistic effect in suppressing PCa cell proliferation as a potential strategy to overcome the development of chemotherapy resistance in advanced prostate cancer patients. We found that combinatorial treatment of docetaxel with PRGL493 or our candidate inhibitors 7 and 10 led to a further suppression of cell viability (Figure 21A, B). This synergistic effect was more evident in DU145, a cell line that was relatively more resistant to single treatment of docetaxel and ACSL4 inhibitors (Figure 21A, B). These results suggest that inhibition of ACSL4 could serve as a therapeutic strategy in combination with chemotherapy which significantly improved the therapeutic benefit through both suppression of cell viability and re-sensitizing PCa cells to chemotherapeutic agents such as docetaxel.

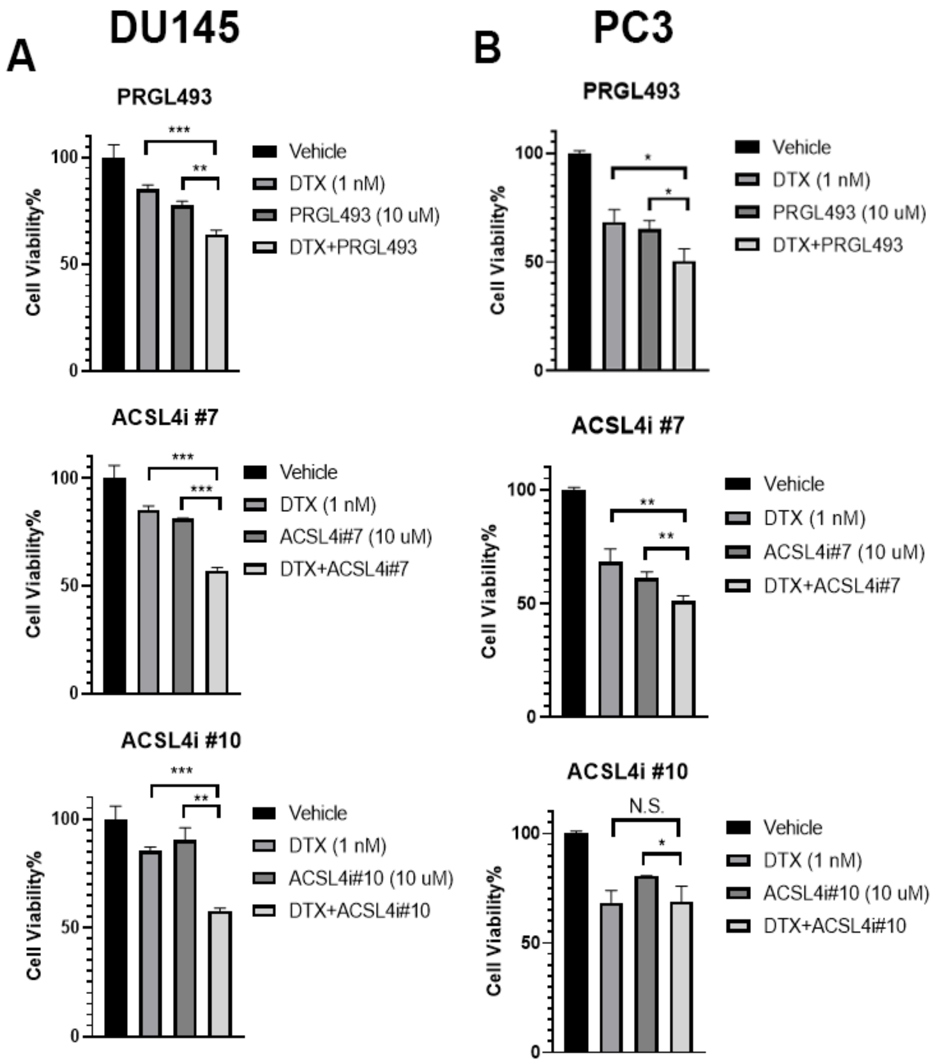

Figure 21. Combinatorial treatment of ACSL4 inhibitors and docetaxel showed synergistic effect in the suppression of PCa cell growth. 20A. Treatment of DU145 with combined docetaxel and ACSL4 inhibitors (PRGL493, ACSL4i #7, ACSL4i #10). 20B. Treatment of PC3 with combined docetaxel and ACSL4 inhibitors (PRGL493, ACSL4i #7, ACSL4i #10). **P* < 0.05, ***P* < 0.01, ****P* < 0.001. Data are shown as the mean ± SD from n=3 biological replicates.

8.3.2 ACSL4 Overexpression Does Not Affect PCa Sensitivity to Anti-Androgen Treatment

AR signaling is one of the most important oncogenic drivers and biomarkers during both initiation and progression of prostate cancer, and it plays an essential role in the development of anti-androgen therapy resistance. We first examined if ACSL4 OE had any effect on AR signaling activation, as suggested by RNA-seq analysis (Figure 12). Consistently, we found that the AR signaling in LNCaP-ACSL4 OE cells, especially upon DHT stimulation was slightly upregulated as indicated by higher PSA level (Figure 21A). Since 22Rv1 cells express the AR-V7 variant independent of androgen signaling, we did not observe any significant difference in AR and no PSA was expressed in both 22Rv1-Ctrl and 22Rv1-ACSL4 OE cells (Figure 22A). In addition, we found that LNCaP-ACSL4 OE cells were slightly more resistant to enzalutamide treatment, although no statistical significance was detected between the Ctrl and ACSL4 OE groups (Figure 22B). 22Rv1-ACSL4 OE cells did not respond to enzalutamide treatment (Figure 22A, B). Collectively, these results suggest that ACSL4 OE has a minimal effect on AR signaling activation and the sensitivity of PCa cells to anti-AR treatment.

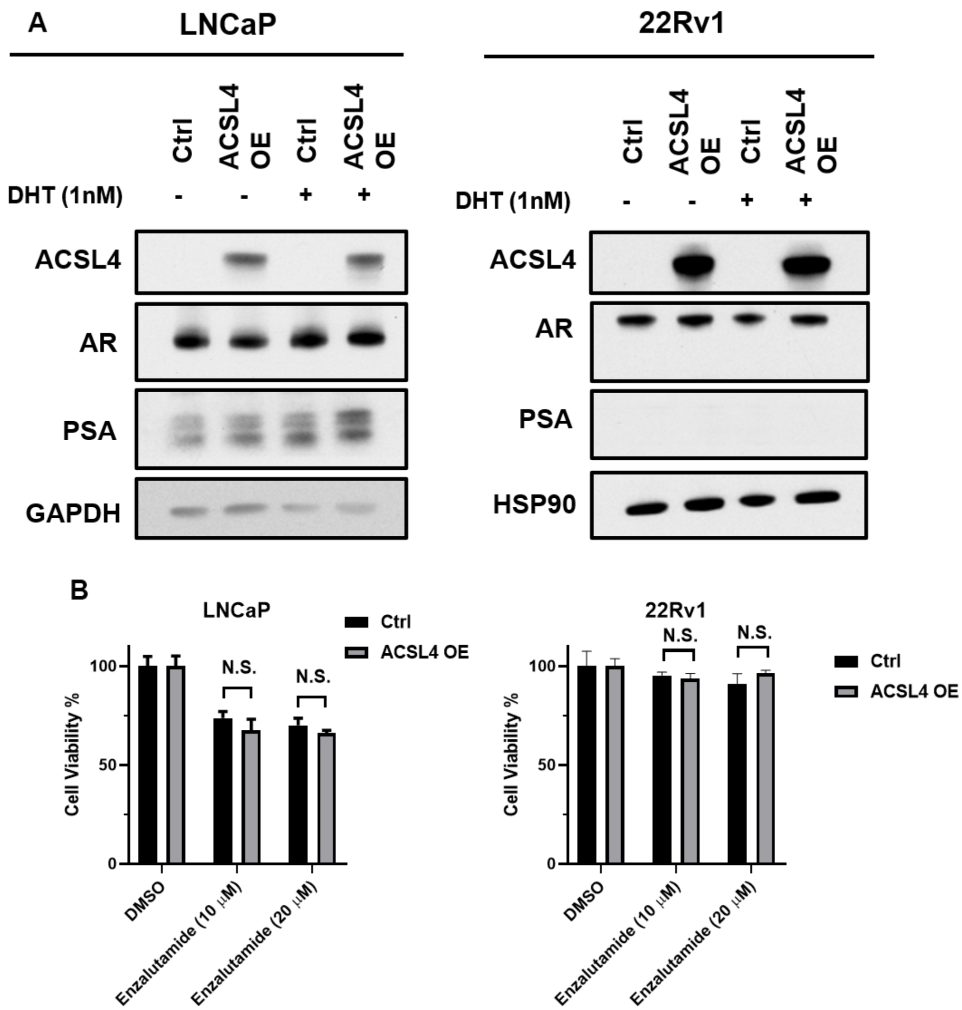

Figure 22. ACSL4 overexpression slightly increased AR signaling while did not change PCa sensitivity to enzalutamide treatment. 21A. Western blotting showing the level of AR and PSA in ACSL4-Ctrl and ACSL4 OE cells following DHT treatment. 21B. Treatment of Ctrl and ACSL4 OE LNCaP and 22Rv1 cells with enzalutamide for 48 h. Data are shown as the mean ± SD from n=3 biological replicates.

8.4 Discussion

In this chapter, we discussed the potential for the clinical application of ACSL4 inhibitors in the context of advanced prostate cancer through exploring possible combinatorial treatment with the chemotherapeutic agent docetaxel. In Chapter 6 we found that ACSL OE enhanced the chemotherapy resistance in PCa cells, possibly through the modification of extracellular matrix that impairs the physical penetration of chemotherapeutic drugs, as well as the development adaptability to stress due to altered cellular phospholipid component and increased energy production. Indeed, in addition to the inhibitory effects on cell viability as shown in Chapter 7, here we also showed that inhibition of ACSL4 could also re-sensitize PCa cells to docetaxel treatment. The development of chemotherapy resistance is frequently observed during the progression of advanced prostate cancer. Therefore, overcoming such drug resistance as PCa progresses will be a major breakthrough since chemotherapeutic agents such as docetaxel still have the indispensable role in the improvement of clinical outcomes and prolonging patients' survival. Previous studies have suggested the association between chemotherapy-induced ROS generation and ferroptosis, and the potential involvement of ferroptosis during chemotherapy treatment. [146] Therefore, inhibition of ACSL4 might have a negative effect on the clinical benefit of chemotherapy in certain contexts. However, our study showed that in prostate cancer, cell death induced by docetaxel treatment only involved apoptosis without the presence of ferroptosis, indicating that inhibited ACSL4 activity will not impair the efficacy of docetaxel. Moreover, given the result that AR signaling remains unchanged in ACSL4 OE cells, and that ACSL4 OE did not change LNCaP sensitivity to enzalutamide treatment, it is likely that the combinatorial treatment could be used in both AR-dependent and AR-independent PCa.

9. Conclusions and Future Directions

In this paper, we discussed the role of the fatty acyl-CoA ligase ACSL4 in prostate tumorigenesis, with a focus on its function in promoting prostate tumor growth and enhancing chemotherapy resistance, as well as the discovery of novel ACSL4 inhibitors that effectively suppresses prostate cancer cell growth with better efficacy and target selectivity. Dysregulated fatty acid metabolism is a hallmark of prostate cancer through upregulating energy production and *de novo* lipid synthesis. [1] Targeting the aberrant signaling pathways in fatty acid metabolism has been proven effective as a potential anti-cancer therapy, while the major limitations of the current small molecule inhibitors are the low selectivity on desired targets and severe side effects. [118] Our previous study identified ACSL4 as a downstream target of RB1/E2F signaling in prostate cancer, and previous studies have established an association between ACSL4 level and poor survival in advanced prostate cancer patients including CRPC and NEPC. [28] However, the biological function and mechanism of action of ACSL4 in promoting cancer progression, particularly in the context of prostate cancer, has been largely unknown. Through gain-of-function and loss-of-function studies and validated by *in vivo* xenograft experiments, we found that ACSL4 promoted prostate cancer cell proliferation through increased ATP production from excessive fatty acid activation. Consistently, lipidomic profiling analysis confirmed a global upregulation of multiple lipid species upon ACSL4 overexpression, as well as lipid species with ACSL4-modified FA chains. Interestingly, our RNA-seq data validated by *in vitro* assays revealed the altered expression of a group of genes associated with extracellular matrix (ECM) components in ACSL4 overexpressed PCa cells that led to increased migration ability and enhanced resistance to docetaxel treatment, as well as the expression of NEPC markers that might drive the lineage switching with neuroendocrine features. Therefore, we hypothesize that ACSL4 is a critical downstream effector of lethal RB1 loss-driven prostate tumorigenesis and inhibition of ACSL4 could represent a novel therapeutic approach to the treatment of aggressive prostate cancer. Currently, the only published small molecule inhibitor that targets ACSL4 activity is PRGL493, while the IC50 dose of PRGL493 in prostate cancer cells is relatively high with potential off-target effects. [111] Hence, there is an urgent need to develop novel ACSL4 inhibitors with better efficacy and selectivity. Through a structure-based virtual screening (SBVS), we identified 15 small molecules with predicted high binding affinity to ACSL4 enzymatic active sites. Subsequent *in vitro* drug testing confirmed the pharmacological effects on suppressing PCa cell proliferation in 4 of these 15 drugs. We found that these candidate ACSL4 inhibitors demonstrated higher efficiency in our previously generated isogenic ACSL4 OE PCa cells, while ACSL4 KO cells were resistant to ACSL4 inhibitors treatment. An isotope labeled ACSL4 activity assay showed that inhibitors 7 and 10 demonstrated high selectivity in reducing ACSL4 activity, which serve as promising lead compounds for the development of treatment for advanced prostate cancers. Further exploration of the clinical application of these ACSL4 inhibitors showed that the combinatorial treatment of ACSL4 inhibitors with docetaxel significantly improved the efficiency of docetaxel, which provided an option for resolving chemotherapy resistance in advanced prostate cancer patients.

In this study, we hypothesized that ACSL4 promoted prostate cancer progression through increased energy production that supports rapid proliferation. However, as suggested by our IHC data where ACSL4 OE xenograft tumors expressed not only significantly higher level of Ki67, but also showed a significantly lower to no caspase-3 expression indicating inhibited apoptosis. Indeed, it has been reported that unesterified AA is a critical signal for apoptosis induced by NSAIDs, and that overexpression of ACSL4 in cancer samples may contribute to the depletion of unesterified AA and removing of proapoptotic signal to promote carcinogenesis. [29] Therefore, future studies may focus on a more comprehensive role of ACSL4 in tumorigenesis by considering the overall impacts of increased cell proliferation, reduced apoptosis, as well as enhanced drug resistance. It would also be interesting to investigate changes in apoptosis signaling in ACSL4 OE cells to further dissect the underlying mechanisms. In addition, our RNA-seq data have suggested a change in the NEPC marker genes upon ACSL4 OE. However, it remains unclear how these genes are regulated by ACSL4 activity, or how these changes may contribute to the progression of NEPC. Since inhibition of ACSL4 effectively suppressed the cell viability of NEPC cells, it would be interesting for future studies to elucidate the essential role of ACSL4 in NEPC to discover novel therapeutic options that effectively target this malignant and lethal type of prostate cancer. To this end, future studies may refer to our RNA-seq data where we identified altered NEPC genes, particularly the upregulation of BRINP family genes in ACSL4 OE cells. Given the functions of the majority of these NEPC genes are largely unknown, it would be valuable to investigate them through further functional analyses. Lastly, although our candidate inhibitors, particularly 7 and 10 were proven promising as lead compounds, there is still room for the improvement of efficacy and specificity. One future direction is to improve the bioavailability of the candidate inhibitors through structural modification that could potentially enhance drug uptake or reduce/delay degradation to improve efficacy. Subsequent studies will also focus on performing PD/PK analyses for our candidate inhibitors with a goal of achieving success in the *in vivo* test of ACSL4 inhibitors.

Appendix A

Supplemental Figures

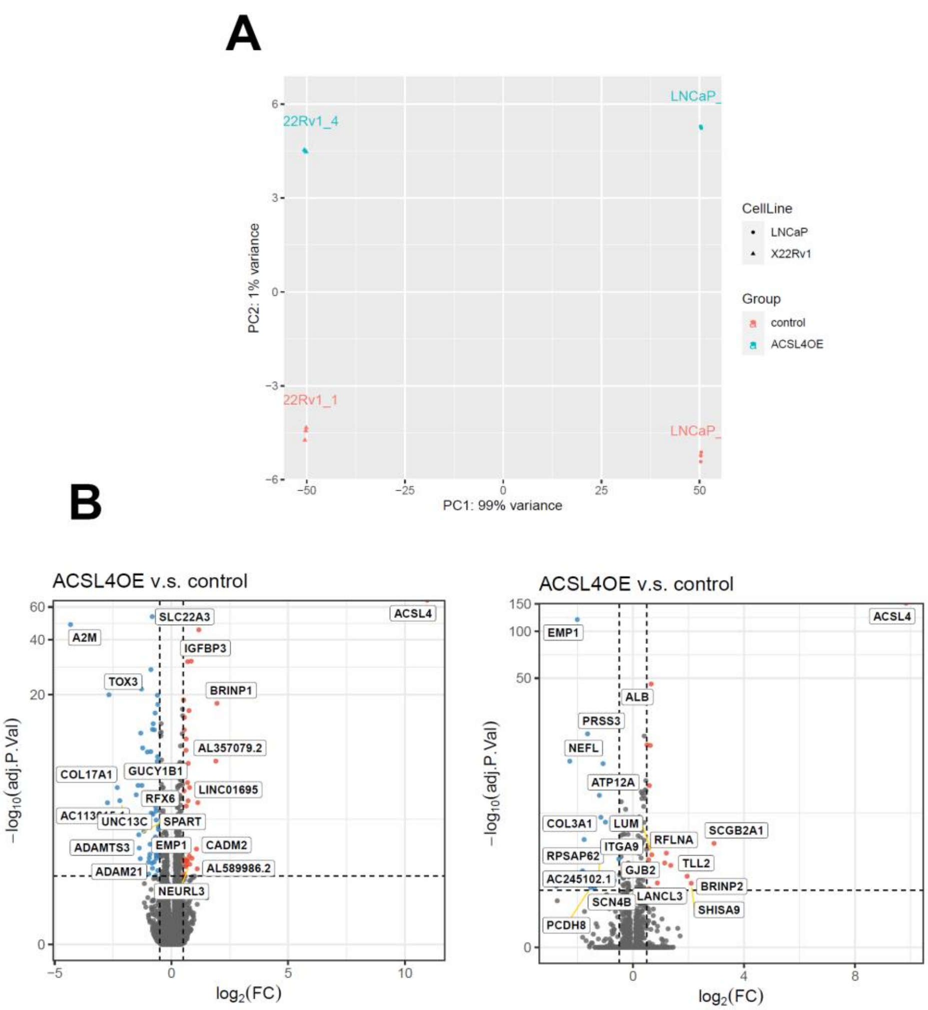

Supplemental Figure S1: RNA-seq analysis revealed distinct transcriptomic profiles in LNCaP- and 22Rv1-ACSL4 OE cells. S1A. Principal Component Analysis (PCA). S1B. Volcano plots showing the top changed genes in LNCaP (left) and 22Rv1 (right) after ACSL4 OE.

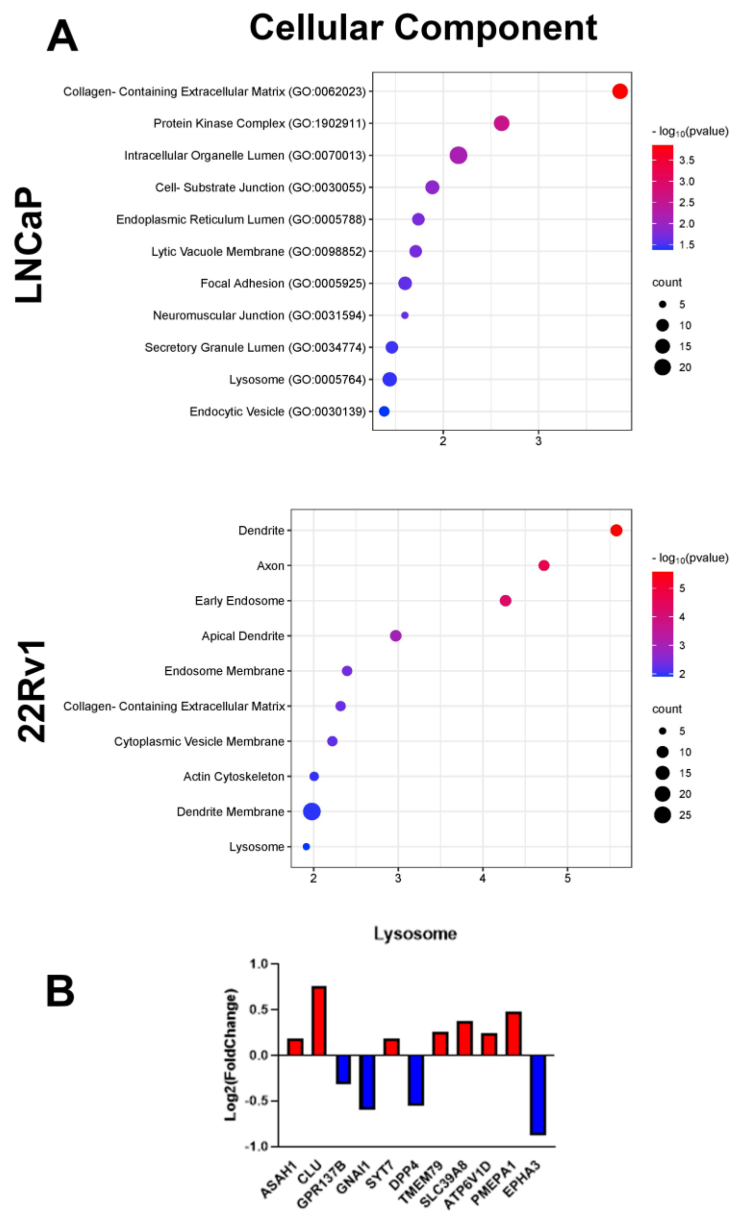

Supplemental Figure S2: RNA-seq analysis revealed cellular component change associated with lysosome. S2A. Enrichment analysis showing the cellular component enriched in LNCaP (top) and 22Rv1 (bottom) upon ACSL4 OE. S2B. Lysosome gene change in LNCaP-ACSL4 OE.

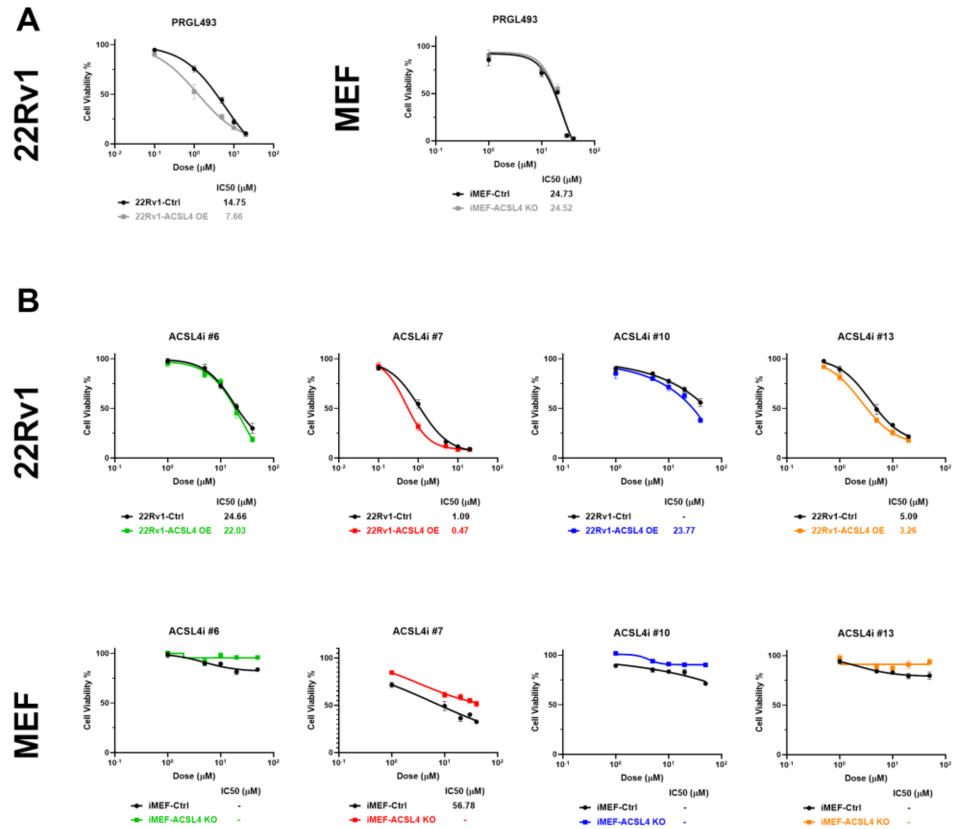

Supplemental Figure S3. ACSL4 inhibitor treatment led to shifted dose-response in 22Rv1-ACSL4 OE and iMEF-ACSL4 KO cells. S3A. Dose-response of PRGL493 treatment in 22Rv1-ACSL4 OE and iMEF-ACSL4 KO cells. S3B. Dose-response of candidate ACSL4 inhibitors treatment in 22Rv1-ACSL4 OE and iMEF-ACSL4 KO cells.

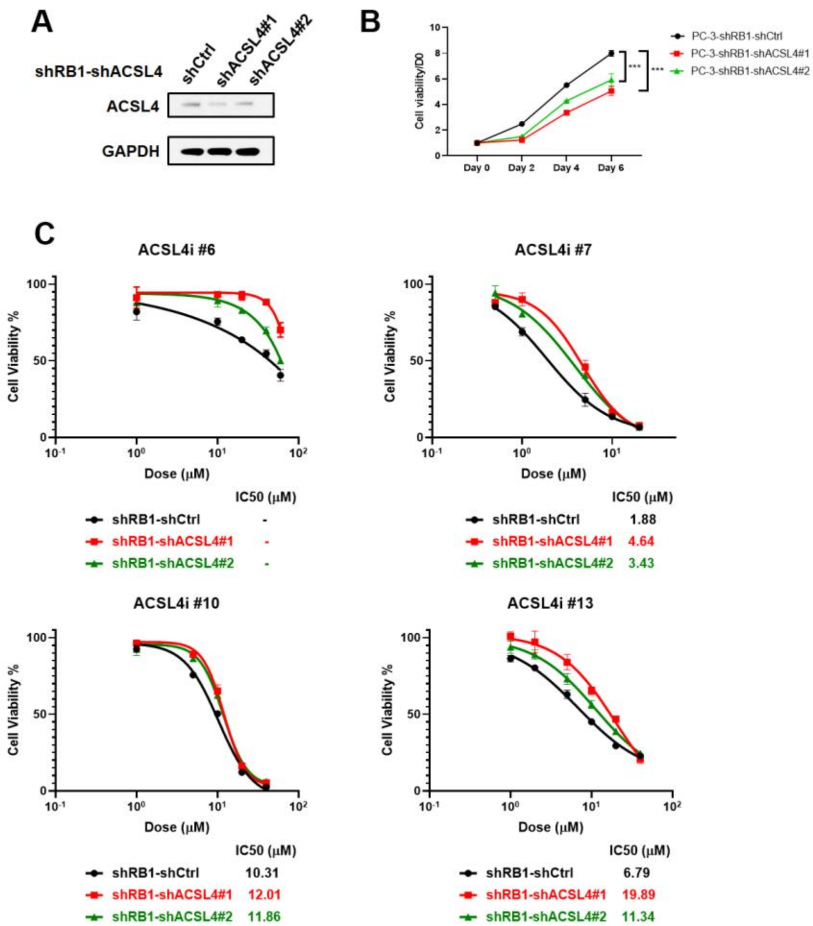

Supplemental Figure S4. Double KD of RB1 and ACSL4 led to significantly decreased PC3 proliferation rate and increased resistance to ACSL4 inhibitors treatment. S4A. Western blotting showing the knockdown of ACSL4 in PC3-shRB1 cells. S4B. 6-day cell proliferation of PC3-shRB1 and PC3-shRB1-shACSL4 determined by crystal violet assay. S4C. Dose-response of PC3-shRB1 and PC3-shRB1-shACSL4 to the treatment of ACSL4 inhibitors. ***P<0.001. Data are shown as the mean ± SD from n=3 biological replicates.

Appendix B

Supplemental Materials and Methods

Supplemental Table 1: sgRNA sequences for CRIPSR knock-out experiments.

Primer Name	Sequence (5' to 3')
ACSL4 sgRNA #1 Forward	TTACTTTGTTTTAGACCGA
ACSL4 sgRNA #1 Reverse	TCGGTCTAAAACAAAGTAA
ACSL4 sgRNA #2 Forward	TCCAGGGATACGTTCACAC
ACSL4 sgRNA #2 Reverse	GTGTGAACGTATCCCTGGA

Lipidomic Profiling Supplemental Data

Supplemental Table 2: Nomenclature of detectable lipid classes

Lipid Name	Abbreviations
Acyl carnitine	AcCa
Bismethyl phosphatidic acid	BisMePA
Cardiolipin	CL
Ceramides	Cer
Ceramides phosphate	CerP
Simple Glc series 2 GNAc1	CerG2GNAc1
Cholesteryl Ester	ChE
Carboxymethylethanolamine	CmE
Coenzyme Q10	Co Q10
Coenzyme Q7	Co Q7
Diglyceride	DG
Diglycosylmonoradylglycerol	DGMG
Fatty acid	FA
Ganglioside 3	GM3
hexosylceramide	Hex1Cer
dihexosylceramide	Hex2Cer
Trihexosylceramide	Hex3Cer
Lysophosphatidylcholine	LPC
Lysophosphatidylethanolamine	LPE

Lysophosphatidylglycerol	LPG
Lysophosphatidylinositol	LPI
Lysophosphatidylserine	LPS
Monoglyceride	MG
Monogalactosyldiacylglycerol	MGDG
Monogalactosylmonoacylglycerol	MGMG
Monolysocardiolipin	MLCL
Monoetherphosphatidylcholin	MePC
(O-acyl)-1-hydroxy fatty acid	OAHFA
Phosphatidic acid	PA
Phosphatidylcholine	PC
Phosphatidylethanol	PEt
Phosphatidylethanolamine	PE
Phosphatidylglycerol	PG
Phosphatidylinositol	PI
Phosphatidylinositol monophosphate	PIP
Phosphatidylmethanol	PMe
Phosphatidylserine	PS
Sphingomyelin	SM
Stigmasteryl ester	StE
Triglyceride	TG
Wax ester	WE
Zymosteryl ester	ZyE
Dimethylphosphatidylethanolamine	dMePE
Phytosphingosine	phSM

Supplemental Table 3: List of Significantly Altered Lipid Ions in ACSL4 OE Cells Compared with Control Cells.

Lipid Ion	LNCaP-Ctrl	LNCaP-ACSL4 OE
TG(22:1_22:4_22:5)+NH4	2431763.289	27147095.08
PI(18:0_18:0)-H	2936194.672	9232337.38
PS(20:2_22:4)-H	4751393.339	6486750.309
PC(40:4)+H	157504.781	2387330.249
TG(61:4+3O)+H	9574674.036	63588149.16
LPE(17:0)-H	47360.61367	1454839.516

PE(15:0_20:4)-H	0	1164819.894
PC(45:1)+(CH3CH2)3NH	6873472.315	47944461.95
PC(18:0_20:4)+H	425347809.9	1348624741
PG(20:3_22:6)+NH4	552029.1897	30351640.64
PC(15:0_22:6)+H	355916852	695143514.6
PE(18:0_22:6)+H	351305513.9	688186131
PG(22:6_22:6)-H	2461115.026	63329946.64
PIP(18:2+O_22:6)-H	102463.8233	2903555.081
PI(18:2+6O_22:6)-H	86600.682	2069360.99
TG(18:0_6:0_6:0)+(CH3CH2)3NH	0	4189132.736
TG(18:1_20:2_22:5)+NH4	49458079.41	367205308
TG(20:2_22:3_22:4)+NH4	14061161.83	79544075.34
PC(18:0_13:0)+H	610619.5315	3944666.919
PC(19:1_22:3)+H	14698450.71	86937295.27
PG(22:5_22:6)+NH4	1293698.101	42440112.85
DG(24:1e)+NH4	5807925.159	16069030.06
DG(26:1e)+NH4	18538864.8	42996993.85
TG(59:3+3O)+H	24581296.69	144742858.7
TG(20:2_20:2_22:4)+NH4	55642981	204596394.6
TG(19:1_20:3_22:5)+NH4	533921.5728	19440131.54
PC(16:0_16:1)+H	12284049649	35780741761
PG(20:3_22:6)-H	1854043.781	54266059.05
ChE(22:6)+NH4	27927495.2	113049760.5
PC(47:6)+H	485841.553	10498466.75
TG(22:3_22:4_22:4)+NH4	1373954.328	34391829.09
DG(24:2)+H	715127.2322	3096561.526
TG(22:3_22:3_22:3)+NH4	6502982.744	30413291.85
PG(22:4_22:6)-H	2394699.611	31596354.64
AcCa(17:0)+H	8274084.255	92717007.52
TG(59:5+3O)+H	3864891.555	95984759.65
DG(20:1_22:4)+NH4	4718332.673	28744800.53
TG(18:1_22:5_22:5)+NH4	6808898.805	137301741.9
TG(16:0_22:5_22:5)+NH4	14157763.26	181103300.1
PG(22:5_22:6)-H	1929237.75	37298350.84
TG(16:1_10:3_10:4)+(CH3CH2)3NH	2577275.374	13932464.75
TG(4:0_11:4_20:4)+(CH3CH2)3NH	5311616.752	17917200.33
TG(16:1_18:1_22:6)+NH4	41239189.94	185243922.1
SM(d44:0)+HCOO	22866.8214	426244.1489

PG(20:4_22:6)-H	913173.3787	12374901.33
PC(15:0_20:5)+HCOO	0	700317.0327
SM(d40:2)+H	299415946	904523319.6
TG(20:1_22:5_22:6)+NH4	2533217.123	64020965.93
TG(18:1_18:1_22:6)+NH4	89545923.08	447621311.8
ChE(22:5)+NH4	23123514.95	99794010.69
TG(18:1_22:5_22:6)+NH4	2053020.159	71050546.42
DG(25:1e)+NH4	19616643.47	53837791.59
Hex1Cer(d20:1_24:0)+H	1624645.094	20418396.15
TG(51:0e)+NH4	630301.4897	3055017.622
PG(18:1_20:4)+NH4	14477742.36	56718478.54
TG(18:1_14:0_22:5)+NH4	132542966.7	464436740.5
LPC(19:0)+H	436295.468	6805834.828
TG(22:3_22:4_22:5)+NH4	1073351.163	34567424.84
LPG(22:6)-H	815127.5463	12638538.39
DG(36:5e)+NH4	4781792.739	16590657.43
TG(18:1_22:4_22:4)+NH4	36302092.65	205854986.7
TG(16:0_22:6_22:6)+NH4	608827.145	30640629.76
PG(22:6_22:6)+NH4	2290999.851	87184415.17
PC(33:6)+H	5565339.758	23590682.09
PC(22:6_22:6)+H	3417596.651	16994244.17
PC(18:0e_22:2)+H	1020777.708	4839315.805
PC(16:1_22:6)+H	71836562.83	344735662.8
TG(18:0e_20:1_22:6)+NH4	474538.2479	2334403.306
TG(19:1_20:2_22:4)+NH4	7133475.533	31716122.35
TG(13:0_10:2_11:3)+NH4	5042278.155	1769029.08
DG(25:1e)+H	12446809.26	34118731.19
TG(14:0_22:4_22:6)+NH4	3696755.851	37392271.84
DG(38:6e)+NH4	3533355.707	16549260.13
PS(38:5e)-H	11452628.27	8473887.812
TG(18:1_18:2_22:6)+NH4	18510843.2	140455950.9
TG(16:0_16:1_22:6)+NH4	61904141.07	277421473.8
PC(17:0_22:6)+H	10536764.15	30778012.8
PC(16:1_13:0)+H	228049062.5	47212699.76
PG(20:2_22:6)+NH4	16655897.52	89839155.69
PC(36:6e)+HCOO	155596.8717	1454925.095
PC(18:0_15:0)+H	6950115.292	16964414.57
PG(20:1_22:6)+NH4	11880656.74	46051649.21

PC(32:4e)+H	2455540.107	13635015.27
PC(22:6_22:6)+HCOO	292152.1053	2045607.703
TG(22:4_22:4_22:6)+NH4	3060292.21	31481829.13
PEt(16:0_17:0)+H	2025082.241	27405249.02
StE(22:5)+NH4	2741574.333	13571909.89
PG(22:4_22:6)+NH4	1535172.571	26225732.4
TG(16:1_18:1_22:5)+NH4	152118029.4	657694540.3
DG(18:0_22:6)+NH4	3092120.581	19948374.2
PI(18:0e_18:1)-H	3127399.021	4021713.233
ChE(22:4)+NH4	55390008.27	162630183.4
PG(18:2_22:6)-H	8132346.275	45991188.4
PC(38:6COOH)+H	86703487.12	233693021.4
PS(18:0_22:6)+H	86703487.12	233693021.4
PC(12:1e_22:6)+H	7652538.839	32158054.89
PC(44:10)+H	3953423.764	24970384.72
WE(39:5)-H	493357.5313	1733186.231
PC(14:1e_20:4)+HCOO	599068.6258	2753341.453
TG(11:0COOCH3_16:0_18:1)+(CH3CH2)3NH	130159114.5	590604076.5
PC(27:0)+H	2775998.298	15171892.97
PC(43:5e)+H	1063630.768	6246740.255
PG(18:1_22:6)+NH4	80946066.07	365354660.7
PG(14:0_22:6)-H	699103.1261	4947135.282
TG(18:0e_18:1_22:6)+NH4	8050610.325	23218185.93
DG(18:3e)+H	86912504.46	455394767.3
PG(22:4_22:5)-H	2080370.859	12350663.82
PE(17:1_16:1)-H	659938.8903	2518375.777
PI(18:0_22:6)+NH4	27132075.64	67393274.47
DG(40:7e)+NH4	4867571.666	23709721.36
PC(17:1_22:6)+H	85345967.77	215038572.3
PI(43:6+OO)-H	2594357.539	1318029.016
DG(38:7e)+NH4	13568670.33	51248073.06
PC(17:1_22:6)+HCOO	86456.128	1071716.265
TG(18:1_20:2_22:4)+NH4	152475383.4	408366129.2
PI(18:0_20:2)+H	3025438.067	16655169.39
TG(16:1_18:2_22:6)+NH4	3375995.864	44772106.94
PE(16:1_14:0)-H	1845594.974	7292101.241
TG(63:6+3O)+H	0	12030193.98
PG(20:5_22:6)-H	264117.7387	4257092.626

PE(16:0p_22:6)+H	861271029.7	2452330065
TG(19:1_18:1_22:4)+NH4	24881089.14	63888261.65
TG(20:0_16:0_19:0)+NH4	1597252.294	5031983.085
PC(34:1+O)+H	3954436.491	12655941.21
PC(20:0e_17:0)+H	457871.3827	3120850.545
PC(18:0_22:6)+H	669235354.8	2185969087
PC(16:1e_22:6)+HCOO	6087173.405	21539318.62
PI(20:5+6O_22:6)-H	936346.3333	3029713.877
PE(14:0p_22:6)+H	11523586.19	49405804.52
PI(38:5e)-H	1725169.776	577772.512
TG(16:1_17:1_22:4)+NH4	16435614.47	55458967.95
PC(18:0_20:4)+HCOO	58486348.15	190579495.4
PC(18:1_20:5)+HCOO	13005499.07	43427200.59
PC(16:1_20:5)+H	77004735.1	322272918.6
PC(18:1_18:2)+CH3COO	6.806	760068.273
PC(36:3+2O)+H	44407986.2	177264686.2
ChE(20:5)+NH4	9380922.256	27411102.29
BisMePA(16:2e_16:1)+NH4	8179376.733	27795903.74
PG(33:0)-H	1320600.46	9823310.16
PE(18:0p_18:1)+H	1073976.561	2933041.135
TG(19:1_18:1_22:5)+NH4	13206159.23	60726072.21
TG(22:2_22:3_22:3)+NH4	8212136.553	31340310.8
TG(16:0_12:0_22:6)+NH4	11360594.16	63772056.37
PC(32:0)+H	43085650.89	155277948.5
TG(14:0e_9:0_10:0)+NH4	5288984.15	13071427.03
TG(4:0_12:0_14:0)+NH4	517516.8048	1725620.615
PI(18:0_20:4)+NH4	270431263.8	628120136.4
PS(34:3)-H	4226012.672	1627149.737
Cer(t42:3)+HCOO	225166.4558	1680257.782
PC(14:1e_20:4)+H	37350107.36	123108322.2
AcCa(22:0)+H	9817133.041	39744693.29
BisMePA(16:2e_14:0)+NH4	11227759.39	32774959.44
DG(16:0_20:4)+NH4	16791439.11	53231830.88
TG(16:1_17:1_18:2)+NH4	21023252.64	65057176.36
PC(18:1_22:5)+HCOO	13193142.8	41567110.89
PC(22:5_20:4)+HCOO	839993.3737	3837677.576
PC(34:4+4O)+H	513767.1703	5063961.504
PE(18:0p_22:6)+H	307475394.1	866047930.9

Hex1Cer(t16:0_18:1)+HCOO	12854268.2	26704504.88
PC(19:1_20:4)+H	115172219.8	323430722.9
TG(22:4_22:4_22:5)+NH4	4543024.059	33383877.45
PE(18:0p_20:2)+H	44899565.46	109986536.9
DG(15:0_18:1)+NH4	19332834.56	45161552.96
PE(18:1p_22:6)+H	374597146.3	1031441711
BisMePA(18:2e_22:5)+NH4	42182017.36	99811474
PC(20:0e_22:6)+HCOO	838629.027	3472205.391
WE(41:5)-H	4156936.462	9795905.947
TG(18:1_14:1_22:6)+NH4	10545337.62	59658233.7
PMe(36:4+OO)-H	2078019.592	9802093.193
PC(16:1e_20:4)+CH3COO	0.296333333	1402017.279
PC(16:1e_22:6)+H	158533703.6	375188061
PI(16:0_22:6)+NH4	15329749.21	47044704.17
PC(16:0_22:6)+H	2064317071	7270035360
PC(20:4_22:6)+HCOO	1683132.333	6869919.37
PC(16:1e_20:4)+H	721608631.3	2004756084
PC(16:0_22:6)+HCOO	86002587.23	275400195.4
PG(18:2_22:6)+NH4	9310246.598	42716137.51
PC(26:0_20:4)+H	1076154.326	3556439.715
PI(18:0_18:1)+H	15552102.29	28506664.91
SM(t42:0)+HCOO	903018.9392	2683174.908
PI(36:3+6O)-H	1523624.658	4185125.69
PE(16:0p_22:5)+H	91377655.94	187733734.1
PI(18:1_22:6)-H	819016.181	3014251.203
PC(22:5_22:6)+H	7304285.825	28410492.68
PC(20:4_22:6)+H	23901488.35	93937449.17
PC(32:1)+H	69172713.35	214845966.2
PS(18:0_22:5)-H	62528871.53	166636055.6
PC(36:5+OO)+H	27311487.35	65642928.59
TG(20:2_22:3_22:3)+NH4	25807508.86	83757772.61
TG(18:1_12:0_22:6)+NH4	22949754.06	101804823.7
PG(18:1_22:4)+NH4	39978883.29	124993482.4
PC(20:1_22:5)+HCOO	254323.4406	1565518.199
TG(12:0_14:0_22:6)+NH4	3526574.782	14397924.68
TG(14:0_14:0_17:1)+NH4	300987.1172	895215.881
PC(18:2e_24:1)+H	15291476.14	51962569.52
Cer(d18:2_18:0)+H	2462684.938	7538046.88

Cer(t18:1_18:0)+H-H2O	2462684.938	7538046.88
DG(16:0_14:0)+NH4	25888266.53	76277549.05
PG(19:1_22:6)-H	1009975.793	10665220.83
PC(18:0_22:6)+HCOO	24496589.17	88990660.41
PC(16:1_20:5)+HCOO	8206358.43	30229044.73
PS(36:3)-H	29228769.49	22965494.14
ChE(16:0)+NH4	1267174.228	5541023.542
PC(18:0_22:5)+HCOO	4537996.289	14691858.4
PC(12:0_14:0)+H	10509003.51	46051668.01
BisMePA(18:3e_14:0)+NH4	95137132.5	305107865.6
PE(16:0p_16:1)+H	95137132.5	305107865.6
FA(18:1+2O)-H	80340846.42	175080719
PIP(36:3+O)-H	2400062.437	6417083.421

Lipid Ion	**22Rv1-Ctrl**	**22Rv1-ACSL4 OE**
PC(42:9)+H	71226245.4	47654145.05
PC(37:1)+H	1088370.557	13020930.83
SM(d40:3)+H	1501582.63	2471963.091
PIP(38:5+8O)-H	511711.2343	73515.00467
PE(16:1p_22:5)+H	43784205.6	20934217.21
PC(27:2)+H	11618679.64	19190800.43
OAHFA(42:10)-H	8159464.603	45246816.43
PE(35:3)-H	8786320.468	10806679.55
dMePE(18:3+7O_20:5)-H	766804.426	324304.895
TG(16:0_14:0_17:1)+NH4	110906917.4	164594172.8
AcCa(17:0)+H	14826597.26	28094292.36
TG(18:0_6:0_6:0)+(CH3CH2)3NH	16128206.97	10787576.85
SM(t42:0)+HCOO	9210977.39	4501760.663
DG(21:1e)+H	31106598.52	47568656.48
PC(38:5)+H	5062735.504	312516.8575
LPE(20:3)+H	15042158.4	27503571.42
DG(24:1e)+NH4	12785061.96	21309140.23
PC(17:0_20:2)+H	84855650.76	302312686.1
PC(25:0COOCH3)+H	12642692.92	23010438.52
TG(4:0_12:0_12:0)+NH4	11123627.04	21220618.08
PE(18:0_22:6)+H	477782608.7	360610943.4
PC(26:3+3O)+H	2623714.735	7049486.744

dMePE(16:0_18:1)-H	13401766.31	26654019.12
Hex1Cer(t16:0_18:1)+HCOO	33748268.36	56595215.95
PG(38:5+5O)-H	515559.8855	1356051.038
PI(39:3)-H	0	807204.3507
MePC(36:1)+(CH3)2NH2	4191559.393	9936101.762
TG(14:0_22:4_22:6)+NH4	4074719.513	705388.0038
SM(11:1COOH)+HCOO	6410084.452	11532221.7
PC(20:0e_16:0)+CH3COO	2108577.654	8194453.808
PG(22:6_22:6)-H	8834607.211	2590539.88
LPC(20:3)+H	379600238.1	735575458
PC(18:3+OO_18:0)+HCOO	3632853.3	2579955.313
PG(22:5_22:6)-H	1166846.53	298450.5553
PC(19:1_20:4)+HCOO	2273058.292	6259754.706
dMePE(17:0_18:1)-H	1431396.128	1074985.417
PS(16:0_16:1)+(CH3CH2)3NH	5478152.327	9707690.57
WE(4:0_16:4)+H	31808474.85	86512763.07
PG(22:6_22:6)+NH4	14027430.99	3001900.391
PC(16:1e_22:2)+H	22467062.82	28791537.55
LPC(22:6)+HCOO	7830688.171	11399221.62
PC(20:5+Ox_18:1)+CH3COO	2457212.536	1927552.041
PC(36:4)+H	33605506.33	7920072.201
PC(26:1_20:4)+H	27584120.88	41702590.79
PC(8:0_11:1)+H	73554618.14	141423034.8
TG(12:0_10:2_10:3)+NH4	1255157.805	5277799.489
LPC(20:1e)+H	10318800.08	17150406
PC(33:1)+H	14626864.41	3873695.653
LPC(22:4)+H	19450385.21	38563487.43
PI(18:0_20:3)+H	3218411.53	0
PE(16:1_14:0)-H	486358.0887	1058341.283
Cer(t18:0_23:0)+H-2H2O	13336483.24	15892974.71
PC(16:0COOCH3_20:4)+HCOO	1582726.651	2865528.649
PG(19:1_22:4)-H	999518.816	5968412.273
PC(18:0e_22:6)+H	1682285507	2260223654
PC(20:4_14:4)+CH3COO	1962227.107	991503.391
TG(16:1_14:0_18:1)+NH4	564310691.8	810199352.7
TG(9:0_10:2_10:2)+(CH3CH2)3NH	5108501.01	9355172.392
DG(38:6e)+NH4	83180621.73	55919233.49
TG(8:0_8:0_14:0)+NH4	6879876.969	37689679.31

RNA-seq Supplemental Data

Supplemental Table 4: List of Significantly Altered Gene Expression in ACSL4 OE Cells Compared with Control Cells.

LNCaP-ACSL4 OE vs. LNCaP-Ctrl

Gene	baseMean	log2FoldChange	padj
ATP1B1	8080.456684	-0.821970884	5.914E-54
A2M	125.6171793	-4.321966664	5.7485E-49
SLC22A3	1113.634347	1.1740248	6.7995E-46
IGFBP3	1309.273884	0.847153225	3.0946E-31
ADRA2A	2796.495239	0.695204199	4.5619E-31
EPHA3	930.9544359	-0.878387366	3.6021E-28
LIN7A	310.4229113	-1.283985661	3.6463E-22
TOX3	72.44243955	-2.676101032	1.1966E-20
GNAI1	2568.345046	-0.599462854	1.555E-20
HMGCS2	2562.619962	0.520647549	2.1843E-19
BRINP1	99.51309725	1.952486772	1.3881E-18
TSC22D3	1749.807036	-0.583444962	2.4685E-18
CBLN2	5134.848503	0.475304503	2.6253E-17
CLU	686.4540331	0.752241534	5.4892E-17
TNFRSF19	1145.709466	-0.698693708	1.7832E-16
PMEPA1	3024.26183	0.483483543	6.1001E-16
AL591069.1	1914.978589	0.555656046	1.3536E-15
CLSTN1	9665.679528	-0.442549186	1.8871E-14
SALL2	532.121079	-0.780920259	1.9667E-14
PXDN	477.7053576	-0.812378101	1.8612E-13
UGT2B10	552.3875422	-0.730947794	2.2571E-13
MALT1	2831.186621	0.54716483	2.2571E-13
KCNMA1	2654.829703	-0.445439119	5.0931E-13
CCDC74A	141.4483551	-1.315134604	7.713E-13
CAPN5	2043.736299	-0.467929167	7.713E-13
H2AJ	3480.977364	0.463923567	9.6758E-13
ATP11A	2570.380045	-0.45050062	2.0258E-12
ID1	1240.683139	0.626556626	6.134E-12
ACPP	2841.691125	0.391070366	6.0073E-11
PHLDA1	155.2091649	-1.23062987	1.1227E-10
IL1RN	622.3329416	0.624884447	2.2908E-10

ANKRD29	259.4523126	-0.886650021	3.3584E-10
RALYL	210.8105456	-1.030786844	3.7603E-10
EPHA6	682.3481891	-0.590690829	1.4049E-09
SEPTIN3	1323.020764	-0.426486824	3.4595E-09
AL357079.2	51.18536878	1.902449504	4.6854E-09
RDH10	744.9242424	-0.608124202	5.0866E-09
KLK3	59803.59501	0.36616492	6.5331E-09
PEG3	2591.057354	0.468754059	8.4904E-09
PCDH11Y	582.5454369	0.719382025	8.5521E-09
H2BC21	3152.703846	0.33714549	9.129E-09
ZNF608	186.4638425	-0.948147437	1.9887E-08
LINC00161	953.2636323	0.456887137	2.1005E-08
ZNF350	548.5123831	0.570817031	2.8389E-08
ADAMTS1	20087.09673	0.304679384	2.8389E-08
SCD	21356.99139	-0.285913556	3.7188E-08
LAMC1	13519.16107	0.327156776	6.128E-08
COL5A2	336.5356578	-0.681208746	6.8057E-08
NAP1L1	14459.55729	-0.354756385	9.1424E-08
SOX4	3008.96502	-0.348744202	1.3259E-07
KLK2	11413.15017	0.338014231	1.3745E-07
SEMA3C	2661.430346	0.419490978	1.8776E-07
ADGRG6	10164.27074	0.333292667	1.8776E-07
GRIN3A	980.6143128	0.45010248	1.9039E-07
ID3	2016.624417	0.470774968	2.3787E-07
ELL2	1988.519424	0.348951721	2.4883E-07
SLC39A8	1548.069178	0.376169817	3.6759E-07
EFS	1000.40174	0.42173819	4.1667E-07
S100P	325.4038533	0.686429319	6.604E-07
QSER1	919.0233206	-0.430466028	8.9976E-07
SMAD9	662.661306	0.473042537	9.4863E-07
H1-2	2393.989619	0.338411248	1.1275E-06
ABCA12	1331.323093	0.383930453	1.1284E-06
GUCY1B1	71.26800683	-1.430786487	1.161E-06
ACOX2	79.7991988	-1.266192733	1.161E-06
CDYL2	2056.100491	0.326695776	1.2208E-06
UNC13B	4660.599856	0.263965225	1.4151E-06
SPRY4	213.4274203	0.777201609	1.721E-06
CDH26	1123.651804	-0.389109733	1.721E-06

COL17A1	27.89989546	-2.320774082	1.7461E-06
LPAR3	2123.403648	-0.352998853	1.7461E-06
MCCC2	12865.37342	0.271075554	1.8779E-06
DEFB132	429.0080624	0.543059756	3.2104E-06
PCDHB8	81.58437863	-1.171174524	5.5457E-06
HSPH1	4957.3252	0.252330111	5.5486E-06
RFX6	56.21898902	-1.507681735	6.4673E-06
H2AC6	1609.16038	0.362678306	7.0791E-06
TUBA1A	1015.960964	-0.397813554	1.0287E-05
SECTM1	1135.403966	0.400974606	1.0761E-05
H4C8	998.2953836	0.392685037	1.2391E-05
AC109782.1	137.1219086	-0.930102193	1.36E-05
EME2	2309.018457	0.317627414	1.36E-05
ARHGEF2	857.5115567	-0.398644167	1.3786E-05
UNC13C	28.04607892	-2.209449276	1.739E-05
HPGD	235.8792127	0.71331688	1.769E-05
GFM1	4378.822049	0.275438222	1.8658E-05
BAMBI	1414.994497	-0.344747273	1.8688E-05
PTGFR	2007.397079	-0.312461489	1.8967E-05
VASH2	436.5474155	-0.532077746	2.2254E-05
AC113615.1	19.13521722	-2.738633462	2.4052E-05
LINC01695	78.42829433	1.130501376	2.4052E-05
AL162582.1	870.4208146	0.385602935	3.4348E-05
DNAH8	275.3734791	0.633858167	4.0297E-05
PYGL	231.2468878	-0.665615548	4.9223E-05
LCP1	6047.67333	0.250025143	4.9223E-05
AAK1	2785.200392	0.283881644	5.0986E-05
DAPK1	451.3870953	-0.489484514	7.906E-05
RPS6KA3	1847.601091	-0.352367052	7.906E-05
ST6GAL1	203.1892061	-0.659704151	8.4901E-05
TRPM8	630.814903	0.413000934	8.4901E-05
AL606500.1	966.4492816	0.374518036	8.4901E-05
CAVIN1	118.6707191	-0.865777864	0.00011235
SI	182.1354333	-0.788380833	0.00013067
MIPEP	1024.478612	-0.350010068	0.00013067
MTERF4	2584.637541	0.280979367	0.00013067
H2BC12	1836.962817	0.284588117	0.00016311
TTC6	1100.371318	-0.374905368	0.00019615

H2BC5	515.7068541	0.440955866	0.00021984
CBWD1	1826.920907	0.328002224	0.00024371
AL357139.2	310.743873	0.545900613	0.00026042
CENPN	4171.804564	0.25229812	0.00026572
FBLIM1	206.1189087	-0.649128664	0.00028125
MAGEA4	147.6767556	0.733649868	0.00040614
PCDHB5	714.9780241	-0.370215278	0.00041515
APP	8404.13741	0.209047444	0.00044712
REPS2	853.5992236	-0.407990566	0.00045449
GLYATL2	376.7072718	0.470575123	0.00051572
H2BC8	316.9915419	0.504349899	0.0005592
BTG1	2878.112699	0.244060857	0.00058379
SESN3	3816.709732	-0.346199223	0.00062381
DPP4	224.0029656	0.590544222	0.00064091
EPHB2	260.1744782	-0.555449487	0.0006643
ACADVL	18258.60403	0.179011268	0.00074242
PDE4D	246.4842504	-0.55043342	0.00088924
MAST4	909.5083102	0.319742758	0.00094921
GDF15	18750.87951	0.23720863	0.00096041
ADD3	2717.509241	0.245221248	0.00105415
PLD1	53.64156407	-1.176831944	0.00105789
NQO1	3826.569132	0.225617193	0.00105789
ABCC5	2821.603952	0.267588426	0.00108187
MAP3K5	1151.53676	0.310574075	0.00112317
OTULINL	741.6753604	0.351766637	0.0011807
RSL24D1	3152.429828	-0.283005457	0.00119652
TFPI	3203.581743	-0.237624381	0.00121848
ETV1	5912.404223	0.207469218	0.00122249
MEX3A	1044.7298	-0.310122862	0.00123249
GPR158	3817.011917	0.229795307	0.00131462
RNF187	16511.65505	-0.21907179	0.00156682
F2R	351.491849	-0.447517359	0.00156933
VTA1	6294.998999	-0.227183386	0.00156933
SPART	35.0234841	-1.397901752	0.00157696
KIFC2	1794.099892	0.292174438	0.00163208
MAPK13	512.2673743	0.387332691	0.00193037
PCDHB13	146.765083	-0.683777883	0.00196883
RASEF	2684.513489	0.2406924	0.00196883

ATP6V1D	2142.419084	0.24919444	0.00203392
MYCBP2	5021.118858	0.250367035	0.00226337
IGF1R	752.3231514	0.363377352	0.00227942
ALDH2	576.5731137	-0.377952534	0.00241389
ZNF385B	397.2238109	-0.430813101	0.00255457
H2BC18	295.2944267	0.510059514	0.00256232
PSAT1	9108.49914	-0.216729927	0.00258035
ID2	527.5674757	0.391000615	0.00299205
GLYATL1P2	354.1441503	0.458988849	0.00301813
GLUL	4390.515359	-0.196724676	0.00304024
C9orf64	235.2999217	-0.528151194	0.00323497
HOXC13-AS	195.2704661	0.569427164	0.00345798
NFRKB	2923.232083	0.234112937	0.00362027
ALCAM	2175.456958	0.246358186	0.00371088
GULP1	10498.31626	0.199499538	0.00371088
PITPNM1	1205.556643	0.27830312	0.0038969
S1PR3	445.0226962	0.408155617	0.00392921
PCDHB11	78.14722319	-0.913568253	0.00407112
FAXDC2	436.5897548	0.400891104	0.00407112
LRP1	575.5376292	-0.391344167	0.00407112
RDX	3873.397608	0.227257993	0.00407112
RHOBTB3	378.3973826	-0.410087921	0.00407189
CITED2	1412.667341	-0.282146333	0.00420869
ACSL1	8475.427828	-0.209866512	0.00432065
JUNB	1502.483231	0.260533253	0.00436295
NOTCH3	989.6985717	-0.304119037	0.0043923
HSD11B2	1791.220819	0.257230824	0.0051118
SLC16A6	563.3699576	0.354925189	0.00546798
CRYM	205.1678514	0.531885387	0.00554745
NAXD	1381.914769	0.248234254	0.00566582
ADAMTS3	34.70457933	-1.37932588	0.00583059
CAB39L	2896.199569	0.201833993	0.00589062
CADM2	49.00402243	1.073806253	0.00637133
PODXL	1753.501784	-0.247339883	0.00639156
DIO1	302.8995936	-0.461519098	0.00645101
TMSB10	3051.592871	-0.237612242	0.00649741
ACKR3	1843.705425	-0.272834199	0.00689184
AJUBA	1320.029853	-0.252917502	0.00720133

BIRC3	377.3853434	0.412125227	0.00724909
ST6GALNAC1	816.6291142	0.32292562	0.00724909
HES6	1491.275727	-0.273873496	0.00726182
NRP1	4233.357938	0.20263295	0.00800776
GGCT	3651.503895	-0.206185161	0.00814738
BBS10	875.6001773	-0.323595918	0.00857295
PRKCD	3672.366859	-0.199300147	0.00943276
ZNF812P	180.4744905	-0.54312468	0.0094589
PRUNE2	16554.26071	0.193028849	0.0094589
FN1	32114.96015	0.409131169	0.00968318
ITPRID2	5864.259075	0.193621405	0.00996023
MID1	61.57954673	-0.923369997	0.0101177
STC2	2978.601001	-0.196867349	0.0101177
DHRS3	128.3408926	-0.64772766	0.01022073
IFT57	1630.034758	0.235954727	0.01024735
SHC1	5530.271816	0.172244824	0.01024735
MMP11	289.9801805	-0.431360685	0.01041977
TUBB4A	563.8893209	-0.336039086	0.01081567
AF165147.1	252.5671194	0.463612465	0.01122731
TEX2	3151.574694	0.195135247	0.01138378
MAGEC1	88.94721841	0.766801402	0.01156745
GOLGA2P5	122.5848842	-0.643192052	0.01156745
MAP2K6	205.9234494	-0.510764813	0.01156745
RIN2	313.9532915	-0.445871783	0.01156745
CACNA1H	343.4584819	0.406285009	0.01156745
AGR2	2718.572616	0.212304537	0.01156745
RTN4	7217.303424	0.162748865	0.01156745
STMN1	3993.908416	-0.192923112	0.01201456
THBS1	512.7265545	0.340026021	0.01213336
SAMD11	848.4222235	0.305811728	0.01226413
SESN1	2802.82496	-0.224397677	0.01238695
KIF3C	330.9014775	-0.428245293	0.01243265
SQSTM1	9665.878405	0.169459189	0.01262852
FADS2	18523.6653	-0.214760083	0.012776
KRT6C	55.48560935	-0.947840654	0.01355069
ASAH1	5176.279437	0.180316826	0.01367052
LNX2	1043.078224	0.305605287	0.01377846
EMP1	64.1421242	0.878108259	0.01398558

TTR	130.3016009	-0.651059603	0.01418177
TMEM45B	426.96828	0.382542691	0.01418177
ADAM21	30.43829613	-1.33474368	0.01437428
NIPSNAP1	6008.069732	-0.182109085	0.01447832
ANGPT2	170.010161	0.596123305	0.01512305
AC092718.4	457.6747663	0.36819595	0.01536034
NPDC1	5907.210829	0.183774376	0.01548959
MBOAT2	4028.203837	0.179217391	0.01632972
KRT20	142.8049117	0.686462605	0.01656653
DNAH8-AS1	114.2901098	0.640040883	0.01668036
FOXRED2	3819.234669	-0.186309794	0.01714701
GLP1R	207.8194133	0.501731252	0.01772798
FOXN3	1490.837009	-0.247434966	0.01774531
AC010168.2	157.9034567	0.602052252	0.01781112
DSG2	6764.280629	-0.168222472	0.01829182
UGT8	85.04016111	-0.736374701	0.01858106
GPR137B	513.1572898	-0.322835263	0.01858106
LMO4	854.4645835	-0.291879686	0.01858106
COL6A2	1044.920859	-0.244883929	0.01858106
HOXC10	47.37358486	-0.977450528	0.01884846
KREMEN1	979.9850742	-0.252830444	0.01884846
EIF4EBP1	3748.840093	-0.239610909	0.01902695
LTN1	1103.316119	0.278639805	0.0191027
AMACR	589.4970546	0.302171042	0.01954934
TACC1	3109.332812	0.205488439	0.01980513
NUP93	9556.51837	0.169133724	0.02011025
PIK3CD-AS2	65.98165274	-0.829426092	0.02018872
ERRFI1	1328.392187	0.229582042	0.02020513
ACTR3	7331.826762	0.159452072	0.02043112
NFKB2	1997.482165	0.210440876	0.02113911
TMEM179	482.8554109	0.347779698	0.02141737
NEURL3	74.54797303	0.784820232	0.02211433
ADPGK	2970.480181	0.176869356	0.02311343
BANK1	537.822482	0.354221294	0.02330524
ABCC4	8880.701678	0.175576272	0.02330524
ACHE	127.3584317	0.639988246	0.02364805
PLK2	892.2341092	-0.263888983	0.02364805
CELSR1	720.9386047	-0.28710501	0.02367582

TMEM79	959.8722619	0.256249564	0.02367582
CHPT1	5331.726197	-0.160301255	0.02380503
ACAP3	3222.761759	0.186018794	0.02409249
FAM162A	5455.321791	0.221150214	0.02429841
DIO3	768.9548379	0.299901036	0.02501536
ATF4	14010.81777	-0.183921595	0.02551849
NFE2L3	486.0592808	-0.318147501	0.02589888
H2BC4	208.7588938	0.481666551	0.02592366
DNASE1	1683.139705	0.217879518	0.02592366
CTAG2	112.0145591	0.617252869	0.02613665
RAB29	2168.28842	-0.198159686	0.02739917
USP54	9646.036006	0.157732412	0.02788135
AQP3	680.4427263	0.314792199	0.02808216
ADM2	1945.768554	-0.211469113	0.02808216
EGLN3	911.9832569	0.245347665	0.02852022
CRIP2	330.3615858	0.421431095	0.02857936
TMEM164	2528.113007	0.195683682	0.02919933
ABAT	2011.870698	0.195322849	0.02919933
PLEKHG6	67.78966974	-0.813397252	0.02956272
MKLN1	1691.730411	0.224006205	0.02956272
SHROOM3	3728.930835	0.196864735	0.02956272
TMEM144	892.5275466	-0.276801597	0.03018534
SLC44A1	2375.431085	-0.202950088	0.03018534
AL589986.2	34.55202873	1.105998911	0.03085325
DUSP2	690.4641761	0.274884336	0.03085325
NOS3	770.2365546	0.295005098	0.032769
SYT7	2845.490451	0.186774949	0.03323301
ALKBH2	956.0911085	-0.278429228	0.03402857
LRRN1	1096.196796	0.233577302	0.03402857
WDR90	2928.154513	0.174935163	0.0342769
BX255925.3	2574.452045	0.178047352	0.03430902
IGF2BP3	121.6625467	-0.583731106	0.03484216
WDFY2	419.6178718	0.328488282	0.03486955
GNPTAB	2466.429103	-0.203128808	0.03578111
ARHGAP28	279.0685742	-0.386421926	0.03625892
FRY	303.4809053	-0.381573665	0.03654119
MTMR9	878.3668839	0.243866784	0.03782852
CROT	1262.593433	0.22015784	0.03890116

PCDH1	814.9748048	0.258238169	0.03943947
CCDC159	763.8423294	0.271693468	0.04163147
DRAIC	520.8952407	-0.300206933	0.04166597
LIN9	475.5161092	-0.309862198	0.04221207
TMC6	1950.986831	0.190142285	0.04221207
RNF145	2903.216226	-0.174729081	0.04221207
LINC02718	575.9912226	0.339132075	0.04274712
SERPINB5	295.5502822	-0.396650212	0.0435691
LGMN	2847.780515	-0.179780174	0.0436092
SMOC2	40.86356671	-0.972803419	0.04407083
PGC	142.4682235	0.5476726	0.04407083
UGT2B28	260.9449549	-0.415718521	0.04437729
APLP1	1372.373194	0.216771586	0.04526334
LINC02593	740.7810821	0.255720047	0.04536082
NUCB2	1806.559592	-0.199540465	0.04536082
MAP4K4	3435.655775	-0.171860387	0.04703626
ASPHD1	2440.724026	0.212801331	0.04731196
TMEM123	5298.833636	-0.178421881	0.04765545
OR51E1	95.75174217	-0.674960308	0.04838197
GPRC5C	429.1668305	-0.33058265	0.04838197
METTL7A	1816.780541	-0.21635158	0.04838197
KRT19	151.3381169	0.56357013	0.04852084
HS3ST1	238.0432784	-0.40276138	0.04900864
HES4	1134.561786	0.239969519	0.04928502

22Rv1-ACSL4 OE vs. 22Rv1-Ctrl

Gene	baseMean	log2FoldChange	padj
EMP1	746.4946598	-2.007978552	9.010836e-120
ALB	6543.453883	0.654183475	1.481221e-46
PRSS3	189.8515048	-1.637079784	2.428279e-22
COLCA1	4413.995064	0.404186118	1.240487e-21
PFKP	1807.03239	0.503328596	5.497634e-19
SPOCK2	1064.046488	0.622334894	8.042844e-19
NEFL	68.32089775	-2.278746105	6.744738e-15
AC093001.1	272.6209348	-1.080245087	2.325432e-14
RELN	435.766612	-0.703951561	2.231807e-11

GDF15	1216.814828	0.460072763	3.820855e-11
ADRA2A	714.512894	0.587912947	2.402133e-10
ALDH1A1	1118.583083	0.440590685	1.022558e-09
SMOC1	1379.790115	0.466224901	1.421306e-09
ERBB2	6125.733651	0.296011801	1.911269e-09
MAOA	3169.080202	0.320366886	3.352776e-09
SLC45A3	1627.487018	0.383128432	5.879904e-09
ATP12A	120.6424828	-1.213426871	6.114499e-09
SPOCK1	1010.710109	0.438657624	1.609575e-08
RHOU	6291.664504	0.319101364	1.626430e-08
GABRA1	1034.494419	-0.42401315	4.082576e-08
PHETA2	1121.640001	0.383793728	1.484795e-07
HIF1A	3896.388658	-0.266711402	3.095710e-07
EPHA3	5741.091334	0.224425205	1.908485e-06
NTRK1	91.83037491	-1.157932499	2.052358e-06
IFT57	2867.70983	0.279909384	2.567493e-06
FLNB	8629.535562	-0.221148394	4.152469e-06
IRX3	4380.658442	0.225700441	4.315292e-06
NXPH1	115.0778107	-0.993868749	5.896940e-06
HLA-DQB1	898.1354018	0.390759151	6.336749e-06
PRSS21	1187.846756	0.323687445	3.205005e-05
S100A6	1066.429921	-0.364029337	6.104658e-05
MAP1B	1331.98785	-0.307975782	6.104658e-05
NKX3-1	20708.62769	-0.178905156	6.104658e-05
CNTNAP2	542.7628798	-0.441977766	7.438747e-05
LRRC8A	16198.98876	0.182713226	7.856443e-05
BEX1	1598.516943	0.278801779	0.0001123
COL3A1	37.94624465	-1.762520932	0.0001469
DKK1	775.164973	0.394812183	0.0001661
SCGB2A1	15.55900826	2.918085108	0.0002723
SMARCA1	990.2427216	0.32898703	0.0002723
NEDD4L	4377.348876	0.193246923	0.0002723
DOK6	1290.759039	-0.288969714	0.0002756
MYO1D	3589.900628	-0.212019229	0.0002785
ALS2	1528.121856	0.269437272	0.0003182
TSPAN1	2741.72532	-0.264204703	0.0003333
PTCH1	2282.714656	-0.227134895	0.0004643
C1QL4	330.4942933	0.561119347	0.00052

PCDH19	378.2899076	0.482327354	0.0006605
ALDH3A2	45234.57185	0.167631508	0.0007491
RFLNA	60.94894511	1.199495191	0.0010979
ARFGEF3	6048.086257	0.205734766	0.0011406
LUM	169.8786158	0.674503151	0.0013544
GABRB2	510.4392401	-0.429780866	0.0017414
NR2F2	1093.501074	0.290482821	0.0020342
LUZP2	294.6796636	-0.510410232	0.0023176
ZNF727	224.2621581	0.559363659	0.0025554
GJB2	53.40825866	1.140329261	0.003708
IGF2R	4223.000228	-0.171723345	0.003708
LAMC1	10492.16252	0.139923696	0.0044675
TLL2	38.81224879	1.358885279	0.0048842
MARCKS	8952.568607	0.191361449	0.0050571
MKI67	11489.01566	-0.166871465	0.0050929
MUC13	1830.220543	-0.228043592	0.0053581
PLAAT3	885.70411	0.282867081	0.0059607
PMEPA1	8537.112076	0.148921377	0.0064503
UBE2E3	3950.59214	-0.17751426	0.0068822
NUPR1	4340.304009	0.197043946	0.0071726
RPSAP62	22.6453448	-1.817356277	0.0087861
XK	208.0617712	0.565640965	0.0094217
EPHB2	138.8976223	0.644381597	0.0102279
LPL	586.9202149	-0.333187025	0.0102279
UGT2B15	767.6124302	0.319825355	0.0102279
EEF1A2	7909.809765	0.164522761	0.0102279
IL1R1	483.3051229	-0.373694066	0.01053
CTNNA2	241.9848118	-0.486797296	0.0130612
BRINP2	16.82578739	1.947244324	0.0149271
CPT1A	4508.669426	-0.157051705	0.0159414
SYTL2	2863.660901	0.201979465	0.01752
TDRD9	498.9447585	-0.357868711	0.0176801
VCAN	515.5855894	-0.337842533	0.0176801
SCRN1	920.3152479	0.263567853	0.0178651
ITGA9	36.20861682	-1.261448675	0.0213024
LXN	403.5350214	0.36342812	0.0216302
SEMA3D	114.2730222	-0.677048091	0.021977
ELL2	6167.505012	0.176506778	0.0240442

LANCL3	66.91210833	0.875923142	0.0275175
AC002456.1	43.91961381	-1.090711539	0.0275937
ACSL3	4485.34876	-0.177668441	0.0275937
NPR3	880.7443029	-0.25862801	0.0281468
SHISA9	14.86811174	2.098498583	0.0281602
CNN3	1308.266268	0.231608473	0.0298478
PAFAH1B3	2496.860123	-0.176997388	0.0298478
HOXB6	380.9214204	-0.36614952	0.0318366
F3	692.6184907	0.281094039	0.0329342
AC245102.1	9.103742641	-2.761459102	0.0359663
EDN2	491.8014093	-0.333535954	0.0359663
SPRY4	689.2004962	0.286161105	0.0359663
ERBB3	5372.294622	-0.150483335	0.0359663
UNC13B	11765.92296	0.132648232	0.0378415
AC110285.6	335.5190207	0.391274465	0.0404574
PCDH8	22.65484055	-1.528238048	0.0404647
SCN4B	26.02075941	-1.385020383	0.0419745
TUBA1A	4252.850368	-0.172163707	0.0419745
GLUL	3196.238144	0.162567869	0.0438002
REEP2	138.3728003	0.578761219	0.043919
CA12	1332.668816	0.229511601	0.044107
HSPA8	61164.38742	0.121320171	0.0460572
SOGA1	6045.533094	-0.164054096	0.047382
KIAA1324	5593.752492	-0.143085942	0.0496497
HEBP2	5141.238949	0.137566015	0.0496497
ENC1	1577.750389	-0.20135637	0.0498111

Structural-Based Virtual Screening Supplemental Data

Supplemental Table 5: List of the Top 15 ACSL4 Candidate Inhibitors by Virtual Screening.

Structure	COMPOUND _ID	Product_name	MDL#	MW	Name
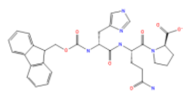	JFD02942	1-(5-amino-2-{[2-{[(9H-9-fluorenylmethoxy)carbonyl]amino}-3-(1H-4-imidazolyl)propanoyl]amino}-5-oxopentanoyl)-2-pyrrolidinecarboxylic acid	MFCD01312595	602.25	ACSL4i #1
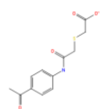	PD00665	2-{[2-(4-acetylanilino)-2-oxoethyl]thio}acetic acid	MFCD01935529	267.3	ACSL4i #2
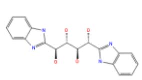	XBX00163	1,4-di(1H-benzo[d]imidazol-2-yl)butane-1,2,3,4-tetraol	MFCD00114547	354.36	ACSL4i #3
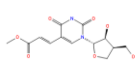	BTBS00021	methyl 3-{1-[3-hydroxy-4-(hydroxymethyl)tetrahydrofuran-2-yl]-2,4-dioxo-1,2,3,4-tetrahydropyrimidin-5-yl}acrylate	MFCD00829806	312.28	ACSL4i #4

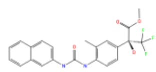	JFD02160	methyl 3,3,3-trifluoro-2-hydroxy-2-(3-methyl-4-{[(2-naphthylamino)carbonyl]amino}phenyl)propanoate	MFCD00789258	432.4	ACSL4i #5
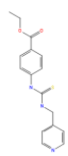	DSHS01220	ethyl 4-({[(4-pyridylmethyl)amino]carbothioyl}amino)benzoate	MFCD00121913	315.39	ACSL4i #6
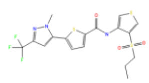	KM05324	N2-[4-(propylsulfonyl)-3-thienyl]-5-[1-methyl-3-(trifluoromethyl)-1H-pyrazol-5-yl]thiophene-2-carboxamide	MFCD00097107	463.51	ACSL4i #7
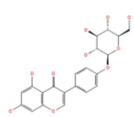	RJC00214	5,7-dihydroxy-3-(4-{[3,4,5-trihydroxy-6-(hydroxymethyl)tetrahydro-2H-pyran-2-yl]oxy}phenyl)-4H-chromen-4-one,80<90%	MFCD00205548	418.27	ACSL4i #8
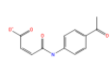	S03356	4-(4-acetylanilino)-4-oxobut-2-enoic acid	MFCD00157791	233.22	ACSL4i #9
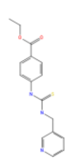	DSHS01227	ethyl 4-({[(3-pyridylmethyl)amino]carbothioyl}amino)benzoate	MFCD00121920	315.39	ACSL4i #10

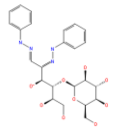	BTB12004	3,5,6-trihydroxy-2-(2-phenylhydrazono)-4-{[3,4,5-trihydroxy-6-(hydroxymethyl)tetrahydro-2H-pyran-2-yl]oxy}hexanal 1-phenylhydrazone	MFCD00205402	520.54	ACSL4i #11
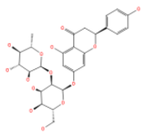	NRB04426	7-({4,5-dihydroxy-6-(hydroxymethyl)-3-[(3,4,5-trihydroxy-6-methyltetrahydro -2H-pyran-2-yl)oxy]tetrahydro-2H-pyran-2-yl}oxy)-5-hydroxy-2-(4-hydroxyphenyl)chroman-4-one	MFCD00204244	580.54	ACSL4i #12
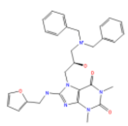	NRB03553	7-[3-(dibenzylamino)-2-hydroxypropyl]-8-[(2-furylmethyl)amino]-1,3-dimethyl-2,3,6,7-tetrahydro-1H-purine-2,6-dione	MFCD00831326	528.61	ACSL4i #13
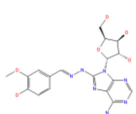	HTS09787	4-hydroxy-3-methoxybenzaldehyde N-{6-amino-9-[3,4-dihydroxy-5-(hydroxymethyl)tetrahydro	MFCD03056017	431.41	ACSL4i #14

		-2-furanyl]-9H-purin-8-yl}hydrazone			
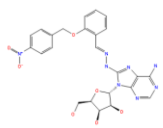	HTS11450	2-[(4-nitrobenzyl)oxy]benzaldehyde N-{6-amino-9-[3,4-dihydroxy-5-(hydroxymethyl)tetrahydro-2-furanyl]-9H-purin-8-yl}hydrazone	MFCD03406964	536.5	ACSL4i #15

References

1. Faubert, B., A. Solmonson, and R.J. DeBerardinis, *Metabolic reprogramming and cancer progression.* Science, 2020. **368**(6487).

2. Harayama, T. and H. Riezman, *Understanding the diversity of membrane lipid composition.* Nat Rev Mol Cell Biol, 2018. **19**(5): p. 281-296.

3. Zhu, J. and C.B. Thompson, *Metabolic regulation of cell growth and proliferation.* Nat Rev Mol Cell Biol, 2019. **20**(7): p. 436-450.

4. Rohrig, F. and A. Schulze, *The multifaceted roles of fatty acid synthesis in cancer.* Nat Rev Cancer, 2016. **16**(11): p. 732-749.

5. Su, X. and N.A. Abumrad, *Cellular fatty acid uptake: a pathway under construction.* Trends Endocrinol Metab, 2009. **20**(2): p. 72-7.

6. Rysman, E., et al., *De novo lipogenesis protects cancer cells from free radicals and chemotherapeutics by promoting membrane lipid saturation.* Cancer Res, 2010. **70**(20): p. 8117-26.

7. Kopecka, J., et al., *Phospholipids and cholesterol: Inducers of cancer multidrug resistance and therapeutic targets.* Drug Resist Updat, 2020. **49**: p. 100670.

8. Viswanathan, V.S., et al., *Dependency of a therapy-resistant state of cancer cells on a lipid peroxidase pathway.* Nature, 2017. **547**(7664): p. 453-457.

9. Mika, A., et al., *Preferential uptake of polyunsaturated fatty acids by colorectal cancer cells.* Sci Rep, 2020. **10**(1): p. 1954.

10. Scott, J.S., et al., *Monounsaturated Fatty Acids: Key Regulators of Cell Viability and Intracellular Signaling in Cancer.* Mol Cancer Res, 2022. **20**(9): p. 1354-1364.

11. Watt, M.J., et al., *Suppressing fatty acid uptake has therapeutic effects in preclinical models of prostate cancer.* Science Translational Medicine, 2019. **11**(478).

12. Dibble, C.C., et al., *PI3K drives the de novo synthesis of coenzyme A from vitamin B5.* Nature, 2022. **608**(7921): p. 192-198.

13. Gouw, A.M., et al., *The MYC Oncogene Cooperates with Sterol-Regulated Element-Binding Protein to Regulate Lipogenesis Essential for Neoplastic Growth.* Cell Metab, 2019. **30**(3): p. 556-572 e5.

14. Sancho, P., et al., *MYC/PGC-1alpha Balance Determines the Metabolic Phenotype and Plasticity of Pancreatic Cancer Stem Cells.* Cell Metab, 2015. **22**(4): p. 590-605.

15. Kinnaird, A., et al., *Metabolic control of epigenetics in cancer.* Nat Rev Cancer, 2016. **16**(11): p. 694-707.

16. Butler, L.M., et al., *Lipidomic Profiling of Clinical Prostate Cancer Reveals Targetable Alterations in Membrane Lipid Composition.* Cancer Res, 2021. **81**(19): p. 4981-4993.

17. Lima, A.R., et al., *Comprehensive Metabolomics and Lipidomics Profiling of Prostate Cancer Tissue Reveals Metabolic Dysregulations Associated with Disease Development.* J Proteome Res, 2022. **21**(3): p. 727-739.

18. Zhang, Z.L., et al., *New insights into lipid metabolism and prostate cancer (Review).* International Journal of Oncology, 2023. **62**(6).

19. Migita, T., et al., *ACSL3 promotes intratumoral steroidogenesis in prostate cancer cells.* Cancer Sci, 2017. **108**(10): p. 2011-2021.

20. Balaban, S., et al., *Extracellular Fatty Acids Are the Major Contributor to Lipid Synthesis in Prostate Cancer.* Mol Cancer Res, 2019. **17**(4): p. 949-962.

21. Falchook, G., et al., *First-in-human study of the safety, pharmacokinetics, and pharmacodynamics of first-in-class fatty acid synthase inhibitor TVB-2640 alone and with a taxane in advanced tumors.* EClinicalMedicine, 2021. **34**: p. 100797.

22. Al-Jameel, W., et al., *Inactivated FABP5 suppresses malignant progression of prostate cancer cells by inhibiting the activation of nuclear fatty acid receptor PPARgamma.* Genes Cancer, 2019. **10**(3-4): p. 80-96.

23. Liu, Q., et al., *Targeting lipid metabolism of cancer cells: A promising therapeutic strategy for cancer.* Cancer Lett, 2017. **401**: p. 39-45.

24. Kang, M.J., et al., *A novel arachidonate-preferring acyl-CoA synthetase is present in steroidogenic cells of the rat adrenal, ovary, and testis.* Proceedings of the National Academy of Sciences of the United States of America, 1997. **94**(7): p. 2880-2884.

25. Kuwata, H. and S. Hara, *Role of acyl-CoA synthetase ACSL4 in arachidonic acid metabolism.* Prostaglandins Other Lipid Mediat, 2019. **144**: p. 106363.

26. Chen, J., et al., *ACSL4 promotes hepatocellular carcinoma progression via c-Myc stability mediated by ERK/FBW7/c-Myc axis.* Oncogenesis, 2020. **9**(4): p. 42.

27. Qiu, Y., et al., *ACSL4-mediated membrane phospholipid remodeling induces integrin beta1 activation to facilitate triple-negative breast cancer metastasis.* Cancer Res, 2024.

28. Wu, X., et al., *ACSL4 promotes prostate cancer growth, invasion and hormonal resistance.* Oncotarget, 2015. **6**(42): p. 44849-63.

29. Cao, Y., et al., *Intracellular unesterified arachidonic acid signals apoptosis.* Proc Natl Acad Sci U S A, 2000. **97**(21): p. 11280-5.

30. Li, Y.J., et al., *Fatty acid oxidation protects cancer cells from apoptosis by increasing mitochondrial membrane lipids.* Cell Rep, 2022. **39**(9): p. 110870.

31. Liu, H., Y. Liu, and J.T. Zhang, *A new mechanism of drug resistance in breast cancer cells: fatty acid synthase overexpression-mediated palmitate overproduction.* Mol Cancer Ther, 2008. **7**(2): p. 263-70.

32. Tang, Y., et al., *Fatty acid activation in carcinogenesis and cancer development: Essential roles of long-chain acyl-CoA synthetases.* Oncol Lett, 2018. **16**(2): p. 1390-1396.

33. Wang, M.E., et al., *RB1-deficient prostate tumor growth and metastasis are vulnerable to ferroptosis induction via the E2F/ACSL4 axis.* J Clin Invest, 2023. **133**(10).

34. Hartman, E.J., S. Omura, and M. Laposata, *Triacsin C: a differential inhibitor of arachidonoyl-CoA synthetase and nonspecific long chain acyl-CoA synthetase.* Prostaglandins, 1989. **37**(6): p. 655-71.

35. Rossi Sebastiano, M. and G. Konstantinidou, *Targeting Long Chain Acyl-CoA Synthetases for Cancer Therapy.* Int J Mol Sci, 2019. **20**(15).

36. Koundouros, N. and G. Poulogiannis, *Reprogramming of fatty acid metabolism in cancer.* Br J Cancer, 2020. **122**(1): p. 4-22.

37. Ma, Y., et al., *Fatty acid oxidation: An emerging facet of metabolic transformation in cancer.* Cancer Lett, 2018. **435**: p. 92-100.

38. Martinez-Reyes, I. and N.S. Chandel, *Mitochondrial TCA cycle metabolites control physiology and disease.* Nat Commun, 2020. **11**(1): p. 102.

39. Fagone, P. and S. Jackowski, *Membrane phospholipid synthesis and endoplasmic reticulum function.* J Lipid Res, 2009. **50 Suppl**(Suppl): p. S311-6.

40. Ladanyi, A., et al., *Adipocyte-induced CD36 expression drives ovarian cancer progression and metastasis.* Oncogene, 2018. **37**(17): p. 2285-2301.

41. D Calvo, D.G.-C., Y Suárez, M A Lasunción, M A Vega, *Human CD36 is a high affinity receptor for the native lipoproteins HDL, LDL, and VLDL.* J Lipid Res, 1998. **39**(4): p. 777-788.

42. Olzmann, J.A. and P. Carvalho, *Dynamics and functions of lipid droplets.* Nat Rev Mol Cell Biol, 2019. **20**(3): p. 137-155.

43. Baenke, F., et al., *Hooked on fat: the role of lipid synthesis in cancer metabolism and tumour development.* Dis Model Mech, 2013. **6**(6): p. 1353-63.

44. Shimano, H. and R. Sato, *SREBP-regulated lipid metabolism: convergent physiology - divergent pathophysiology.* Nat Rev Endocrinol, 2017. **13**(12): p. 710-730.

45. Collins, J.M., et al., *De novo lipogenesis and stearoyl-CoA desaturase are coordinately regulated in the human adipocyte and protect against palmitate-induced cell injury.* J Biol Chem, 2010. **285**(9): p. 6044-52.

46. Marr, N., et al., *Controlling lipid fluxes at glycerol-3-phosphate acyltransferase step in yeast: unique contribution of Gat1p to oleic acid-induced lipid particle formation.* J Biol Chem, 2012. **287**(13): p. 10251-10264.

47. Wendel, A.A., T.M. Lewin, and R.A. Coleman, *Glycerol-3-phosphate acyltransferases: rate limiting enzymes of triacylglycerol biosynthesis.* Biochim Biophys Acta, 2009. **1791**(6): p. 501-6.

48. Ren, H., et al., *A phosphatidic acid binding/nuclear localization motif determines lipin1 function in lipid metabolism and adipogenesis.* Mol Biol Cell, 2010. **21**(18): p. 3171-81.

49. Ying, H., et al., *Oncogenic Kras maintains pancreatic tumors through regulation of anabolic glucose metabolism.* Cell, 2012. **149**(3): p. 656-70.

50. Gao, P., et al., *c-Myc suppression of miR-23a/b enhances mitochondrial glutaminase expression and glutamine metabolism.* Nature, 2009. **458**(7239): p. 762-5.

51. Yuneva, M., et al., *Deficiency in glutamine but not glucose induces MYC-dependent apoptosis in human cells.* J Cell Biol, 2007. **178**(1): p. 93-105.

52. Hao, Y., et al., *Oncogenic PIK3CA mutations reprogram glutamine metabolism in colorectal cancer.* Nat Commun, 2016. **7**: p. 11971.

53. Menendez, J.A. and R. Lupu, *Fatty acid synthase and the lipogenic phenotype in cancer pathogenesis.* Nat Rev Cancer, 2007. **7**(10): p. 763-77.

54. Ward, P.S. and C.B. Thompson, *Signaling in control of cell growth and metabolism.* Cold Spring Harb Perspect Biol, 2012. **4**(7): p. a006783.

55. Berwick, D.C., et al., *The identification of ATP-citrate lyase as a protein kinase B (Akt) substrate in primary adipocytes.* J Biol Chem, 2002. **277**(37): p. 33895-900.

56. Yecies, J.L., et al., *Akt stimulates hepatic SREBP1c and lipogenesis through parallel mTORC1-dependent and independent pathways.* Cell Metab, 2011. **14**(1): p. 21-32.

57. Menendez, J.A. and R. Lupu, *Oncogenic properties of the endogenous fatty acid metabolism: molecular pathology of fatty acid synthase in cancer cells.* Curr Opin Clin Nutr Metab Care, 2006. **9**(4): p. 346-57.

58. Xing, X., et al., *The ets protein PEA3 suppresses HER-2/neu overexpression and inhibits tumorigenesis.* Nat Med, 2000. **6**(2): p. 189-95.

59. Williams, K.J., et al., *An essential requirement for the SCAP/SREBP signaling axis to protect cancer cells from lipotoxicity.* Cancer Res, 2013. **73**(9): p. 2850-62.

60. Bustos, S.O., et al., *Secretory Autophagy Forges a Therapy Resistant Microenvironment in Melanoma.* Cancers (Basel), 2022. **14**(1).

61. Tomasetti, M., et al., *MicroRNA-126 induces autophagy by altering cell metabolism in malignant mesothelioma.* Oncotarget, 2016. **7**(24): p. 36338-36352.

62. Lin, J., et al., *The roles of glucose metabolic reprogramming in chemo- and radio-resistance.* J Exp Clin Cancer Res, 2019. **38**(1): p. 218.

63. Botzer, L.E., et al., *Hexokinase 2 is a determinant of neuroblastoma metastasis.* Br J Cancer, 2016. **114**(7): p. 759-66.

64. Menendez, J.A., L. Vellon, and R. Lupu, *Antitumoral actions of the anti-obesity drug orlistat (XenicalTM) in breast cancer cells: blockade of cell cycle progression, promotion of apoptotic cell death and PEA3-mediated transcriptional repression of Her2/neu (erbB-2) oncogene.* Ann Oncol, 2005. **16**(8): p. 1253-67.

65. Veigel, D., et al., *Fatty acid synthase is a metabolic marker of cell proliferation rather than malignancy in ovarian cancer and its precursor cells.* International Journal of Cancer, 2015. **136**(9): p. 2078-2090.

66. Menendez, J.A. and R. Lupu, *Fatty acid synthase (FASN) as a therapeutic target in breast cancer.* Expert Opinion on Therapeutic Targets, 2017. **21**(11): p. 1001-1016.

67. Zaytseva, Y.Y., et al., *Preclinical evaluation of novel fatty acid synthase inhibitors in primary colorectal cancer cells and a patient-derived xenograft model of colorectal cancer.* Oncotarget, 2018. **9**(37): p. 24787-24800.

68. Hatzivassiliou, G., et al., *ATP citrate lyase inhibition can suppress tumor cell growth.* Cancer Cell, 2005. **8**(4): p. 311-21.

69. Gutierrez, M.J., et al., *Efficacy and safety of ETC-1002, a novel investigational low-density lipoprotein-cholesterol-lowering therapy for the treatment of patients with hypercholesterolemia and type 2 diabetes mellitus.* Arterioscler Thromb Vasc Biol, 2014. **34**(3): p. 676-83.

70. Filippov, S., S.L. Pinkosky, and R.S. Newton, *LDL-cholesterol reduction in patients with hypercholesterolemia by modulation of adenosine triphosphate-citrate lyase and adenosine monophosphate-activated protein kinase.* Curr Opin Lipidol, 2014. **25**(4): p. 309-15.

71. Shah, S., et al., *Targeting ACLY sensitizes castration-resistant prostate cancer cells to AR antagonism by impinging on an ACLY-AMPK-AR feedback mechanism.* Oncotarget, 2016. **7**(28): p. 43713-43730.

72. Peck, B. and A. Schulze, *Lipid desaturation - the next step in targeting lipogenesis in cancer?* FEBS J, 2016. **283**(15): p. 2767-78.

73. Ma, M.K.F., et al., *Stearoyl-CoA desaturase regulates sorafenib resistance via modulation of ER stress-induced differentiation.* J Hepatol, 2017. **67**(5): p. 979-990.

74. Potze, L., et al., *Betulinic Acid Kills Colon Cancer Stem Cells.* Curr Stem Cell Res Ther, 2016. **11**(5): p. 427-33.

75. Vriens, K., et al., *Evidence for an alternative fatty acid desaturation pathway increasing cancer plasticity.* Nature, 2019. **566**(7744): p. 403-406.

76. Mortensen, M.S., J. Ruiz, and J.L. Watts, *Polyunsaturated Fatty Acids Drive Lipid Peroxidation during Ferroptosis.* Cells, 2023. **12**(5).

77. Penzo, D., et al., *Effects of fatty acids on mitochondria: implications for cell death.* Biochim Biophys Acta, 2002. **1555**(1-3): p. 160-5.

78. Pham, D.V. and P.H. Park, *Adiponectin triggers breast cancer cell death via fatty acid metabolic reprogramming.* J Exp Clin Cancer Res, 2022. **41**(1): p. 9.

79. Lee, J.Y., et al., *Polyunsaturated fatty acid biosynthesis pathway determines ferroptosis sensitivity in gastric cancer.* Proc Natl Acad Sci U S A, 2020. **117**(51): p. 32433-32442.

80. Magtanong, L., et al., *Exogenous Monounsaturated Fatty Acids Promote a Ferroptosis-Resistant Cell State.* Cell Chem Biol, 2019. **26**(3): p. 420-432 e9.

81. Nath, A., et al., *Elevated free fatty acid uptake via CD36 promotes epithelial-mesenchymal transition in hepatocellular carcinoma.* Sci Rep, 2015. **5**: p. 14752.

82. Kuda, O., et al., *CD36 Protein Is Involved in Store-operated Calcium Flux, Phospholipase A2 Activation, and Production of Prostaglandin E2.* Journal of Biological Chemistry, 2011. **286**(20): p. 17785-17795.

83. Yang, Y., et al., *ACSL3 and ACSL4, Distinct Roles in Ferroptosis and Cancers.* Cancers (Basel), 2022. **14**(23).

84. Ding, K., et al., *Acyl-CoA synthase ACSL4: an essential target in ferroptosis and fatty acid metabolism.* Chin Med J (Engl), 2023. **136**(21): p. 2521-2537.

85. Siddappa, M., et al., *Identification of transcription factor co-regulators that drive prostate cancer progression.* Sci Rep, 2020. **10**(1): p. 20332.

86. Burkhart, D.L. and J. Sage, *Cellular mechanisms of tumour suppression by the retinoblastoma gene.* Nat Rev Cancer, 2008. **8**(9): p. 671-82.

87. Knudsen, E.S. and K.E. Knudsen, *Tailoring to RB: tumour suppressor status and therapeutic response.* Nat Rev Cancer, 2008. **8**(9): p. 714-24.

88. Ku, S.Y., et al., *Rb1 and Trp53 cooperate to suppress prostate cancer lineage plasticity, metastasis, and antiandrogen resistance.* Science, 2017. **355**(6320): p. 78-83.

89. Walter, D.M., et al., *RB constrains lineage fidelity and multiple stages of tumour progression and metastasis.* Nature, 2019. **569**(7756): p. 423-427.

90. Chen, W.S., et al., *Genomic Drivers of Poor Prognosis and Enzalutamide Resistance in Metastatic Castration-resistant Prostate Cancer.* Eur Urol, 2019. **76**(5): p. 562-571.

91. Doll, S., et al., *ACSL4 dictates ferroptosis sensitivity by shaping cellular lipid composition.* Nat Chem Biol, 2017. **13**(1): p. 91-98.

92. Dixon, S.J., et al., *Ferroptosis: an iron-dependent form of nonapoptotic cell death.* Cell, 2012. **149**(5): p. 1060-72.

93. Shimbara-Matsubayashi, S., et al., *Analysis on the Substrate Specificity of Recombinant Human Acyl-CoA Synthetase ACSL4 Variants.* Biol Pharm Bull, 2019. **42**(5): p. 850-855.

94. Chen, F., et al., *The ACSL4 Network Regulates Cell Death and Autophagy in Diseases.* Biology (Basel), 2023. **12**(6).

95. Kuch, E.M., et al., *Differentially localized acyl-CoA synthetase 4 isoenzymes mediate the metabolic channeling of fatty acids towards phosphatidylinositol.* Biochim Biophys Acta, 2014. **1841**(2): p. 227-39.

96. Soupene, E. and F.A. Kuypers, *Mammalian long-chain acyl-CoA synthetases.* Exp Biol Med (Maywood), 2008. **233**(5): p. 507-21.

97. Munir, R., et al., *Lipid metabolism in cancer cells under metabolic stress.* Br J Cancer, 2019. **120**(12): p. 1090-1098.

98. Gan, B., *ACSL4, PUFA, and ferroptosis: new arsenal in anti-tumor immunity.* Signal Transduct Target Ther, 2022. **7**(1): p. 128.

99. Killion, E.A., et al., *A role for long-chain acyl-CoA synthetase-4 (ACSL4) in diet-induced phospholipid remodeling and obesity-associated adipocyte dysfunction.* Mol Metab, 2018. **9**: p. 43-56.

100. Natarajan, R. and J.L. Nadler, *Lipid inflammatory mediators in diabetic vascular disease.* Arterioscler Thromb Vasc Biol, 2004. **24**(9): p. 1542-8.

101. Manna, P.R., et al., *Synergistic activation of steroidogenic acute regulatory protein expression and steroid biosynthesis by retinoids: involvement of cAMP/PKA signaling.* Endocrinology, 2014. **155**(2): p. 576-91.

102. Cao Y, D.K., Doan TP, Prescott SM., *Fatty acid CoA ligase 4 is up-regulated in colon adenocarcinoma.* Cancer Research, 2001(61): p. 8429–8434.

103. Ma, L.L., et al., *Tumor suppressor miR-424-5p abrogates ferroptosis in ovarian cancer through targeting ACSL4.* Neoplasma, 2021. **68**(1): p. 165-173.

104. Zhang, Y., et al., *High-fat diet impairs ferroptosis and promotes cancer invasiveness via downregulating tumor suppressor ACSL4 in lung adenocarcinoma.* Biol Direct, 2021. **16**(1): p. 10.

105. Ndiaye, H., et al., *Immunohistochemical staining reveals differential expression of ACSL3 and ACSL4 in hepatocellular carcinoma and hepatic gastrointestinal metastases.* Biosci Rep, 2020. **40**(4).

106. Jemal, A., et al., *Cancer statistics, 2008.* CA Cancer J Clin, 2008. **58**(2): p. 71-96.

107. Harris, W.P., et al., *Androgen deprivation therapy: progress in understanding mechanisms of resistance and optimizing androgen depletion.* Nat Clin Pract Urol, 2009. **6**(2): p. 76-85.

108. Penning, T.M., *Androgen biosynthesis in castration-resistant prostate cancer.* Endocr Relat Cancer, 2014. **21**(4): p. T67-78.

109. Xinyu Wu, G.D., Peng Lee, and Marie E Monaco, *Lipid metabolism in prostate cancer.* Am J Clin Exp Urol, 2014. **2**(2): p. 111–120.

110. Monaco, M.E., et al., *Expression of Long-chain Fatty Acyl-CoA Synthetase 4 in Breast and Prostate Cancers Is Associated with Sex Steroid Hormone Receptor Negativity.* Transl Oncol, 2010. **3**(2): p. 91-8.

111. Castillo, A.F., et al., *New inhibitor targeting Acyl-CoA synthetase 4 reduces breast and prostate tumor growth, therapeutic resistance and steroidogenesis.* Cell Mol Life Sci, 2021. **78**(6): p. 2893-2910.

112. Orlando, U., et al., *Characterization of the mouse promoter region of the acyl-CoA synthetase 4 gene: role of Sp1 and CREB.* Mol Cell Endocrinol, 2013. **369**(1-2): p. 15-26.

113. Wu, J., et al., *Intercellular interaction dictates cancer cell ferroptosis via NF2-YAP signalling.* Nature, 2019. **572**(7769): p. 402-406.

114. Dattilo, M.A., et al., *Regulatory mechanisms leading to differential Acyl-CoA synthetase 4 expression in breast cancer cells.* Sci Rep, 2019. **9**(1): p. 10324.

115. Kan, C.F., et al., *PPARdelta activation induces hepatic long-chain acyl-CoA synthetase 4 expression in vivo and in vitro.* Biochim Biophys Acta, 2015. **1851**(5): p. 577-87.

116. Brown, C.W., et al., *The alpha6beta4 integrin promotes resistance to ferroptosis.* J Cell Biol, 2017. **216**(12): p. 4287-4297.

117. Kan, C.F., et al., *Arachidonic acid downregulates acyl-CoA synthetase 4 expression by promoting its ubiquitination and proteasomal degradation.* J Lipid Res, 2014. **55**(8): p. 1657-67.

118. Cheng, M., Z.M. Bhujwalla, and K. Glunde, *Targeting Phospholipid Metabolism in Cancer.* Front Oncol, 2016. **6**: p. 266.

119. Kato, M., et al., *Dendritic cell adenosylhomocysteine hydrolase-like protein 1 (AHCYL1) and inositol phospholipid signaling are potential targets for modulating their function.* Blood, 2006. **108**(11): p. 917a-918a.

120. Parlani, M., C. Jorgez, and P. Friedl, *Plasticity of cancer invasion and energy metabolism.* Trends Cell Biol, 2023. **33**(5): p. 388-402.

121. Eidelman, E., et al., *The Metabolic Phenotype of Prostate Cancer.* Front Oncol, 2017. **7**: p. 131.

122. Wang, T., F. Ma, and H.L. Qian, *Defueling the cancer: ATP synthase as an emerging target in cancer therapy.* Molecular Therapy-Oncolytics, 2021. **23**: p. 82-95.

123. Fiorillo, M., et al., *High ATP Production Fuels Cancer Drug Resistance and Metastasis: Implications for Mitochondrial ATP Depletion Therapy.* Front Oncol, 2021. **11**: p. 740720.

124. Poulose, N., et al., *Genetics of lipid metabolism in prostate cancer.* Nat Genet, 2018. **50**(2): p. 169-171.

125. Allott, E.H., E.M. Masko, and S.J. Freedland, *Obesity and prostate cancer: weighing the evidence.* Eur Urol, 2013. **63**(5): p. 800-9.

126. Kliewer, S.A., et al., *Fatty acids and eicosanoids regulate gene expression through direct interactions with peroxisome proliferator-activated receptors alpha and gamma.* Proc Natl Acad Sci U S A, 1997. **94**(9): p. 4318-23.

127. Golej, D.L., et al., *Long-chain acyl-CoA synthetase 4 modulates prostaglandin E(2) release from human arterial smooth muscle cells.* J Lipid Res, 2011. **52**(4): p. 782-93.

128. Huang, J., et al., *Extracellular matrix and its therapeutic potential for cancer treatment.* Signal Transduct Target Ther, 2021. **6**(1): p. 153.

129. Kesh, K., et al., *Therapy Resistance, Cancer Stem Cells and ECM in Cancer: The Matrix Reloaded.* Cancers (Basel), 2020. **12**(10).

130. Chen, M., et al., *An aberrant SREBP-dependent lipogenic program promotes metastatic prostate cancer.* Nat Genet, 2018. **50**(2): p. 206-218.

131. Beltran, H., et al., *Divergent clonal evolution of castration-resistant neuroendocrine prostate cancer.* Nat Med, 2016. **22**(3): p. 298-305.

132. Yuan, T.C., S. Veeramani, and M.F. Lin, *Neuroendocrine-like prostate cancer cells: neuroendocrine transdifferentiation of prostate adenocarcinoma cells.* Endocr Relat Cancer, 2007. **14**(3): p. 531-47.

133. Grabner, G.F., et al., *Metabolic regulation of the lysosomal cofactor bis(monoacylglycero)phosphate in mice.* J Lipid Res, 2020. **61**(7): p. 995-1003.

134. Showalter, M.R., et al., *The Emerging and Diverse Roles of Bis(monoacylglycero) Phosphate Lipids in Cellular Physiology and Disease.* Int J Mol Sci, 2020. **21**(21).

135. Berg, A.L., et al., *Cellular transformation promotes the incorporation of docosahexaenoic acid into the endolysosome-specific lipid bis(monoacylglycerol)phosphate in breast cancer.* Cancer Lett, 2023. **557**: p. 216090.

136. Orlando, U.D., et al., *Acyl-CoA synthetase-4, a new regulator of mTOR and a potential therapeutic target for enhanced estrogen receptor function in receptor-positive and -negative breast cancer.* Oncotarget, 2015. **6**(40): p. 42632-50.

137. Motomiya, M., et al., *Activity-dependent regulation of BRINP family genes.* Biochem Biophys Res Commun, 2007. **352**(3): p. 623-9.

138. Berkowicz, S.R., et al., *Brinp1(-/-) mice exhibit autism-like behaviour, altered memory, hyperactivity and increased parvalbumin-positive cortical interneuron density.* Mol Autism, 2016. **7**: p. 22.

139. Dos Santos, R.N., L.G. Ferreira, and A.D. Andricopulo, *Practices in Molecular Docking and Structure-Based Virtual Screening.* Methods Mol Biol, 2018. **1762**: p. 31-50.

140. Kim, J.H., T.M. Lewin, and R.A. Coleman, *Expression and characterization of recombinant rat Acyl-CoA synthetases 1, 4, and 5. Selective inhibition by triacsin C and thiazolidinediones.* J Biol Chem, 2001. **276**(27): p. 24667-73.

141. Wang, T., O.I. Pulkkinen, and T. Aittokallio, *Target-specific compound selectivity for multi-target drug discovery and repurposing.* Front Pharmacol, 2022. **13**: p. 1003480.

142. Tannock, I.F., et al., *Docetaxel plus prednisone or mitoxantrone plus prednisone for advanced prostate cancer.* N Engl J Med, 2004. **351**(15): p. 1502-12.

143. Hwang, C., *Overcoming docetaxel resistance in prostate cancer: a perspective review.* Ther Adv Med Oncol, 2012. **4**(6): p. 329-40.

144. Sekino, Y. and J. Teishima, *Molecular mechanisms of docetaxel resistance in prostate cancer.* Cancer Drug Resist, 2020. **3**(4): p. 676-685.

145. Oh, S.J., et al., *Mitochondrial event as an ultimate step in ferroptosis.* Cell Death Discov, 2022. **8**(1): p. 414.

146. Sha, R., et al., *Predictive and prognostic impact of ferroptosis-related genes ACSL4 and GPX4 on breast cancer treated with neoadjuvant chemotherapy.* EBioMedicine, 2021. **71**: p. 103560.

147. Vellky, J.E. and W.A. Ricke, *Development and prevalence of castration-resistant prostate cancer subtypes.* Neoplasia, 2020. **22**(11): p. 566-575.

Biography

Jinjin Wu obtained her Bachelor of Science degree in Environmental Sciences from Peking University in China in 2015, where she developed strong interest in studying neurodegenerative health outcomes from environmental exposure. As a student researcher, she designed and conducted an environmental toxicology study, which was published on *Environmental Research* entitled “Effects of prenatal exposure to silver nanoparticles on spatial cognition and hippocampal neurodevelopment in rats”. To pursue her career goal in the healthcare field, Jinjin completed her Master of Public Health degree in Columbia University in 2017, and this experience provided her with solid foundation in clinical research and statistical analysis. Driven by her passion in translational research and pathology, Jinjin joined Dr. Yiping Li’s lab as a research scientist, where she focused on disease modeling and bone biology, and her work resulted in three NIH R01 awards, as well as multiple publications on *Journal of Biological Chemistry*, *eLife, and International Journal of Biological Sciences* etc.

During her PhD study at Duke University, Jinjin focused on targeted therapy/drug development and cancer genetics research. She was awarded 2023 School of Medicine OBGE and Precision Genomics Collaboratory Pilot Grant and 2024 Graduate School Conference Travel Award, and she presented her findings from her thesis work at multiple conferences such as AACR and SBUR Annual Conferences. Jinjin also served as a Graduate Student Peer Mentor from the year 2023 to 2024.